Polypyrrole with improved solubility, synthesized using different doping techniques for applications in energy storage devices

Thesis submitted to

Cochin University of Science and Technology

in partial fulfillment of the requirements

for the award of the degree of

Doctor of Philosophy

By

Joseph John
Reg No: 4434

Department of Physics
Cochin University of Science and Technology
Cochin-682 022, Kerala, India

March 2019

Polypyrrole with improved solubility, synthesized using different doping techniques for applications in energy storage devices

Ph.D. thesis in the field of Material Science

Author

Joseph John
Division for Research in Advanced Materials
Department of Physics
Cochin University of Science and Technology
Cochin-682 022, Kerala, India
E-mail: joseph.john.kp@gmail.com

Supervising Guide

Dr. S. Jayalekshmi
Emeritus Professor
Division for Research in Advanced Materials
Department of Physics
Cochin University of Science and Technology
Cochin-682 022, Kerala, India
E-mail: jayalekshmi@cusat.ac.in

March 2019

DEPARTMENT OF PHYSICS
COCHIN UNIVERSITY OF SCIENCE AND TECHNOLOGY
KOCHI - 682022, INDIA

Dr. S. Jayalekshmi
Emeritus Professor

Certificate

Certified that the thesis entitled **"Polypyrrole with improved solubility, synthesized using different doping techniques for applications in energy storage devices"** submitted by **Mr. Joseph John** in partial fulfillment of the requirements for the award of degree of Doctor of Philosophy in Physics to Cochin University of Science and Technology, is an authentic and bonafide record of the original research work carried out by him under my supervision at the Division for Research in Advanced Materials Laboratory of the Department of Physics. Further, the results embodied in this thesis, in full or part, have not been submitted previously for the award of any other degree. All the relevant corrections and modifications suggested by the audience during the pre-synopsis seminar and recommended by the Doctoral Committee have been incorporated in the thesis.

Cochin - 22
March 2019

Dr. S. Jayalekshmi
(Supervising Guide)

Declaration

I hereby declare that the work presented in the thesis entitled **"Polypyrrole with improved solubility, synthesized using different doping techniques for applications in energy storage devices"** is based on the original research work done by me under the guidance and supervision of Dr. S. Jayalekshmi, Emeritus Professor, Department of Physics, Cochin University of science and Technology, Cochin-22, India and no part of it has been included in any other thesis submitted previously for the award of any degree.

Cochin - 22
March 2019

Joseph John

Dedicated to

My Family

&

Teachers

****

"The fear of the LORD is the beginning of wisdom,
and knowledge of the Holy One is understanding"

(Proverbs 9:10)

The Holy Bible

****

Words of gratitude...

At this moment of accomplishment, it is a pleasure to express my sincere thanks to all those who have contributed in many ways to the successful completion of my efforts. During the entire course of time, I was assisted by many people and it is indeed my pleasure to express my gratitude to all of them.

At this fortuitous moment, I take this opportunity to express my profound gratitude to my supervising guide Dr. S. Jayalekshmi, Emeritus Professor, Department of Physics, CUSAT, for initiating in me the drive, motivation and enthusiasm to pursue a research oriented Physics carrier and for her exemplary guidance, monitoring and constant encouragement throughout the course of the PhD programme. She has been a continuous source of inspiration for me since my M.Sc and M.Phil days in CUSAT and after that she gave me an opportunity to join for research under her guidance. In all my walks through the dark worlds of doubts and uncertainties, she lighted the way and showed the way. I take this opportunity to sincerely thank her for giving me the opportunity to work under her guidance. Without her sincere help and competent advice, I am sure, my work would not have been completed.

I am extremely thankful to Prof. M. Junaid Bushiri, Head of the Department of Physics, CUSAT and all former Heads of the Department of Physics for providing all the necessary facilities and environment to carry out fruitful research and for their support and co-operation.

I have been privileged throughout the period of research work to be associated with Prof. M. K. Jayaraj and Prof. K. P. Vijayakumar, Doctoral Committee members of my Ph.D. programme for their co-operation and unlimited support. I take this opportunity to thank all the faculty members of the Department of Physics, for their encouragement and co-operation. I would like to express my gratitude towards Prof M. R. Anantharaman, for his valuable suggestions during my pre-synopsis presentation.

I convey my sincere thanks to the administrative, library and laboratory staff of the Department of Physics for their help and assistance.

I consider myself fortunate to have been associated with Dr. Sajeev U.S, Assistant Professor, Government College, Nattakom during my research work. He has been a well-wisher and a strong motivator. The help extended by Parvathy G., FIP substitute is also gratefully acknowledged.

I express my gratitude towards Manoj M and Dr. Pradeep V. S who familiarized me with the synthesis of polymers and the assembling of Li ion cells. I also express my gratitude towards Dr. Anilkumar K. M, Assistant Professor, MSM College, Kayamkulam for his support and advices.

I am truly grateful to Divya N.G, Nano Functional Materials Lab, for her enormous support and encouragement. Her willingness and ready availability to offer help and her helping hand in writing the thesis are worth mentioning.

I am extremely thankful to Anuroop R, Solid State Physics Lab, for the help and support rendered by him throughout the period of my research. He inspired me a lot and helped me whenever I faced roadblocks in my research.

I consider it a privilege to thank my colleagues in the DREAM laboratory, Department of Physics, Mr. Abhilash A, Dr. Sreekanth J. Varma, Dr. Anand, Jinisha B, Dr. Saheeda, Dr. Sabira, Soumya and Merin, for being with me, extending all sorts of help during the entire period of my research work. My special thanks are also extended to Mrs. Ranjini R Mohan for the sincere help extended, whenever necessary.

I acknowledge with thanks the services rendered by STIC CUSAT and FESEM facility centre of CUSAT.

I am extremely thankful to Rev. Fr. Johnson Chirmmel, Manager and Mrs. Bridgit Jeeji C. J, Principal of Aquinas College for their support, encouragement and blessings. I am also grateful to University Grants

Commission, Government of India for providing the teacher fellowship under the FIP programme.

I acknowledge with deep affection the love, support, patience and benevolence of my mother Annie John, wife Mary Leejia P.J and my daughter Ann Maria Joseph, without whose care, consideration and prayers, it would not have been possible to bring my efforts to a successful completion. I am also thankful to my father in law and mother in law for the consideration and care extended. I remember the prayers of my father (Late K. J. John) who was highly concerned about my research.

Above all, I bow my head before the Almighty for the everlasting blessings showered on me, without whose grace, this report would not have emerged in the present form.

Joseph John

Preface

Interest in conducting polymers such as polypyrrole, polyaniline and polythiophene has increased tremendously during the last few decades on account of their tunable electronic properties for applications in rechargeable batteries, electrochromic devices, optical switching devices and as functional electrodes, sensors and smart materials. Conducting polymers or electroactive conjugated polymers are materials that conduct electricity and exhibit good electrical and optical properties that are conventionally shown by inorganic systems. Electrically conducting organic polymers with conjugated structure possess semiconducting and metallic properties depending upon the extent of doping and have incredible potential for applications in light emitting diodes, sensors, photovoltaic cells, energy storage devices, corrosion inhibition devices, micro-actuators and anti-electrostatic coatings. Among the conducting polymers, polypyrrole (PPy) is a widely studied conjugated polymer owing to its many advantageous features which include easily oxidizable nature, high electrical conductivity, good solubility, eco-friendliness, availability of precursor materials and unique redox properties. It has attracted the attention of scientists in interdisciplinary fields due to the ease of synthesis, good environmental stability and biocompatibility, which make it a promising material for commercial applications. Even though the polymerized form of pyrrole is widely studied, its electrical transport properties have been not completely understood. Most of the studies on PPy available in literature are on the electrochemically synthesized form. There are also reports on the ionic conductivity and the charge transfer mechanisms in PPy.

Polypyrrole is electrochemically active and permits the penetration of the electrolyte into the polymer mass, which makes it a prospective

electrode material for applications in rechargeable batteries. By the insertion and extraction of lithium ions, polypyrrole is found to be electrochemically active in the voltage range of 2.0-4.5V versus Li/ Li+ with a theoretical capacity of 72 mAh/g. Apart from its electrochemically active nature, PPy also functions as a conductive additive, thereby reducing the inert weight associated with the preparation of the cathode materials. It has also attracted much attention as an effective additive material to enhance the performance of anode materials in lithium-ion cells. As a conducting polymer, polypyrrole shows good compatibility with sulphur and organic electrolytes. The morphology of polypyrrole is ideal to enrich the electrochemical behaviour of the sulphur cathode in lithium- sulphur rechargeable cells.

The present thesis is divided into eight chapters. The work presented in the first part of the thesis is centred on the synthesis of polypyrrole using plasma polymerization and chemical oxidative polymerization techniques. Since the conductivity of the plasma polymerized PPy thin films is low, chemical oxidative polymerization technique using different oxidants and dopants is attempted to synthesize polypyrrole with higher electrical conductivity and solubility. Studies show that the poor solubility of polypyrrole is because of the presence of long chain conjugated structure, strong intramolecular interactions among the polymer chains and weak interactions of polypyrrole with the solvent, which limits its processability, characterization and applications. Even though much work has been devoted to increase the solubility of polypyrrole, the structural, morphological and electrical conductivity studies of the polymer doped with different dopants and soluble in various solvents have not been pursed in detail. The first phase of the thesis is mainly focussed on detailed investigations on the solubility, electrical conductivity, compositional aspects, structural morphology, optical

characteristics and stability of polypyrrole samples both in bulk and thin film forms, synthesized using plasma polymerization and chemical oxidative polymerization techniques.

The second phase of the work presented in the thesis is devoted to develop novel approaches to grow PPy based, cathode active materials for applications in Li secondary cells. Polymers like polypyrrole (PPy), polythiophene (PTh) and polyaniline (PANI) are being extensively studied as active electrode materials for lithium cells, because they can be easily switched between the oxidized and the reduced states. However, many of the PPy based cathodes have several problems related to low capacity and poor charge –discharge curves. In the present work, attempts have been made to assess the suitability of lithium enriched polypyrrole as the cathode active material for lithium based cells. Detailed studies have been carried out to enhance the electrochemical performance of the lithium substituted PPy based Li-ion cells by modifying the synthesis techniques. The suitability of the composite of the lithium enriched PPy with graphene to effect surface modification of the sulphur cathode to realize lithium - sulphur cells with high capacity and cycling stability has also been investigated in detail in the second phase of the research work.

Chapter 1 gives an introductory approach to polypyrrole and its synthesis using various techniques, emphasizing the importance of the oxidants and dopants in determining the structure, solubility and the electrical transport properties. The versatile applications of polypyrrole in different technological fields are reviewed, with special emphasis on its applications in lithium based rechargeable cells. The prime objectives of the present work are also highlighted in this chapter.

The growth of polypyrrole (PPy) thin films by ac plasma polymerization technique in the pristine and iodine doped forms and the detailed studies on the electrical conduction mechanism, presence of defect states and the optical characteristics form the focal theme of **chapter 2** The electrical transport studies of the aluminium-polymer film-aluminium structures have been carried out and the space charge limited conduction (SCLC) mechanism is identified as the most probable mechanism of carrier transport in these polymer films. Optical band gap and related constants are estimated from the optical absorption studies in the UV-visible-NIR spectral region. The investigations carried out to understand the defect levels created in the pristine and iodine doped PPy thin films, using Urbach tail analysis, also form a major part of this chapter.

Chapter 3 deals with the attempts carried out to synthesize polypyrrole with better solubility and higher electrical conductivity using chemical oxidative polymerization technique, compared to the PPy samples obtained using plasma polymerization method and the detailed structural, morphological, electrical and optical characterization of the synthesized PPy samples. Soluble polypyrrole with higher electrical conductivity is synthesized by chemical oxidative polymerization using ammonium persulfate (APS) as the oxidant and di (2-ethylhexyl) sulfosuccinic acid sodium salt (NaDEHS), dodecylbenzene sulfonic acid (DBSA) and dodecylbenzene sulfonic acid sodium salt (NaDBSA) as dopants. The work highlights the prospects of utilizing the solubility of doped PPy samples in various solvents for applications in the field of electronic gadgets.

The attempts made to improve the solubility and conductivity of polypyrrole films by synthesizing polypyrrole/graphene composite films, soluble in organic solvents, using chemical oxidative polymerization

method, with dodecylbenzene sulfonic acid (DBSA) as the dopant and ammonium persulfate (APS) as the oxidant, form the core theme of **chapter 4.** Thin films of polypyrrole /graphene composites are obtained on glass substrates by spin coating and electrospraying methods. The morphological, structural, optical, and electrical properties of the spin coated and electro-sprayed thin films are found to depend on the solvents used to dissolve the composites.

Chapter 5 introduces a relatively less expensive lithium salt, n-butyllithium in hexanes (n-BuLi)as the dopant for developing lithium substituted polypyrrole, to be used as the cathode active material in rechargeable Li ion cells. Polypyrrole is synthesized by chemical oxidative polymerization method, with ferric chloride as the oxidant and lithium substitution is achieved by treating with n-BuLi, in an argon filled glove box for four different volume concentrations of *n*-BuLi to improve lithium substitution or metalation. The lithium enriched PPy samples are subjected to detailed structural characterization using XRD, FTIR spectroscopy, FESEM and TEM techniques. The structural analysis confirms the successful lithium substitution and the enhanced crystallinity/order in Li substituted samples compared to pure PPy. The coin cells assembled using the lithium substituted PPy as the cathode, lithium metal as the anode and lithium hexaflurophosphate ($LiPF_6$) as the electrolyte show an open circuit voltage of 3.3 V. The assembled cells are electrochemically characterized using cyclic voltammetry and charge-discharge cycling techniques and it is seen that the Li substituted polypyrrole based Li-ion cells are electrochemically active. All the four cells show stable charge - discharge cycling behaviour up to 60 cycles, specific capacity about 30.03 mAh/g for the cell with maximum lithium substitution of 21.56 % and coulombic efficiency around 85 %. The

specific capacity of the cells can be further improved by optimizing the lithium doping concentrations.

Chapter 6 highlights the modifications undertaken to enhance the electrochemical performance of lithium substituted polypyrrole, used as the active cathode material for Li-ion cells, discussed in the previous chapter. The capacity and the cycling stability of the cells can be enhanced by synthesizing polypyrrole by chemical oxidative polymerization, using ammonium persulfate (APS) as the oxidant, instead of $FeCl_3$, discussed in the previous chapter. The electrochemical characterisation of the cells assembled using Li-substituted polypyrrole as the cathode, lithium metal foil as the anode and lithium hexaflurophosphate ($LiPF_6$) as the electrolyte shows an enhancement in the overall performance of the cells. Specific capacity of about 52.02 mAh/g, close to the calculated theoretical capacity has been obtained for the assembled cells with lithium substitution up to a maximum of 25.8 % for the cathode active material. The Li-ion cells are found to show an open circuit voltage of 3.8 V and an initial discharge capacity of 52.02 $mAhg^{-1}$ and 45.70 $mAhg^{-1}$ at 0.1 C and 0.2 C rates. All the cells show stable charge discharge cycling behaviour up to 85 cycles and coulombic efficiency around 88%.

Chapter 7 of the thesis gives a detailed discussion on the incorporation of PPy, graphene (G) and the composite of PPy with graphene into the conventional sulphur (S) cathode with a view to improve the capacity and the cycling stability of rechargeable lithium - sulphur cells. The electrochemical characterizations are carried out by assembling stainless steel Swagelok type lithium-sulfur cells in an argon filled glove box using PPy-S, S-G, and PPy-(G)-(S) composites as the cathode active materials, lithium metal foil as the anode and 1 M lithium perchlorate in a mixture of 1, 3-dioxolane (DOL) and 1, 2-dimethoxymethane (DME) at a volume ratio of 1:1 including 0.5 M

$LiNO_3$ as the electrolyte. The assembled cells are characterized using cyclic voltammetry and charge discharge cycling techniques and it is seen that the cells are electrochemically active. The discharge capacities of PPy-S, S-G and PPy-S-G composite cathodes based Li-S cells are 1248 mAh/g, 1317 mAh/g and 1444 mAh/g respectively with a capacity retention of 61%, 63% and 69% after 100 cycles. The enhanced capacity of the Li-S cells based on the PPy-G-S composite cathode can be a consequence of the ability of the doped PPy to accommodate large volume of sulphur on its branched structure and the absorption of polysulfides into the pores of PPy, thereby inhibiting the adverse effects of the volume expansion of sulphur during Li intake and the polysulfide shuttling phenomenon.

The summary of the research work carried out and the highlights of the results are presented in the **last chapter**. The future prospects for further investigations based on the results of the present work are also emphasized.

Contents

List of Tables

List of Figures

List of Publications

In Peer Reviewed Journals

1. **Joseph John**, Sajeev Sivaraman, S. Jayalekshmi, and M. R. Anantharaman, films, Investigations on the mechanism of carrier transport in plasma polymerized pyrrole thin films, Journal of Physics and Chemistry of Solids, 71 (2010) 935– 939 (doi:10.1016/ j.jpcs.2010.03.047).

2. **Joseph John**, Sajeev Sivaraman, S. Jayalekshmi, Urbach tail analysis on the defect states of polypyrrole thin films prepared by AC plasma polymerization, e-Polymer, 10(1) (2010) 1618- 7229 (doi:10.1515/epoly.2010.10.1.87).

3. **Joseph John**. M. Manoj. K. M. Anilkumar. V. S. Pradeep. S. Jayalekshmi, Lithium- enriched polypyrrole as a prospective cathode material for Li-ion cells, Ionics, 24 (2018) 2565-2574 (doi: 10.1007/ s11581-017-2398-x).

4. **Joseph John**, P. Saheeda, K. Sabeera, S. Jayalekshmi, Doped polypyrrole with good solubility and film forming properties suitable for device applications, Materials Today: Proceedings 5(10P1) (2018) 21140-21146 (doi: 10.1016/j.matpr.2018.06.512).

Papers presented in International/National conferences

1. **Joseph John**, U.S. Sajeev, S. Jayalekshmi, Plasma Power Dependence on the Optical and Structural Properties of Polypyrrole Thin Films Prepared by ac Plasma Polymerization technique, *National Conference on Current Trends in Materials Science (CTMS-07)*, March 25-27,2007, Christian College, Chengannur, Kerala, INDIA-689 122.

2. **Joseph John**, U.S. Sajeev, S. Jayalekshmi, Plasma Power Dependence on the Optical and Structural Properties of Polypyrrole Thin Films Prepared by ac Plasma Polymerization technique, *National Conference on Current Trends in Materials Science (CTMS-07),* March 25-27,2007, Christian College, Chengannur, Kerala, INDIA-689. 122

3. **Joseph John**, U.S. Sajeev, S. Jayalekshmi, Optical Properties of Pristine And Iodine Doped Polypyrrole Thin Films Prepared under Different Polymerization Conditions, *National Conference on New Horizons in Theoretical and Experimental Physics (NHTEP2007),* October8-10,2007,CUSAT,INDIA.

4. **Joseph John**, U.S. Sajeev, S. Jayalekshmi, The carrier transport mechanism in ac plasma polymerized pyrrole thin films, *National Conference on Nanophotonic Materials,(NCNM-2008),*October,10-12,2008,CUSAT,INDIA.

5. **Joseph John**, U.S. Sajeev, S. Jayalekshmi, Low-k materials based on plasma polymerized pyrrole thin films. *23rd Kerala Science Congress*, January 29-31, 2011, Centre for Earth Science Studies, Akkulam, Thiruvanthapuram. Kerala, INDIA.

6. **Joseph John**, U.S. Sajeev, S. Jayalekshmi, Modification of Surface Structure By Iodine Doping In Plasma Polymerized Thin Films, *National Seminar on Nanotechnology and its Applications,* February 1-3, 2011, Maharaja's College, Ernakulam, Kerala, India.

7. **Joseph John**, U.S. Sajeev, S. Jayalekshmi, Dielectric Properties of ac Plasma Polymerized Pyrrole Thin Films and the Effect of Iodine Doping *20th Swadeshi Science Congress,*November,6-8,2010, CMFRI, Kochi, Kerala, India.

8. **Joseph John**, P Saheeda, K Sabira, S. Jayalekshmi, Doped polypyrrole with good solubility and film forming properties for device applications, *International Conference on Smart Engineering Materials ICSEM-2016*, October 20-22, 2016, RV College of Engineering, Bengaluru.

9. P Saheeda, K Sabira, **Joseph John**, S. Jayalekshmi, Transparent and Flexible Nanocomposite Films of Polyvinyl Alcohol/ Multiwalled Carbon Nanotubes Ffr Optical Limiting Applications. *International Conference on Smart Engineering Materials ICSEM-2016*, October 20-22, 2016, RV College of Engineering, Bengaluru.

10. K Sabira, P Saheeda, **Joseph John**, S. Jayalekshmi, Excellent UV Shielding using Free Standing, Flexible PVDF/ZnO Nanocomposite Films, *International Conference on Smart Engineering Materials*, *ICSEM-2016*, October 20-22, 2016, RV College of Engineering, Bengaluru.

11. **Joseph John**, Adhin Nadh P.S, P Saheeda, K Sabira, S. Jayalekshmi, Lithium Doped Polypyrrole as Cathode Material for Flexible Li-ion Battery, *International Conference on Advanced Materials SCICON-2016*, December 19-21, 2016, Department of Sciences, Amrita Vishwa Vidyapeetham, Coimbatore.

12. P. Saheeda, K. Sabira, **Joseph John**, S. Jayalekshmi, Fluorescent Multi Walled Carbon Nanotube/Polyvinyl Alcohol Nanocomposite Films Synthesised through Green Routes, *International Conference on Advanced Materials SCICON-2016*, December 19-21, 2016, Department of Sciences, Amrita Vishwa Vidyapeetham, Coimbatore.

13. K. Sabira, P. Saheeda, **Joseph John**, S. Jayalekshmi, White Luminescence from Free Standing and Flexible PVDF/ZnO Nanocomposite Films, *International Conference on Advanced Materials SCICON-2016*, December 19-21, 2016, Department of Sciences, Amrita Vishwa Vidyapeetham, Coimbatore.

14. **Joseph John**, P Saheeda, K Sabira, S. Jayalekshmi, Investigations on the structural, morphological, optical and thermal properties of polypyrrole doped with dodecylbenzene sulfonic acid, *International Conference on Advances in Functional Materials (ICAFM-2017)*, January, 6-8, 2017, Anna University, Chennai.

15. **Joseph John**, M. Manoj, K. M. Anilkumar, V. S. Pradeep, S. Jayalekshmi, Electrochemical performance of lithium doped polypyrrole and its composite with $LiFePO_4$ as cathode material for Li-ion battery applications, *1st World Conference on Solid Electrolytes for Advanced Applications: Garnets and Competitors,* September, 6-9, 2017, Pondicherry University, India.

Chapter 1

INTRODUCTION

An overall introduction to the work presented in the thesis is given in this chapter. The chapter begins with a short overview on the history of conducting polymers and the significance of polypyrrole among the class of electrically conducting polymers based on its exceptional structural aspects, fascinating electrical and electrochemical attributes and the wide application prospects. As the title of the thesis illustrates, development of polypyrrole with appreciable solubility and processability suitable for various device applications is addressed with special emphasis on the applications of polypyrrole and its composites in the development of the next generation, flexible energy storage devices. The brief discussion on the objectives of the present studies and the motivation behind the work also forms a vital part of the present chapter.

1.1 Polymers

Polymer science has advanced from humble beginnings to its present dimension of modernity in which sub-atomic building frameworks enable polymer materials to be produced in predetermined specifications [1]. A comprehensive information of the association between the structure and the properties of polymers has enabled the present day engineers to design and synthesize materials with all intents and purposes for any physical attributes that are expected.

A polymer may be defined as a large molecule or a macromolecule built up by repeating structural units joined by the covalent bonds. The word polymer has been derived from the Greek words, poly meaning many and mer, meaning, part. The repeat unit is called the monomer from which the polymer is formed and the process by which the monomer molecules are linked to form a big molecule is called polymerization [2]. The number of repeat units in the chain specifies the length of the polymer chain. This is called the degree of polarization (D P). The molecular weight of the polymer is the product of the molecular weight of the repeat unit and the DP. Depending on the functionality of the monomers used, one can get linear, branched or three-dimensional cross-linked polymers.

W. H. Carothers in 1929, Mark in 1940 and Flory in 1953 recommended that all polymers could be divided into two categories depending upon the mechanism of polymerization, namely condensation polymers and addition polymers [3]. Condensation polymers are those in which the molecular formula of the repeat unit of the polymer chain does not have certain molecules present in the monomer from which it is formed. In polymer formation, condensation takes place between two polyfunctional molecules to produce a large molecule. This is also called step growth polymerization and examples are polyester and polyamide.

On account of their wide scope of applications, both synthetic and natural polymers play an imperative and omnipresent role in customary day to day life due to their mere presence. Polymers range from familiar synthetic plastics such as polystyrene to natural biopolymers such as

DNA and proteins that are essential for biological building and utility. Their substantial atomic mass with respect to small molecular compounds gives rise to extraordinary physical properties, including stiffness, viscoelasticity, and an affinity to form glasses and semi-crystalline structures rather than crystals.

1.2 Intrinsically conducting polymers

Intrinsically conducting polymers (ICPs) or electroactive polymers (EP) are not quite the same as the other conducting polymers, in which a conducting material such as a metal or carbon powder has been uniformly dispersed in a nonconductive polymer [4]. The ICPs or simply the conducting polymers combine the mechanical and chemical properties of insulating polymers with the electrical and optical properties of inorganic semiconductors and metals. This class of polymers has an all-inclusive arrangement of conjugated carbon-carbon double bonds [5]. These polymers are described by sigma (σ) and pi (π) bonds in which the σ electrons are fixed and immobile, due to the formation of covalent bonds between the carbon atoms and the remaining π electrons become delocalized, after doping. The conductivity of ICPs can be increased by doping, which is either the addition of electrons (n-doping) or the removal of electrons (p-doping) from the polymer. Examples of conducting polymers include polypyrrole, polyaniline polythiophene and polyacetylene. The history of development of different types of conducting polymers is quite interesting and is beautifully illustrated in literature [6, 7, 8, 9, 10, 11].

The field of conducting polymers gained attention since 1977, when Alan Heeger, Alan MacDiarmid and Hideki Shirakawa. reported the synthesis of the first intrinsic, electrically conducting organic polymer, doped polyacetylene. The electrical conductivity of polyacetylene increased 10^9 times after it was oxidized (doped) by chlorine, bromine or iodine vapor. These three researchers were awarded the Nobel prize in Chemistry in the year 2000 for their pioneering contributions to nurture the development of conductive polymers. Subsequently, in the past two decades, many research groups have devoted their endeavours for developing new classes of electrically conducting polymer materials and great progress has been accomplished in the growth of newer fields like organic and molecular electronics, polymer optoelectronics and polymer nanophotonics.

In spite of the remarkable progress attained in enhancing the electrical conductivity and achieving perfectly metallic behaviour in polymers, an apt understanding of the origin of metallic transport properties is still constrained by the disordered structure of conducting polymers [12]. Recent years have witnessed the development of advanced production and processing routes for the synthesis of more ordered and homogeneous classes of polymers, both in bulk and thin film forms.

Many research groups have developed new classes of conducting polymers and their derivatives for applications in various fields. These include organic polymers such as polypyrrole (PPy), polyaniline (PANI), polythiophene (PTh), polyfuran and so on.

The chemical structures of the most common conducting polymers are given in figure 1.1.

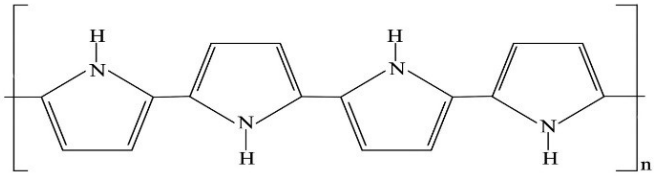

Polypyrrole

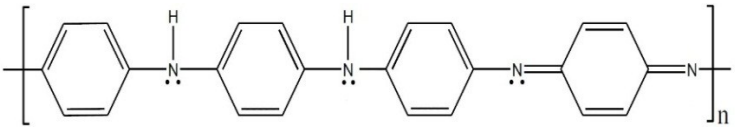

Polyaniline

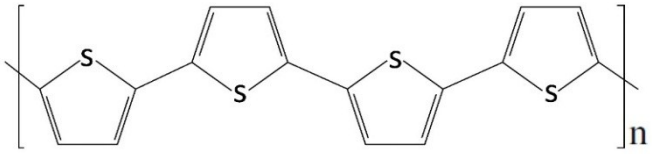

Polythiophene

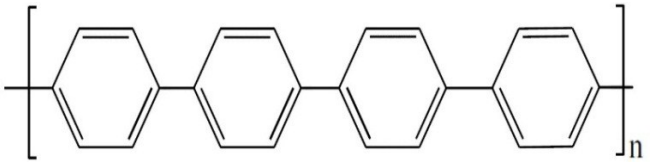

Poly (p-phenylene)

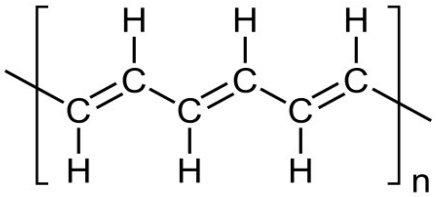

Polyacetylene

Figure 1.1 Chemical structures of conducting polymers

1.3 A brief introduction to polypyrrole

Among the ICPs, polypyrrole is one of the most important and widely investigated polymers. It has received a great deal of attention owing to its high electrical conductivity, promising electrochemical attributes, excellent environmental stability, non-toxic nature and biocompatibility. It finds numerous prospective applications in electronic and electro chromic devices, light-weight batteries, sensors, and optoelectronic and photonic devices [13] and in areas such as bio-imaging, drug delivery, microwave shielding and corrosion protection [14].

1.4 Conduction mechanism of polypyrrole

Investigations on the electrically conducting properties of polypyrrole by different research groups show that they depend upon the temperature during polymerization, the polymer thickness, the nature of the counter ions, the solvent, any substituted functional groups on the pyrrole monomer, the electrochemical polymerization conditions utilized [15] and the presence of structural defects in the polymer. On the other hand, the conduction mechanism and the molecular structure of polypyrrole, are not totally comprehended and there is inconsistency over a few actualities.

The polymer becomes conducting after doping with suitable dopants and counter ions are built up with the charged polymer backbone, conveying a net charge of zero. This technique incorporates dications or dianions (radical ions or bipolarons) which are the charge carriers into the polymer [16]. The electrical conductivity is increased in view of the well-ordered movement of these charge carriers.

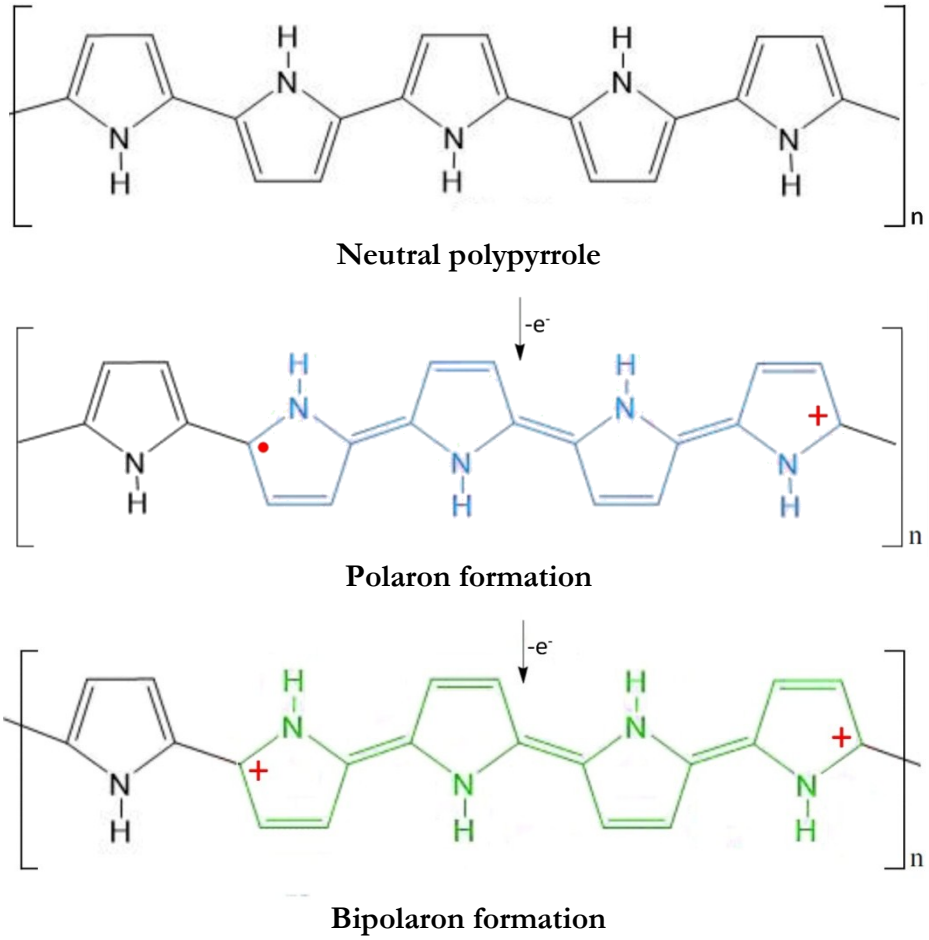

Figure 1.2 The chemical structures of neutral polypyrrole and the oxidative doping of polypyrrole

At the point when still higher doping levels are accomplished, the lattice distortions turn out to be significant to the point that the mid-gap bands of the bipolarons overlap with the valence and conduction bands. Good conductivity is retained, with the electrons as the charge carriers [17, 18]. Indeed, even at the 100% doping level, a band gap still stays in polypyrrole, so that it never achieves the band structure of a genuine

metal. However, the band gap turns out to be small to the point that electrons are promptly promoted at room temperature to produce the partially filled bands essential for electronic conductivity.

An inter- chain or intra - chain charge-hopping mechanism for the bipolarons is essential for polypyrrole to be a powerful conductor, as many basic deformities can emerge in the polymerization process [19]. These deformities disturb the short-range delocalization and overlap of the bipolaron states, which implies that polypyrrole does not behave totally as a one-dimensional conductor.

1.5 Synthesis of polypyrrole

Polypyrrole can be synthesized from the pyrrole monomer by using chemical oxidative polymerization, plasma polymerization and electrochemical polymerization. The synthesis of polypyrrole by oxidation of pyrrole goes back to 1888 and by electrochemical polymerization to 1957.

1.6 Chemical oxidative polymerization

Chemical oxidative polymerization [20] is a typical strategy utilized to synthesize conducting polymers in bulk form. Chemical polymerization is the procedure in which comparatively small molecules, called monomers, join chemically to produce a very large chainlike or network molecule. The monomer molecules may be all similar, or they may represent two, three, or more different compounds. Often, many thousands of monomer units are combined in a single molecule of a polymer.

In this technique, the monomer is dissolved in the dopant acid solution. Oxidants like ammonium peroxydisulfate ($(NH_4)S_2O_8$), hydrogen peroxide (H_2O_2) and salts containing transition metal ions are typically utilized [21]. The oxidant dissolved in the appropriate solvent is added dropwise to the mixture with continuous stirring for 4-24 hours. The precipitate obtained is filtered, washed and dried. This is one of the easiest methods adopted for synthesizing conducting polymers in bulk form.

1.7 Plasma polymerisation

Polymer thin films find a variety of applications in various types of electronic, optoelectronic, photonic and nanophotonic devices (22, 23.24). An overview of the literature reveals that polymers like polyaniline, polypyrrole and polythiophene grown in thin film forms have been investigated in depth with a view to study their structural, electrical and optical properties. Even though different techniques such as spin coating, solution casting and electro chemical deposition are available for the preparation of polymer thin films, plasma polymerization plays a significant role because of its cost viability and simplicity [25].

Plasma polymerization or glow discharge polymerization refers to the formation of polymeric materials under the influence of plasma. It is an excellent technique for the preparation of organic and inorganic thin films on various substrates from a starting monomer [25]. This method is utilized not exclusively to deposit thin films on appropriate substrates but to control the composition of the surface layer of a material for

appropriate applications too. The morphology and composition of plasma polymers are functions of the plasma parameters like power input, monomer flow rate, monomer vapor pressure, substrate temperature and the positioning of the substrates relative to the plasma zone. This method is normally used to produce pinhole free and flawless thin films of organic and inorganic materials on various substrates which include, glass and metal surfaces, quartz plates, fabrics, nanocomposites and nano fibers. [26].

In customary plasma polymerization set up, the monomer is fed into an evacuated chamber and an ac or rf discharge is created which helps the monomer species dissociate into reactant fragments in the form of electrons, ions and free radicals. The result of recombination of these fragments on a substrate is a highly branched and cross linked three dimensional network-a plasma polymer. By controlling the plasma current density, the extent of branching and cross linking can be decreased to some extent with the possibility that the subsequent plasma polymer will have a little extent of conjugation in the structure. The factors that can be promptly controlled during this ionization-deposition process are power density, precursor flow rate, the ratio of precursor vapour pressure to that of an inert carrier gas, reaction time, reactor geometry, plasma frequency and power and temperature of the reactor [27]. The ionized species formed acquire energies typically up to 2 eV, while electrons and metastable species, up to 20 eV. Normally plasma polymerisation reaction occurs at a pressure of around 10^{-2} torr. The gas phase reaction involving polymerisation process can be explained by a modified kinetic theory of gases. The process of plasma

polymerisation involves the fragmentation of the monomer into reactive species and recombination of the fragments on a substrate which is placed inside the plasma chamber [28]. The plasma polymerization method in general includes the use of dc, ac, rf, pulsed and magnetron assisted plasmas. The techniques are suitably adjusted according to the nature of the monomer, the carrier gas, input power, monomer flow rate and the other kinetic and mechanical aspects of plasma polymerization [29, 30, 31, 32, 33, 34]. Being a dry method, plasma polymerization is useful as a polymer thin film deposition technology in the microelectronics industry. Plasma polymerized films have a variety of applications as low dielectric constant intermetallic coatings [35, 36], coatings for surface modifications, barrier coatings and dielectric photo resistant and wave guiding films for microelectronics and photonics [37]. The potential fields of applications of plasma polymers, because of their intriguing photonic and electronic properties also include anti-reflection coatings, polymer LEDs, optical sensors and surface passivation coatings [38].

1.7.1 Urbach tail analysis and the calculation of defect levels of plasma polymerised thin films

In 1953, Urbach proposed an empirical equation for the optical absorption coefficient α, related to the electronic transitions from the valance to conduction band tail in disordered solids [39]. This rule states that $\alpha = \alpha_0 \exp(hv/Eu)$ where α_0 is a constant and Eu is the Urbach energy. Investigations establish that the Urbach absorption edge is practically a universal property of the disordered solids and that the underlying physics is both simple and general and can be connected to polymeric materials too. The presence of impurity levels or the dopants

contributes to the optical absorption in solids since they make charged imperfections and distortion levels [40,41]. The Urbach energy characterizes the slope of the exponential edge region and the inverse of the slope gives the width of the localized states in the band gap. The value of Eu that decides the steepness of the Urbach tail relies upon the structural disorder of the amorphous solid under study.

1.7.2 Space charge limited conduction (SCLC) in plasma polymerized thin Films

When an ohmic contact is made to a metal-polymer-metal (M-I-M) configuration, the carriers can be infused from the metal electrode into the conduction band of the polymer under an applied electric field. In the event that the measure of the infused carriers is beyond that can be transported across the film, a space charge will be built up at the metal polymer interface. Electrons moving through the system under an electric field will be hindered and controlled by the space charge gathered at the metal polymer interface and this gives rise to the phenomenon known as space charge limited conduction (SCLC) [42]. This type of conduction shows a linear region only at low bias voltages, where the equation of conductivity will follow the ohm's law [43]

$$J = \mu n_0 e \frac{V}{d} \qquad (1)$$

where e is the electronic charge, V the voltage applied, μ the carrier mobility, n_0 the equilibrium carrier concentration and d the inter electrode distance or the film thickness of the polymer.

At higher voltages SCLC current density is given by the Mott-Gurney relation

$$J = \frac{9}{8}\varepsilon_0 \varepsilon_r \mu_p \frac{V^2}{d^3} \tag{2}$$

where $\in_o \in_r$ is the permittivity of the polymer, μ_p the hole mobility and d the thickness of the film. From the slope of the *logJ-logV* plot one can observe that the current density J depends quadratically on the voltage V, which is characteristic of SCLC and after this region, the quadratic dependence of J on V changes to a trap filled limit (TFL) situation with slope greater than 2. The slope of the graph in the high voltage region is about 3. The thickness dependence of the space charge limited current follows the relation d^{-n} where n is a parameter, which depends on the trap distribution and is equal to or greater than three in the presence of traps.

The temperature dependence of current density follows the relation

$$J = e\mu N_v \left(\frac{V}{d}\right) \exp\left(-\frac{E_a}{kT}\right) \tag{3}$$

where N_v is the effective density of states in the valence band, k the Boltzmann constant and Ea the activation energy.

1.8 Spin coating

The method of spin coating is a basic procedure for growing thin uniform films on flat surfaces. It is used normally in polymer research, because of its convenience, in spite of the fact that it is not particularly

suited for large-scale film processing [44]. This technique can be applied to inorganic, organic and inorganic/organic solution mixtures. It is utilized for coating of photoresist on silicon wafers, for the coating of sensors, for protective coatings, paint coatings and optical coatings [45].

In spin-coating, the coating solution prepared by dissolving the coating material in an appropriate solvent is dispensed onto the substrate surface, which is then rotated at high speed in order to spread out the solution and, as the solvent evaporates away, a thin film of the coating material is left on the substrate surface.

1.9 Electro-spraying

Electro-spraying is a practical and adaptable strategy that uses electrically charged jet of the solution of the material under study for the collection of particles at micron, submicron and nano scales. It is a method of fluid atomization by electrical forces. It is a one-step method which can possibly produce restricted size distributions of submicrometric particles, with constrained agglomeration of particles and exceptionally high yields [46]. The principle of electro-spraying depends on the capability of an electric field to distort the interface of a liquid drop. The machine was initially built up by Lord Rayleigh in 1882 and was further established by Zeleny in 1917 and Sir Taylor in 1964 [47].

The procedure of electro-spraying is straightforward. The solution of the polymer under study is stacked into a syringe and utilizing a syringe pump, passed through a tiny, however, exceedingly charged narrow capillary gauge needle. The voltage used is commonly up to + or

−30 kV and the collector may be set at 7 to 30 cm away from the capillary. Once the droplets get detached from the Taylor cone, the solvent evaporates, producing dense and solid particles, impelled towards the collector [48].

1.10 Techniques employed for the synthesis of soluble polypyrrole

For practical applications of conducting polymers good solution processability and chemical stability of the polymers are often required. But many reports indicate that, as with most of the conducting polymers, polypyrrole, polymerized either electrochemically or chemically are insoluble in most of the solvents. The presence of long chain conjugated structure and the strong intermolecular and intramolecular interactions and cross-linkings in polypyrrole chains make it insoluble in aqueous/non-aqueous solvents which restrict their processability, characterization and applications [49].

A major development has begun with the alteration of the chemical structure of PPy by adding solubilizing substituents onto the pyrrole monomer unit. The derivatives of PPy comprising alkyl or alkoxy substituents have been observed to be soluble in chloroform, tetrahydrofuran and o-dichlorobenzene [50, 51]. The solubility of polypyrrole can be enhanced by the addition of counter ions to the polymer backbone. The strong intermolecular interactions between conducting polymer chains will diminish because of the introduction of these substituted monomers by doping. The planarity of the polymer is affected by the introduction of long chain substituents to the monomer ring due to steric interference. Doping the polymer with organic sulfonic acids like dodecylbenzenesulfonic acid

(DBSA) and camphorsulfonic acid (CSA) can strongly influence the conductivity, morphology and thermal stability of the bulk polymer [52].

Polypyrrole synthesized by chemical method using DBSA as dopant and APS as oxidant is found to be highly soluble in m-cresol and conditionally soluble in chloroform or dichloroethane. The solubility of the polymer can be attributed to the presence of the huge dopant DBSA, which reduces the inter and intra molecular interactions by placing itself between the polymer molecules. Likewise, the moderate polymerization at 0 ^{o}C reduces the crosslinking reactions, in electrochemical polymerization [53]. The high conductivity of doped polypyrrole is due to the presence of delocalized electrons and higher concentration of bipolarons which can be affirmed by UV/VIS/NIR spectroscopic studies. Numerous reports available on the techniques adopted to enhance the solubility and processability of polypyrrole using different dopants and the effect of doping on the structural, morphological, electrical and optical characteristics of the polymer [54, 55, 56, 57].

1.11 Rechargeable Li-ion cells: An overview

Energy storage is indispensable for the operative improvement of a power-driven economy and execution of renewable energy programmes as well as electricity generation from sun, wind and waves. This requires high performance energy storage innovations, since the energy produced is often irregular and must meet the necessities for large scale applications, including high energy density with environmental friendliness and low cost. Making energy storage systems that ensure uninterrupted power supply with consumer demand is one of the prime

objectives to be accomplished. Among the accessible energy storage systems and technologies, lithium ion cells are established as the most attractive ones due to the high gravimetric and volumetric energy densities they offer and the minimum capacity loss when compared to other rechargeable battery systems [58].

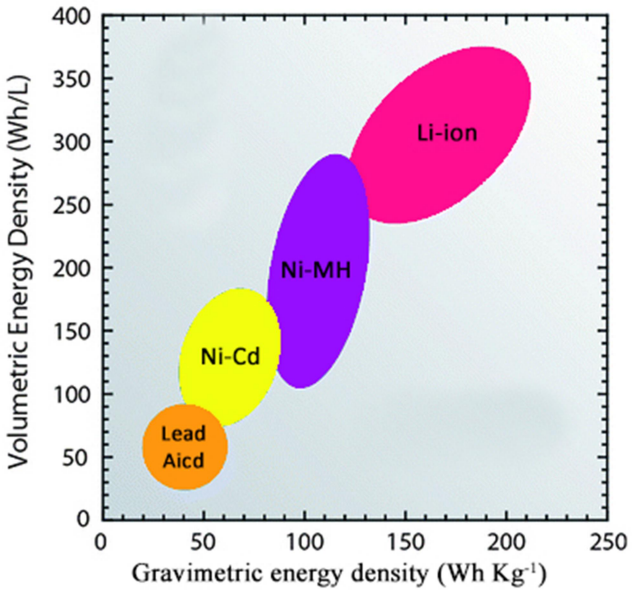

Figure 1.3 Comparison of lithium ion batteries with other rechargeable batteries in terms of volumetric and gravimetric energy densities

The inspiration for the development of Li ion battery technology is the fact that lithium is the lightest and most electropositive metal and along these lines, helps to achieve exceptionally high energy density [59]. The rechargeable lithium ion batteries (LIB), offer much better performance compared to other rechargeable systems and were marketed by Sony in the early 1990s [60] and are generally utilized to power

portable electronic devices, laptop computers, medical implants and hybrid electric vehicles.

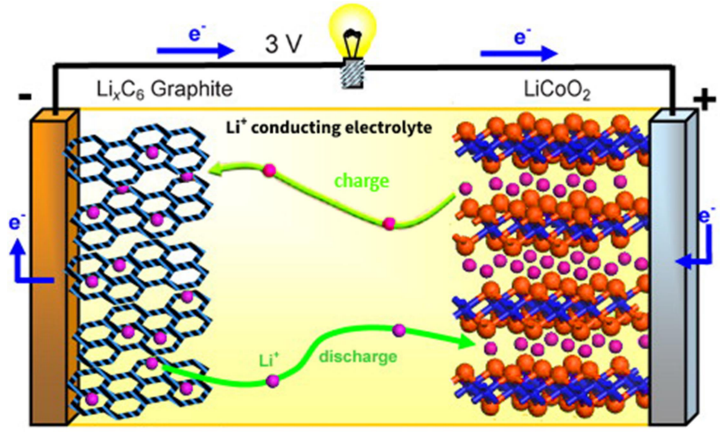

Figure 1.4 Schematic representation of Li-ion cell

A Li-ion cell usually consists of cathode, anode, the electrolyte and the separator which eludes the shorting of the electrodes. The active material for the cathode is lithium metal oxide and for the anode, it is graphite. Because of the electrode potential of the Li^+ions, they are transported between the electrodes through the electrolyte which is normally soaked up in the permeable separator, which acts as a physical barrier avoiding the contact between the electrodes.

The process of lithium moving into the anode or cathode is referred to as intercalation and the reverse process in which lithium moves out of the anode or cathode is referred to as de-intercalation. During the charge process of the graphite/lithium cobalt oxide cell, the graphite (anode) accepts the lithium ions which are de-intercalated into the electrolyte from the cathode. During the discharge of the cell, the reverse process occurs in which positively charged lithium ions are

discharged from the anode into the electrolyte and the ions move towards the cathode and get intercalated into the cathode. Consequently the Li ion cell exploits the electrochemistry of the system by separating the reduction and oxidation processes, storing electrical energy on charging, and releasing electrical energy on discharging of the cell.

The amount of charge that can be stored in $LiCoO_2$ cathode and graphite anode is constrained on account of the intercalation mechanism involved. This intercalation is conceivable in view of the layered structure of the electrode materials. The low theoretical capacities of $LiCoO_2$ and graphite electrode materials make the ordinary Li-ion cells deficient for some applications with high energy needs such as electric vehicles and grid energy storage. Additionally these LIBs are susceptible to short-circuiting and overcharging which impose some safety concerns in their utilization as batteries in vehicles. These restrictions related to the Li-ion batteries such as cost, safety and the limited energy density are constrains to meet the requirements of extended ranges of electric batteries for vehicles [61] which compel the researchers to concentrate on the development of improved battery systems having high energy density, toughness, flexibility, safety and low cost.

1.12 Lithium-sulfur cells

Lithium sulfur (Li-S) cells are promising devices with high theoretical gravimetric energy density of 2500 Wh/kg and high theoretical capacity of 1675 $mAhg^{-1}$ for the next generation energy storage applications [62]. However there are many challenges to be addressed, related to the working of Li-S cells. Both S and Li_2S are

electrically insulating in nature, resulting in poor electrochemical availability, low utilization of the material and low specific capacities. The polysulfide anions formed during cycling can dissolve into the electrolyte which results in ceaseless loss of active material, rapid capacity decay, high self-discharge and reduced safety. These long – chain lithium polysulfides can, likewise, diffuse to Li anode and become reduced chemically, rather than electrochemically, to form short-chain polysulfides (Li_2S_2 and Li_2S) on the Li surface. These unwanted side reactions result in the shuttle effect leading to low coulombic efficiency and poor cycling stability. Similarly sulfur undergoes an extensive volumetric expansion of about 80% upon full lithiation to Li_2S, which causes crushing and structural changes at the electrodes [63, 64].

Significant research effort has been focussed on developing strategies to improve the electrochemical performance of the sulfur cathode in lithium- sulfur cells by introducing conducting agents into the sulphur cathode and also by making composites of sulphur with conducting polymers and carbon nanostructures [65].

1.13 Role of polypyrrole for modifying sulphur cathode

In the present work, sulphur cathode of the Li-S cell is modified by making composites of S with polypyrrole (PPy) and graphene (G). The composite electrodes, polypyrrole/sulphur, sulphur/graphene and polypyrrole/graphene/sulphur, titled respectively as PPyS, SG and PPyGS are used as the cathode active materials to assemble Li-S cells.

1.14 Objectives of the present work

Polypyrrole can be synthesized using plasma, chemical and electrochemical techniques and in various forms and morphologies. It is one of the most popular and extensively studied conducting polymers because of its astounding tunable characteristics. The impacts of dopants and oxidants on the structural and charge transport properties of polypyrrole have been focussed by various research groups. Despite the fact that a great deal of research work has been conducted on polypyrrole, there are certain areas where the unique features of this polymer have not been completely utilized or studied widely. Polymers like polypyrrole (PPy), polythiophene (PTh) and polyanniline (PANI) are being widely inspected as active electrode materials for lithium cells, because they can be easily switched between the oxidized and the reduced states. The present work is devoted to synthesize highly stable, doped polypyrrole and its composites both in bulk and thin film forms for various types of device applications, with special emphasis on energy storage devices.

The objectives of the present work can be summarized as follows.

1) To synthesize polypyrrole (PPy) using different methods and various dopants to suit explicit applications.
2) To investigate the structural, optical and electrical properties of pristine and iodine doped, plasma polymerized pyrrole thin films.

3) Elucidation of the mechanism of conduction and the estimation of the defect levels of pristine and doped, plasma polymerized pyrrole thin films.

4) To synthesize polypyrrole with appreciable solubility and processability using different oxidants and dopants for various device applications.

5) To develop polypyrrole composite films with much enhanced solubility and electrical conductivity by spin coating and electro-spraying methods

6) Synthesis of lithium substituted polypyrrole using different oxidants and cost effective dopants for applications as the cathode active material in rechargeable Li ion cells

7) To investigate the application prospects of polypyrrole and its nanocomposites in the effective modification of the sulphur cathode for developing the next generation Li-S cells with high energy density and excellent cycling stability.

References

[1] J.M.G. Cowie, Polymers: Chemistry and Physics of Modern Materials, Intertext Books, Great Britain (1989)

[2] V.R. Gowariker, N.V. Viswanathan, Jayadev Sreedhar, Polymer Science, Wiley Eastern Limited, (1986)

[3] Fred W. Billmeyer, Jr., Text Book of Polymer Science, John Wiley and Sons, (1984)

[4] Ye.P. Mamunya, V.V. Davydenko, P. Pissis , E.V. Lebedev ., Electrical and thermal conductivity of polymers filled with metal powders, Eur. Polym. J., 38 (2002) 1887-1897

[5] Suresh G Advani, Processing and Properties of Nanocomposites, World Scientific, (2007) 1

[6] Michael S. Freund, Dr. Bhavana A. Deore, Self-Doped Conducting Polymers, Wiley, (2006) 10-12

[7] Inzelt, György., Conducting Polymers A New Era in Electrochemistry, Springer, (2008) 1

[8] G. Çakmak, Z. Küçükyavuz, S. Küçükyavuz and H. Çakmak, Mechanical, electrical and thermal properties of carbon fiber reinforced poly (dimethylsiloxane)/polypyrrole composites, Composites Part A: Applied Science and Manufacturing, 35 (4) (2004) 417-421

[9] R. McNeill, R. Siudak, J. H. Wardlaw and D. E. Weiss, Electronic Conduction in Polymers. I. The Chemical Structure of Polypyrrole, Australian Journal of Chemistry, 16 (6) (1963) 1056-1075

[10] B. A. Bolto, R. McNeill and D. A. Weiss, Electronic Conduction in Polymers. III. Electronic Properties of Polypyrrole, Austrailian Journal of Chemistry, 16 (6) (1963) 1090-1103

[11] I.-Y. Kim, S.-J. Seo, H.-S. Moon, M.-K. Yoo, I.-Y. Park, B.-C. Kim and C.-S. Cho, Chitosan and its derivatives for tissue engineering applications, Biotechnology Advances, 26 (1) (2008) 1-21

[12] Terje A Skotheim, L Ronald, Elsenbaumer, John R Reynolds, Handbook of Conducting Polymers, Marcel Dekker, INC, New York, (1998)

[13] Ansari, R., Polypyrrole conducting electroactive polymers: Synthesis and stability studies, E-Journal of Chemistry, 3 (4) (2006) 186-201

[14] Yang Liu, Ying Chu, Likun Yang, Adjusting the inner-structure of polypyrrole (2006) nanoparticles through microemulsion polymerization, Materials Chemistry and Physics, 98 304-308

[15] F. P. Bradner and J. S. Shapiro, Improvement in the quality of polypyrrole films prepared electrochemically on a mercury anode, Synthetic metals, 26 (1) (1988) 69-77

[16] N. K. Guimard, N. Gomez and C. E. Schmidt, Conducting polymers in biomedical Engineering, Progress in Polymer Science, 32 (2007) 876-921

[17] J. L. Bredas, Handbook of conducting polymers, T.A skotheim (Ed.), Marcel Dekker, New York, 2 (1986) 859

[18] R.R. Chance, D. S. Boudreaux, J. L. Bredas and R. Silby , Handbook of conducting polymers, T.A skotheim (Ed.), Marcel Dekker, New York, 2 (1986), 825

[19] R. Roy, S.K Sen, M. Digar and S.K. Bhattacharyya, Conductivity and thermoelectric power in conducting polypyrrole films, J. Phys., condens. matter, 3(40) (1991) 7849

[20] M Amrithesh, S Aravind, S Jayalekshmi, R S Jayasree, Polyaniline doped with orthophosphoric acid—A material with prospects for optoelectronic applications, J.Alloys Compd,458 (1-2) (2008) 532-535

[21] L.-X. Wang, X.-G. Li and Y.-L. Yang, Preparation, properties and applications of polypyrroles. Reactive and Functional Polymers, 47 (2001) 125-139

[22] Donald L.Wise, Gary E. Wnek, Derbra J.Trantolo, Thomas M.Cooper, Joseph D. Gresser, Photonic Polymer Systems: Fundamentals, Methods and Applications, Marcel Dekker, New York (1998)

[23] Terje A. Skotheim,(Ed), Hand Book of Conducting Polymers, Marcel Dekker, New York, (1986).

[24] Maria Losurdo, Giovanni Bruno and Eugine A.Irene, Anisotropy of optical properties of conjugated polymer thin films by spectroscopic ellipsometry, J.Appl.Phys. 94 (2003) 4923

[25] H.Yasuda, Plasma Polymerization, Academic Press, New York, (1985)

[26] L.S. Hung, L.R.Zheng, and M.G. Mason, Anode modification in organic light- emitting diodes by low-frequency plasma polymerization of CHF3, Appl.Phys.Lett, 78(5) (2001) 673-675

[27] R. Claude and M. Moisan, M.R. Wertheimer, Z. Zakrzewski, Comparison of microwave and lower frequency discharges for plasma polymerization, Appl. Phys. Lett, 50 (1987) 1797

[28] Erika E. Johnston, Buddy D. Ratner, Surface characterization of plasma deposited organic thin films, Journal of Electron Spectroscopy and Related Phenomena, 81 (3) (1996) 303-317

[29] Donglu Shi, S.X. Wang, Wim J, Van Ooji, L.M. Wang, Jiangang Zhao and Zhou Yu, Uniform deposition of ultrathin polymer films on the surfaces of Al2O3 nanoparticles by a plasma treatment, Appl. Phys. Lett, 78 (2001) 1243

[30] Runguang Sun, Junbio Peng, Takayashi Kobayashi, Yuguang Ma, Haifeng Zhang, Shiong Liu, Plasma Polymerization for the Deposition of an Electroluminescent Polymer Layer, Jpn.J.Appl.Phys, 35 (1996) 1506

[31] Donglu Shi, Peng He, Surface modifications of nanoparticles and nanotubes by plasma polymerization, Rev.Adv. Mater. Sci., 7 (2004) 97-107

[32] L.G. Paterno, S Manolache. and F. Denes., Synthesis of polyanniline-type thin layer structures under low-pressure RF-plasma conditions, Synthetic Metals, 130(1) (2002) 85- 97

[33] M. C Kim, S. H Cho, S. B. Lee, Y.Kim, J. H. Boo, Characterization of polymer-like thin films deposited on silicon and glass substrates using PECVD method, Thin Solid Films, 447-448 (2004) 592-598

[34] Ivan D Avramov, Shigeru Kurosowa, Michal Rapp, Piotr Krawczak, Ekaterina I Radeva, Investigations on plasma-polymer-coated SAW and STW resonators for chemical gas-sensing applications, IEEE Transations in Microwave Theory and Techniques, 49 (4) (2001) 827-837

[35] S Saravanan, C Joseph Mathai, M R Anantharaman, S Venkatachalam, Low k thin films based on rf plasma-polymerized aniline, New Journal of Physics 6 (2004) 64

[36] C Joseph Mathai, S Saravanan., M.R Anantharaman, .S Venkitachalam, S Jayalekshmi, Characterization of low dielectric constant polyaniline thin film synthesized by ac plasma polymerization technique, J Phys. D: Appl Phys, 35 (2002) 240-245

[37] H Akther and A. H. Bhuiyan, Electrical and optical properties of plasma-polymerized N,N,3,5-tetramethylaniline thin films, New J. Phys. 7 (2005) 173

[38] D Sakthi Kumar, Kenji Nakamura, Satoko Nishiyama, Shigeru Ishil, Hiromichi Noguchi, Kunihiro Kashiwagi, and Yasuhiko Yoshida , Optical and electrical characterization of plasma polymerized pyrrole films, J.Appl. Phys. 93 (2003), 2705-2711

[39] I. K. Saito and A.J Ikushima, Absorption edge in silica glass, Phys. Rev. B, 62 (2000) 8584-8587

[40] G.D.Cody, T. Tiedje, B. Abeles, B. Brooks, and Y. Golstein, Disorder and the Optical- Absorption Edge of Hydrogenated Amorphous Silicon, Phys,Rev.Lett, 47 (1981) 1480

[41] D.S. Galvao, D.A. dos Santos, B. Laks, C.P.de Melo, M.J. Caldas, Role of disorder in the conduction mechanism in polyanilines, Phys. Rev. Let, 63 (1989) 786

[42] R.H. Fowler, L. Nordheim, Proc. Roy. Soc. London, Electron Emission in Intense Electric Fields A,119 (781) (1928) 173-181

[43] P W M Blom, de Jong and J. J M Vleggaar, Electron and hole transport in poly (p-phenylene vinylene) devices, Appl. Phys. Lett, 68 (1996) 3308

[44] Roar R. Søndergaard,Markus Hösel, Frederik C. Krebs, Roll-to-Roll fabrication of large area functional organic materials, Journal of Polymer Science, Part B:Polymer Physics 51 (1) (2013) 16–34

[45] K. Norrman,, A. Ghanbari-Siahkali, and N. B. Larsen, Studies of spin-coated polymer films. Annu. Rep. Prog. Chem., Sect. C, Phys. Chem., 101 (2005) 174-201

[46] Chul Ho Park, Jonghwi Lee, Electrosprayed polymer particles: Effect of the solvent properties, J. Appl. Polym. Sci. 114 (1) (2009) 430-437

[47] N. Bock, M. A. Woodruff, D. W. Hutmacher, T. R. Dargaville, Electrospraying, a Reproducible Method for Production of Polymeric Microspheres for Biomedical Applications, 3 (1) (2011) 131–149

[48] Raghavan, P., Lim, D. H., Ahn, J. H., Nah, C., Sherrington, D. C., Ryu, H. S., Electrospun polymer nanofibers: the booming cutting edge technology. Reactive and Functional Polymers, 72 (2012) 915-930

[49] H. K. Lim, S. O. Lee, K. J. Song, S. G. Kim, and K. H. Kim, Synthesis and properties of soluble polypyrrole doped with dodecylbenzenesulfonate and combined with polymeric additive poly(ethylene glycol), J. Appl. Polym. Sci., 97 (3) (2005) 1170–1175

[50] K.K. Kanazawa, A.F. Diaz, M.T. Krounbi, G.B. Street, Electrical properties of pyrrole and its Copolymers, Synth Met., 4 (2) (1981) 1l9-130

[51] J.Rühe, T.A.Ezquerra , G.Wegner, New conducting polymers from 3-alkylpyrroles, Synth Met., 28 (1-2) (1989) 177-181

[52] P. Jayamurgan, V. Ponnuswamy, S. Ashokan, and T. Mahalingam, The effect of dopant on structural , thermal and morphological properties of DBSA-doped polypyrrole, Iranian Polymer Journal, 22 (3) (2013) 219–225

[53] J. Y. Lee, D. Y. Kim, and C. Y. Kim, Synthesis of soluble polypyrrole of the doped state in organic solvents, Synth. Met., 74 (2) (1995) 103–106

[54] H.-W. R. Jang, Kwan SikMin-Kyu Songa, Young-Taek Kima, Bum-Seok Kimb, Jinhwan Kimc, Kookheon Chard, A, H. Lee, and B. Moon, Synthesis and characterization of soluble polypyrrole doped with alkylbenzenesulfonic acids, Synth. Met., 141(3) (2004) 315–319

[55] E. J. Oh, K. S. Jang, J. S. Suh, and C. H. Yo, Synthesis and Characteristics of Soluble Polypyrroles with Mixed Dopants, Molecular Crystals and Liquid Crystals 337 (1) (1999) 101–104

[56] Y. Shen and M. Wan, Soluble Conductive Polypyrrole Synthesized By In Situ Doping with β-Naphthalene Sulphonic Acid, Polymer Chemistry, 35(17) (1997) 3689–3695

[57] K.S. Jang, S.S.Han, J.S. Suh, Eun-Jee Oh, Synthesis and characterization of alcohol solule polypyrrole, 119 (1) (2001) 107–108

[58] Preetesh U. Munsh, Jesse Pichel and Elaine S. Kwei, Energy storage: game-changing component of the future grid, February (2009) 41-43

[59] J.M. Tarascon, M. Armand, Issues and challenges facing rechargeable lithium batteries, Nature, 414 (2001) 359–367

[60] X. Yuan, H. Liu, and J. Zhang, Lithium-Ion Batteries: Advanced Materials and Technologies (Green Chemistry and Chemical Engineering), CRC Press (2011)

[61] W. Feng, J. Chen, Improvement of Rate and Cycle Performance by Rapid Polyaniline Coating of a MWCNT/Sulfur Cathode, J. Phys. Chem. C 115 (49) (2011) 24411–24417

[62] Arumugam Manthiram, Yongzhu Fu, Yu-Sheng Su, Challenges and Prospects of Lithium- Sulfur Batteries, Acc. Chem.Res. 46(5) (2012) 1125-1134

[63] Hofmann A.F, Fronczek D.N, Bessler W.G, Mechanistic modeling of polysulfide shuttle and capacity loss in lithium e sulfur batteries, J. Power Sources, 259 (2014) 300-310

[64] Sylwia Walus, Lithium/Sulfur batteries: Development and understanding of the working mechanisms (2015) (Phd Thesis)

[65] Pierre-Etienne Cabelguen, Advanced research on Lithium-Sulfur batteries: Studies of lithium polysulfides (2013) (Phd Thesis).

Chapter 2

MECHANISM OF CARRIER TRANSPORT AND THE ESTIMATION OF DEFECT STATES IN PLASMA POLYMERIZED PYRROLE THIN FILMS

Plasma polymerization is found to be an excellent technique for the synthesis of good quality, pinhole-free, polymer thin films from different monomer precursors. The present chapter deals with the synthesis of polypyrrole (PPy) thin films by ac plasma polymerization technique in their pristine and in situ iodine doped forms and their detailed characterization to understand the effect of iodine doping on their structural, electrical and optical properties.

2.1 Introduction

Polypyrrole, a highly sought after conjugated polymer has been subjected to detailed investigations in its bulk and thin film forms and possess many meritorious characteristics which include, high electrical conductivity, environmental stability, easy availability of the monomer and biocompatibility [1]. In monomer form, pyrrole is a simple heterocyclic organic compound. Polypyrrole (PPy) was first recognized as an electrical conductor by Kanazawa and co-workers and the synthesis route adopted was the electrochemical oxidation of pyrrole [2]. Even though the polymerized form of this material is widely studied, the electrical transport properties of this material are not pursued in depth.

Most of the published work on PPy is based on its electrochemically synthesized form. There are some reports on the ionic conductivity and the charge transfer mechanism in PPy [3]. The dc electrical conductivity of PPy is found to be in the range of 200-500 S/cm in its PF_6 doped form and is a function of the preparation conditions, nature of dopants and temperature. The disorder induced charge localization and the metal insulator transition are also reported in PPy [2, 4].

Plasma polymerization or glow discharge polymerization includes alternating current (ac), radio frequency (rf) and direct current (dc) techniques. It is an excellent technique for the preparation of organic and inorganic polymer thin films on various substrates from a starting monomer. It is an easy and inexpensive technique for growing of PPy thin films on various types of substrates. The optical and electrical properties of PPy films prepared by radio frequency (rf) plasma polymerization technique have been thoroughly studied by Kumar and co-workers [5]. Plasma polymerization, in general is a technique for producing polymer-like-organic materials in the form of thin films with the aid of a plasma discharge. The plasma discharge energizes and dissociates the monomer molecules into neutral particles and reactant fragments in the form of electrons, ions and free radicals. The product of recombination of these fragments on a substrate is a highly branched and cross linked three dimensional network - the plasma polymer. However, by optimizing the plasma parameters or the Yasuda parameters [6], the extent of branching and cross linking in the plasma polymer can be controlled. In the present work, plasma polymerization at 50 Hz

(alternating current a.c) has been chosen as a complementary technique for the preparation of PPy thin films.

The potential fields of applications of plasma polymers, due to their interesting photonic and electronic properties, include anti-reflection coatings, polymer LEDs, optical sensors, surface passivation coatings and low dielectric inter-metallics. Being a dry method, plasma polymerization is suitable as a polymer thin film deposition technology in the microelectronics industry. Plasma polymerized films have variety of applications as low dielectric constant (low-k) intermetallic coatings [7,8], as coatings for surface modifications, barrier coatings, dielectric photo resists and wave guiding films for microelectronics and photonics [9].

The nature of charge carrier transport mechanism in plasma polymer films is highly significant as far as their applications as both, passive and active components in microelectronics and optoelectronics are concerned. The present chapter deals with the investigations carried out to analyse in detail the d.c conduction mechanism in pure and iodine doped PPy films prepared by ac plasma polymerization. Even though reports are available on plasma polymerized pyrrole thin films in pristine and doped forms, a systematic study on the stability and structure of the in situ iodine doped, plasma polymerized pyrrrole thin films, and the effect of doping on the optical and structural properties due to the charged defects created during polymerization process has not been pursued in depth. Urbach tail analysis is a tool, useful for the estimation of defect states in amorphous thin films. But it has not been widely

employed in plasma polymerized thin films. Hence, this chapter is also devoted to explain the modification of the optical and structural properties of the doped polypyrrole films and to have the comparison of defect states in the pristine and iodine doped forms using Urbach tail analysis of the absorption spectrum.

The structural disorders incorporated in amorphous solids are responsible for many of their unique properties. The electric transport properties and the optical behaviour of amorphous materials show dramatic changes depending upon the type and quantity of disorders frozen in these materials. Studying the shape and position of the optical absorption edge as a function of the synthesis conditions is useful for estimating the amount of disorder [10]. Effects of the structural disorders on the electronic properties of amorphous solids can be clearly observed at the band edges**.** The signature of a disordered system is the narrowing of band gap and the formation of localized states within the band tails. The reflections of these effects on the electronic structure of the material can be represented by two separate regions called as the Tauc and the Urbach regions. In doped polymers, the electron accepting or withdrawing groups incorporated during the doping process form defect levels due to the presence of charged species, which will reduce or enhance the binding energy of the charge carriers. As a result, the optical, electrical and the structural properties of the solids are modified [11]. The optical absorption spectrum shows a tail below the absorption edge at a finite temperature. The tail part near the absorption edge in various non- metallic amorphous materials can be expressed empirically as [12]

$$\alpha(E,T) = \alpha_0 \exp\left[-\frac{\sigma(T)(E_0 - E)}{k_B T}\right] \quad (1)$$

where the absorption coefficient α is a function of the photon energy E and the temperature T, E_0 *is* the photon energy, α_0 is the absorption coefficient at $E=E_0$, and $\sigma(T)$ is the steepness coefficient which depends on the temperature and is a measure of the defect states frozen in the amorphous solids. From the analysis of the optical absorption spectrum, the defect levels of doped and pristine thin films can be compared.

2.2 Experimental

2.2.1 Growth of polypyrrole thin films

Polypyrrole thin films were grown on glass substrates by ac plasma polymerization technique and the details of this technique are already reported [8]. The experimental set up consists of two stainless steel electrodes, each of diameter 0.23 m and placed 0.05 m apart. Ultrasonically cleaned glass substrates were placed on the lower electrode for polymer thin film deposition. The schematic diagram of the chamber is shown in figure 2.1. The glow discharge chamber was evacuated using a rotary pump at a pressure of 0.2 Torr. Plasma discharge was obtained in the chamber by applying an ac voltage of 1000 V of frequency 50 Hz between the electrodes and the current was kept at 50 mA and 70 mA. Monomer was injected into the glass chamber at the region between the electrodes by means of a glass sprayer at a monomer vapour pressure of 0.266 mB. The flow rate was

carefully controlled using a needle valve. Polymer films in the thickness range of 100-750 nm could be grown in 30 to 60 minutes on cleaned glass substrates kept in the chamber.

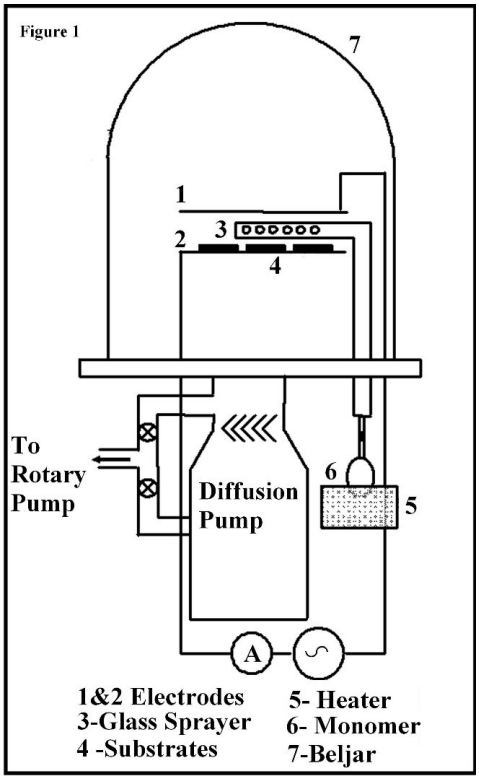

Figure 2.1 Experimental set up for ac plasma polymerization

2.2.2 In situ doping of iodine

Iodine doping was carried out by introducing iodine vapour into the plasma polymerization chamber along with the monomer vapour by means of a separate glass feed through. The introduction of iodine vapour into the chamber was carried out in such a way that the

introduction of the dopant gas did not affect the maintained low pressure inside the vacuum chamber. The thin films prepared in the iodine atmosphere were heated at 340 K for about an hour in a vacuum of 10^{-5} Torr for expelling the part of iodine that was not incorporated inside the polymer matrix.

2.2.3 Preparation of metal-polymer-metal structures and J-V studies

To study the current density-voltage (J-V) characteristics metal-polymer-metal (m-p-m) sandwich structures were prepared. This m-p-m configuration was of the form aluminium-PPy-aluminium with an effective area of 2.5 x 10^{-5} m^2. The Al electrodes of average thickness 100 nm were deposited using the conventional vacuum thermal evaporation unit at a pressure of 10^{-5} Torr [7].

For the electrical conductivity studies, m-p-m structures, shown in figure 2.3 were placed in a home built conductivity cell, shown in figure 2.2. A bias voltage in the range of 1 to 60 V (step 1 V) was applied and the current flowing through the PPy film was measured using an automated Keithley 236 SMU (Source Measurement Unit). All the measurements were taken under dynamic vacuum conditions, with the cell pressure around 10^{-2} Torr.

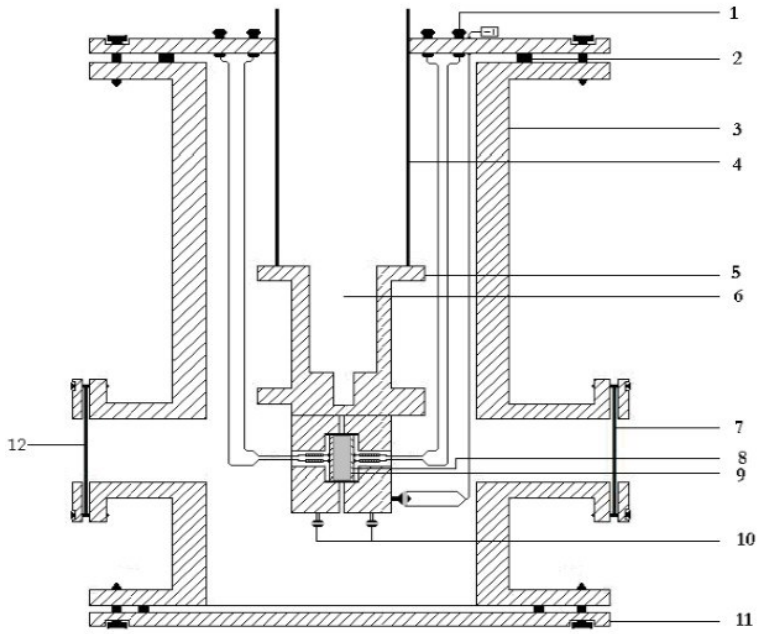

Figure 2.2 Conductivity measurement cell for electrical characterization

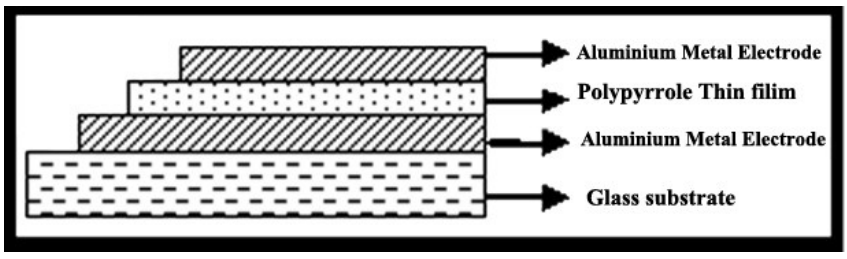

Figure 2.3 Metal-polymer-metal sandwich structure

2.2.4 Film thickness measurement, FTIR spectroscopy and UV-Vis absorption studies

Thickness of the PPy films was measured by a Dektach 6 M thickness profiler. The FTIR spectra of pristine and iodine doped polypyrrole thin films were recorded using Nicolet Avatar 360 FTIR Spectrophotometer in the wavelength range of 400 cm^{-1} - 4000 cm^{-1} under identical conditions. Optical absorption spectra of pure and iodine doped PPy films were recorded using JASCO-V-570 UV-Vis-NIR spectrophotometer. The absorption coefficient α values were calculated from the spectrum by dividing the αd values by the film thickness d and were plotted against the photon energy for pure and iodine doped PPy thin films. The bandgap, E_g of the films was obtained from the Mott plot by plotting the $(\alpha h\nu)^{1/2}$ versus $h\nu$ and then extrapolating the linear portion of the plot to $(\alpha h\nu)^{1/2} = 0$. The dielectric constant of the pure and iodine doped PPy films was measured using the HP 4192A LCR Meter under the dynamic vacuum condition of 10^{-2} Torr pressure, by suitably placing the m-pm structures inside the home built conductivity cell.

2.3 Results and discussions

2.3.1 FTIR spectroscopic studies

The FTIR spectra of monomer pyrrole and plasma polymerized pristine and iodine doped pyrrole films grown under plasma powers of 50 W and 70 W are depicted in figure 2.4. The peaks in the plasma polymerized pyrrole are not sharp when compared with those in monomer pyrrole and most of the IR absorption features of the monomer

pyrrole are noticeable in the spectrum of polypyrrole with small shift in peak positions. The frequencies assigned for different peaks in the FTIR spectra of the monomer and the pristine and iodine doped polypyrrole are shown in Table 2.1.

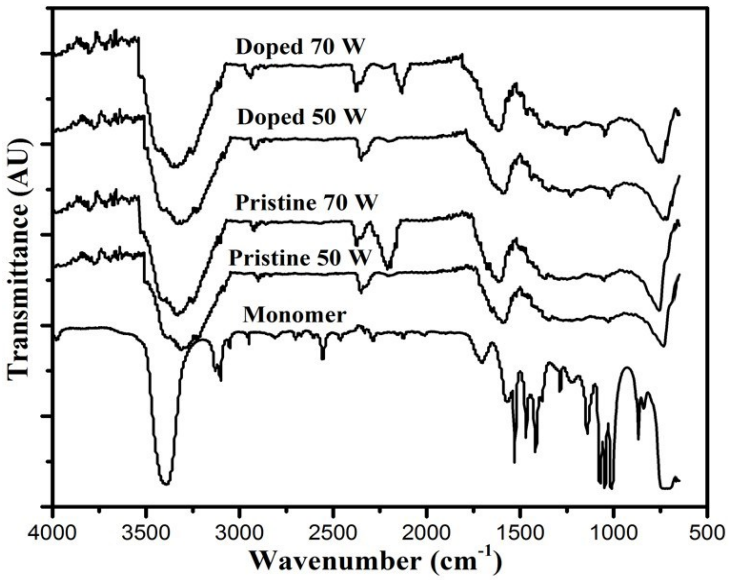

Figure 2.4 FTIR spectra of monomer pyrrole and plasma polymerized pristine and iodine doped pyrrole films grown at plasma powers of 50 W and 70 W

The strong peak due to the NH stretch mode is present at 3400 cm^{-1} in the monomer, at 3332 cm^{-1} in the pristine form and at 3318 cm^{-1} in the iodine doped form. The strong bands at 3119 cm^{-1} representing CH stretch mode and at 1095 cm^{-1} representing CH bend mode in the monomer are relatively weak in the polymer. The reduction in intensity of these bands seems to indicate a corresponding reduction in the number of CH oscillators in the polymer [13]. The peak observed at 1037 cm^{-1} in the

polymer due to the C-N stretching vibration supports the existence of pyrrole rings in the plasma polymer. The peak present at 1705 cm^{-1} in the polymer is due to the C = C stretch mode vibration of the pyrrole ring. The strong peak detected at 740 cm^{-1} in the monomer and polymer indicates the presence of NH out-of-plane bending mode in the monomer and the polymer in its pristine and doped forms. The existence of ring vibrations is seen within the broad band region 1400-1595 $cm^{-1.}$ The slight variations in the exact positions of these peaks may be due to the change of state of the monomer from the liquid state to the polymer in the solid state. These studies show that a good extent of polymerization has taken place through hydrogen abstraction from the CH and NH bonds of the monomer pyrrole ring, which is the most common phenomenon during plasma polymerization [5].

Table 2.1. Peak assignments of the FTIR absorption bands of monomer pyrrole and the undoped and iodine doped polypyrrole

Pyrrole monomer (cm^{-1})	**Polypyrrole (cm^{-1})**	**Iodine doped polypyrrole (cm^{-1})**	**Assignments**
740	740	725	Out-of-plane CH frequencies of aromatic pyrrole ring
1095	1037	1025	C–N stretch
1472	1452	1430	Ring stretch
1577	1595	1586	Ring stretch
1713	1705	1704	C=C stretch of pyrrole ring
3400	3332	3318	N – H Stretch

From Table 2.1, it is seen that shifts in peak position have been observed in the N-H and C-N stretching modes of the iodine doped PPy, compared to the pristine one. The shifts observed in the N-H and C-N stretching vibrations indicate that the dopant atoms might have got attached to the nitrogen lone pair electrons of polypyrrole.

From the analysis of the FTIR spectra it can be concluded that iodine doping modifies the structure of the plasma polymerized pyrrole. Some extent of conjugation is also there in the structure of the plasma polymer, evidenced by the presence of C = C stretch of the pyrrole ring. Because of this extent of conjugation, iodine doping shows frequency shifts in the FTIR spectrum and brings about reduction in the optical band gap and enhancement in dc electrical conductivity as observed in polyaniline thin films by Paterno and co-workers [14]. It can be seen that the FTIR spectrum of polypyrrole, synthesized by polymerization techniques other than plasma polymerization differs considerably from that of the ac plasma polymerized sample. A comparison of prominent IR peaks found in ac plasma polymerized pyrrole thin films with those of the dc plasma polymerized [15], RF plasma polymerized [5] and chemically synthesized [11] polypyrrole films is presented in Table 2.2. A comparison of RF plasma polymerized pyrrole with that of chemically synthesized polypyyrole has been reported by Wang and co-workers [16].

Table 2.2 Comparison of FTIR peaks of ac plasma polymerized pyrrole thin films with those of DC and RF plasma polymerized and chemically polymerized pyrrole thin films.

	Synthesis techniques			
Functional groups	**Ac plasma polymerization (cm^{-1})**	**DC plasma polymerization (cm^{-1})**	**RF plasma polymerization (cm^{-1})**	**Chemical synthesis (cm^{-1})**
Out-of- plane CH vibrational frequencies of aromatic pyrrole ring	740	545,900	102,1060	825
C-N stretch	1037	Not assigned	Not found	1312
Ring stretch	1452	Not assigned	1400	Not assigned
Ring stretch	1595	Not assigned	1510	Not assigned
C=C stretch of pyrrole ring	1705	1620	1600	1530
N – H stretch	3332	3300-3400	3400	3450

2.3.2 UV-Vis absorption studies of pristine and iodine doped PPy at 70 W

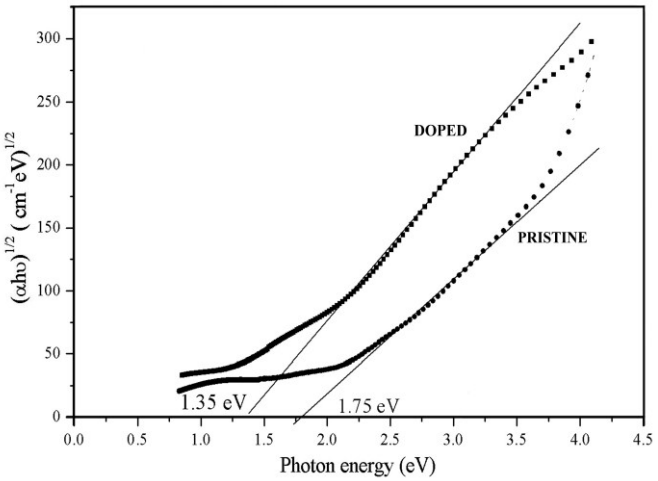

Figure 2.5 Mott plots for the calculation of the band gap of pure and in situ iodine doped PPy thin films

The photon absorption in many amorphous materials is found to obey the Tauc relation [17], which is of the form

$$\alpha h\nu = B\left(h\nu - E_{opt}\right)^{n} \tag{2}$$

where α is the absorption coefficient, $h\nu$ the photon energy, B a constant and the index *n* is connected with the distribution of density of states [18,19].

The plasma polymers at high energies exhibit a linear relationship given by

$$\left(\alpha h\nu\right)^{1/2} = B\left(h\nu - E_{opt}\right) \tag{3}$$

Plots of $(\alpha h\nu)^{1/2}$ against $h\nu$ are given in figure 2.5. These plots are called Mott plots and the transition energies can be evaluated from the plots. The linear portion of the Mott plot when extrapolated to the energy axis gives the threshold of optical absorption. From this, band gap energy is calculated. The optical band gap of pure PPy film is found to be 1.75 eV and that of the iodine doped one is found to be 1.35 eV. The decrease in optical band gap upon iodine doping can be correlated with the increase in electrical conductivity of the iodine doped films, discussed in the next section. A probable reason for the enhancement in electrical conductivity is that, the hole density of the polymer is increased by the doping of iodine. The dopant iodine attracts electrons from the molecular orbitals and produces sublevels or additional levels in the band structure and the band gap between the $\pi \rightarrow \pi^{*}$ states decreases as a result of increase in the length of the conjugated π system [20]. This

contributes for the modification of the Mott plot in the iodine doped PPy films. Similar results are reported in polythiophene thin films [21]. The high electrical conductivity of doped polypyrrole films can be attributed to the formation of a charge transfer complex between the pyrrole ring and the oxidative dopant iodine. The absorption edge obtained at around 1.35 eV in the doped film indicates the presence of bipolarons as reported in the case of plasma polymerized thiophene films by Silverstein and Visoly-Fisher [21].

2.3.3 Current density – Voltage (J-V) studies of pristine and iodine doped PPy, synthesized at 70 W

The J-V characteristics of the pristine and iodine doped polypyrrole films are depicted in figures 2.6, 2.7, 2.8 and 2.9. The thickness values of the films are also indicated in these figures.

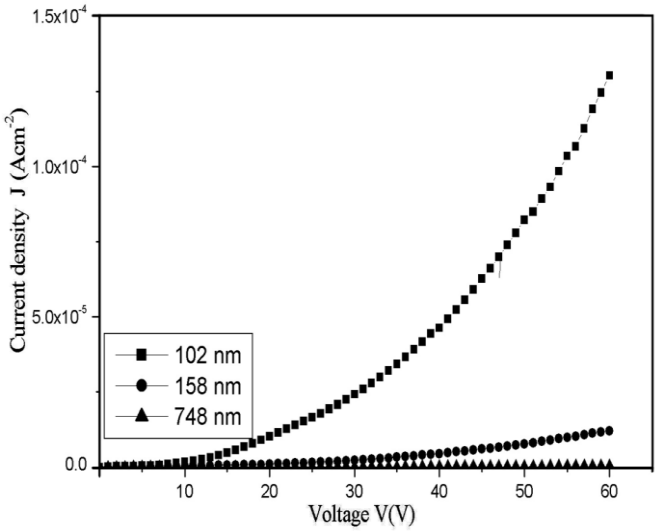

Figure 2.6 J–V characteristics of plasma polymerized pyrrole films in pure form

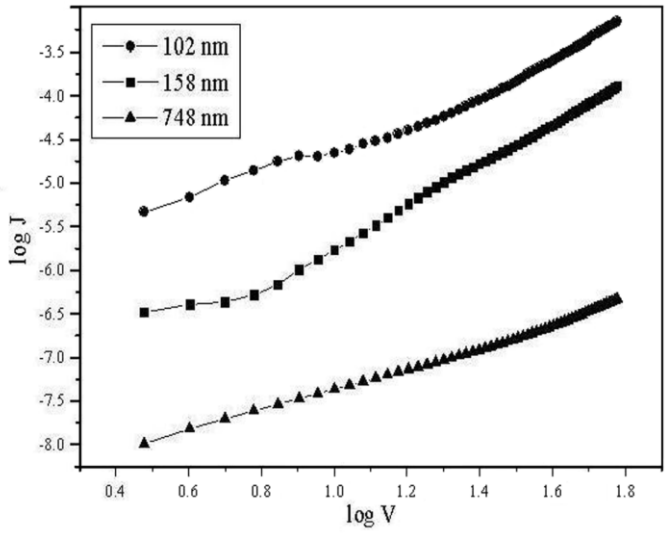

Figure 2.7 Double log(J–V) plots of plasma polymerized pyrrole films in pure form.

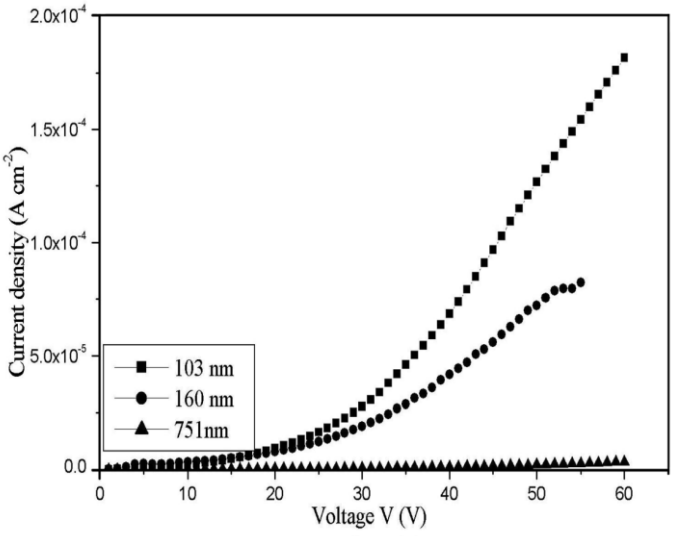

Figure 2.8 J–V characteristics of plasma polymerized pyrrole films in the iodine doped form

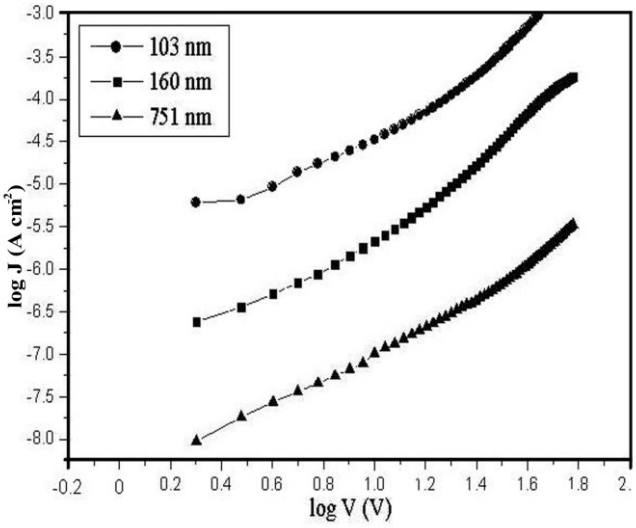

Figure 2.9 Double log (J–V) plots of plasma polymerized pyrrole films in the iodine doped form

The J-V characteristics at room temperature show a non ohmic behaviour at higher voltages and an ohmic behaviour in the low voltage region for both the pure and iodine doped PPy films. It is observed that, there is no breakdown of the films even at higher voltages over 60V for both the pure and iodine doped films. The conductivity values show an order of enhancement in the doped film. The doping of iodine increases the amorphous nature and the irregularities of the polymer film, which leads to low mobility and slow diffusion of charge carriers in the polymer matrix. Due to this, the enhancement of electrical conductivity is not very much pronounced in the iodine doped films, when compared to the situation in electrochemically doped polypyrrole structures.

The double log (J-V) plot of the films shows space charge limited conduction (SCLC) with a linear behaviour at low bias voltages and a nonlinear one at higher voltages. The equation for current density follows Ohm's law at lower voltages, given by [24]

$$J = \mu n_0 e \frac{V}{d} \tag{4}$$

where e is the electronic charge, V the voltage applied, d the inter electrode distance or the thickness of the film, n_o the equilibrium electron density and μ, the mobility of the charge carriers [22]. Here the thickness of the film has a prominent role in the value of J as in the case of voltage dependence according to the relation

$$J = e\mu N_v \left(\frac{\varepsilon_r \varepsilon_0}{ePkT_t} \right)^L \frac{V^{L+1}}{d^{2L+1}} \tag{5}$$

Here P is the trap density per unit energy range at the valence band edge, k the Boltzmann constant, Nv the effective density of states in the valence band, ε_o the permittivity of free space and $\varepsilon_r =$ 2.92 in pure PPy and 2.62 in iodine doped PPy, as calculated from the capacitance measurements. In this equation, L is the ratio T_t /T where T is the ambient temperature and T_t the temperature parameter describing the exponential trap distribution. The change over from ohmic to SCL conduction takes place at a particular voltage Vc known as transition voltage given by the equation,

$$V_c = \left(\frac{p}{N_v} \right)^{1/L} \frac{eN_t d^3}{\varepsilon_0 \varepsilon_r}, \tag{6}$$

Here N_t is the trap density, Nv the effective density of states in the valence band and p the hole density. It is found that, the value of Vc depends on the thickness of the film. The values of Vc for PPy films of different thickness are indicated in the J-V characteristics. At voltages above V_c, the electron current sharply increases from the ohmic behavior. For films of larger thickness a sudden transition from ohmic to SCLC is not observed and in that case diffusion of charge carriers in between the electrodes should also be taken into account. Generally the transition from SCLC to trap filled limit (TFL) is an extremely sharp transition [23]. A more gradual increase is observed in the present case. The absence of a sharp increase in current indicates that the carrier transport in PPy can be regarded as trap free. Due to this, the sharp increase in current, after the space charge region, which is characteristic of a trap filled conduction mechanism has not been observed in both the pristine and the iodine doped films even at high voltages around 60 V.

At voltages greater than Vc, the SCLC current density is given by the Mott-Gurney relation

$$J = \frac{9}{8} \varepsilon_0 \varepsilon_r \mu_p \frac{V^2}{d^3} \tag{7}$$

where $\in_o \in_r$ is the absolute permittivity of the polymer, μ_p the hole mobility and d the thickness of the film. From the slope of the logJ-logV plots (figure 2.7 and figure 2.9) it is to be observed that, the

current density *J* depends quadratically on the voltage V which is characteristic of SCLC and after this region the quadratic dependence of J on V changes to a trap filled limit (TFL) situation with slope greater than 2. The slope of the graph found in the high voltage region is about 3, and an abrupt increase in current is not observed as reported in references [23, 24].

2.3.4 UV-Vis absorption studies of pristine and iodine doped PPy films grown at 50 W

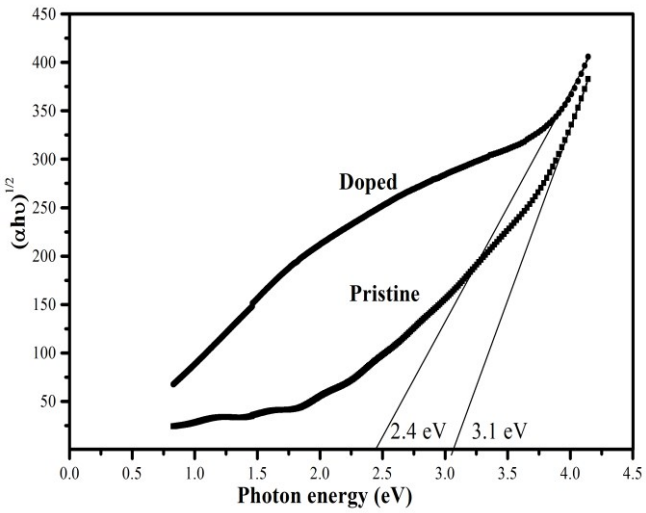

Figure 2.10 Mott plots of polypyrrole thin films in the pristine and iodine doped forms grown at 50 W

The optical absorption spectra of PPy films prepared at 50 W, show an exponential behavior and considerable difference in the case of pristine and doped samples. It is found that sharp absorption edges are not present in the case of the doped films. The Mott plots for the polypyrrole films are given in figure 2.10. In the ac plasma polymerized films, the band gap is found to be 3.1 eV in the pristine and 2.4 eV in the

iodine doped films. For the RF plasma polymerized PPy films, reported by Kumar and co-workers [5], the band gaps are 1.3 eV and 0.8 eV respectively for the pristine and the iodine doped films. Iodine doping results in the creation of charge transfer complexes or molecular aggregates which affects the charge transport properties [25]. Iodine may enter into the polymer chain substitutionally or reside within the defect levels in the amorphous regions. Due to its high electro negativity, iodine interacts with the polymer backbone, leading to structural modifications. This induces additional defect levels in the doped samples indicated by the exponential tail with decrease in photon energy below the band gap. Doping with electron acceptors like iodine increases the electrical conductivity because iodine doping decreases the binding energy of carriers [26].

2.3.5 Urbach tail analysis of polypyrrole thin films grown at 50 W

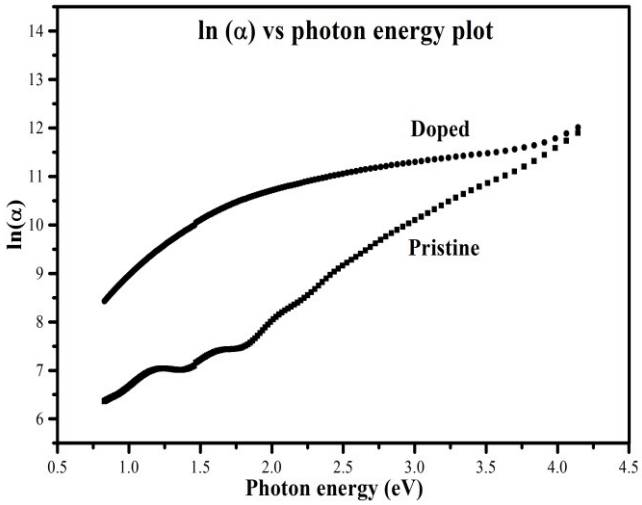

Figure 2.11 ln(α) against photon energy plots of polypyrrole films in the pristine and iodine doped forms, grown at 50 W

The structural disorders in amorphous solids form localized states within the band tails of electronic states, which cause changes in the optical behaviour and the electrical transport processes in these materials, and the amount of disorder is significant to control their structural, electrical and optical properties. The exponential rise in the Urbach edge is the manifestation of the effect of structural and thermal disorder on the electronic properties of semiconductors [27]. The effect of structural disorder on the electronic states of amorphous solids can be clearly recognized at the band edges.

The band tails extending into the band gap generally show an exponential behaviour, appreciable in the low-energy region of the absorption profile. They are characterized by the band tail parameter E_o as

$$\alpha(h\nu) \infty \exp\left(\frac{h\nu}{E_0}\right) \tag{8}$$

where α is the absorption coefficient and $h\nu$, the photon energy. The band tail parameter Eo depends on the carrier concentration n, temperature T and the structural disorder. It $_{is}$ the sum of the interactive and structural contributions and its value can be calculated from the slope of the absorption edge, and is given by

$$E_0 = \frac{d(h\nu)}{d(\ln\alpha)} \tag{9}$$

which is a strong function of temperature [12, 26]

From the FTIR spectral analysis, structural changes have been observed in polymers doped with iodine [21]. These structural modifications induce defect levels within the band gap. The degree of disorder can be calculated using the exponential tail data, estimated from the Urbach tail analysis. The broadening of the Urbach tail increases with increase in defect states of the films. For estimating the defect states, the plot of $\ln\alpha$ against $h\nu$, depicted in figure 2.11 is used. From the inverse of the slope of the $\ln\alpha$ against $h\nu$ plot, the value of the tail width E_0 in eV is calculated, which reflects the defect content in the film. The values of E_0 for the pristine and iodine doped polypyrrole films are calculated and are given in Table 2.3.

Table 2.3 E_0 (in eV) of the pristine and iodine doped polypyrrole films

Photon energy range in eV	**E_0 in eV**	
	Pristine PPy	**Iodine doped PPy**
0.5-1.0	.468	.357
1.0-1.5	.295	.671
1.5-2.0	.612	.816
2.0-2.5	.436	1.446
2.5-3.0	.545	2.099
3.0-3.5	.665	2.836
3.5-4.0	.708	1.685

The information obtained from the table suggests that in the high energy region, the value of E_0 for different absorption energy ranges, is higher in the case of doped films, compared to the pristine ones. This

indicates that the defect states created in this energy range is more pronounced in the doped films. From the absorption spectrum it can be seen that when compared to the pristine films, a considerable increase in optical absorption can be observed in doped films within the UV-Vis region. It is evident that the defect states created by the doping of iodine enhance the optical absorption in the UV-Vis region.

The E_0 value of the pristine PPy (0.468 eV) is higher than that of the doped one (0.357 eV) in the NIR region. This indicates that the defect states or additional energy levels created by doping are more prominent in the visible region than in the NIR region. The increase in the value of E_0 in the doped polypyrrole films in the visible region shows the enhancement of the charged defect states when the polymerization is carried out in the iodine atmosphere.

The increase of the dc electrical conductivity and the decrease in the band gap of the doped polypyrrole can be attributed to the fact that p type doping with iodine leads to removal of electrons from the polypyrrole system which brings about increase in the hole density. Due to this, the molecular orbitals of the polymer shift towards smaller binding energy with respect to the Fermi level [28]. As a result of the reduction in the binding energy the conductivity of the polymer increases.

2.3.6 J-V studies of pristine and iodine doped PPy grown at 50 W

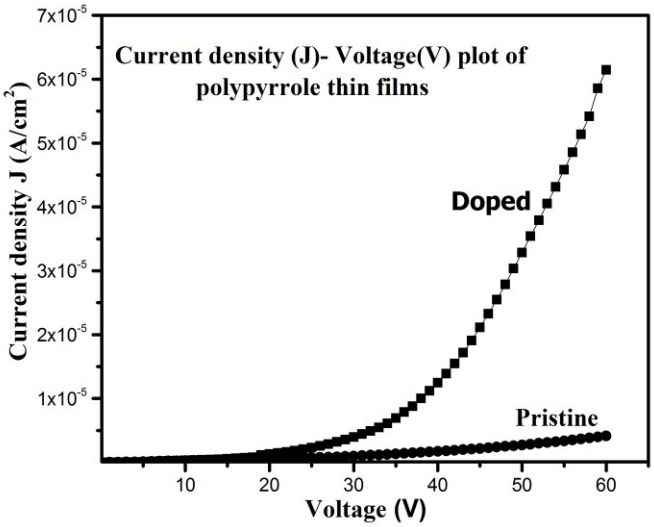

Figure 2.12 J-V characteristics of polypyrrole films in the pristine and doped forms prepared at 50 W

The current density versus voltage (J-V) characteristics of the pristine and doped polypyrrole thin films of thickness 210 nm are shown in figure 2.12.

The J-V characteristics at room temperature show non ohmic behaviour at higher voltages and ohmic behavior in the lower region of the applied voltage in the case of both the pristine and the iodine doped polypyrrole films. The graph shows that there is no breakdown in the films even at higher voltages around 60V for the pristine and the doped films. The log J versus log V plots of PPy films are given in figure 2.13.

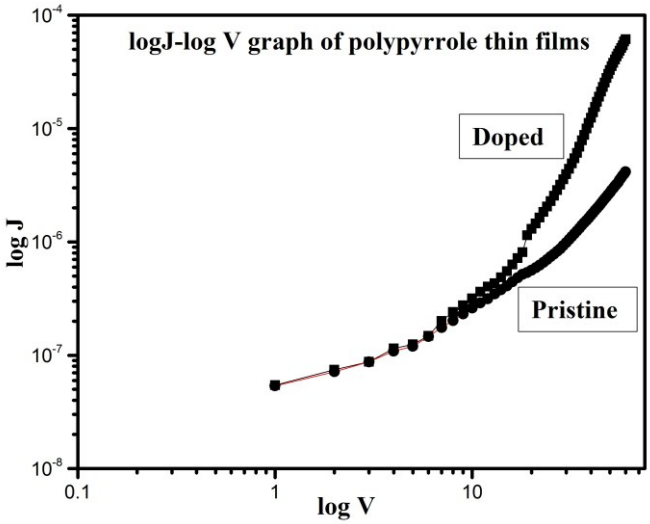

Figure 2.13 Log J-log V plots of plasma polymerized pyrrole thin films of thickness 210 nm in the pristine and iodine doped forms.

In the lower voltage region, the value of the slope of log J versus log V plot is found to be unity which is the ohmic region where the current is proportional to the applied voltage such that the famous relation $J = \mu n_0 e \frac{V}{d}$ holds. Here the mobility μ and the density of thermally generated charge carriers n_o are assumed to be constant at a given temperature and *e* is the electronic charge, V the voltage applied and *d,* the inter electrode distance or the film thickness [22]. For voltages above the critical voltage V_c = 10V, for the pristine film and V_c = 5.8 V for the doped film, the electron current strongly increases. The occurrence of an abrupt increase in the current at a certain critical voltage V_c is characteristic of an insulator with traps and at this voltage the electrical conduction mechanism switches to the SCLC mode. At

higher voltages, SCLC type current density is characterized by the Mott-Gurney relation given by equation (7).

From the slope of the log J-log V plot, it is observed that the current density J shows SCLC type dependence on the applied voltage up to a region 30 V for the pristine and 18 V for the doped films. After this region the dependence of J on V changes to the trap filled limit type (TFL) with slope higher than 2. The slope of the graph in the high voltage region for the pristine film is about 3 and for the doped film it is about 3.6, which indicates the enhancement of trap density in the doped films. Space charge limited (SCLC) type conduction is an indication of the presence of structural defects typically resulting in the creation of discrete trap states within the energy gap [34], which has been observed in the optical absorption studies as well.

The conductivity values show an order of enhancement in the doped PPy films. Reduction of band gap and the modification of the absorption spectrum of the iodine doped polypyrrole film, compared to the pristine one are the highlights of the optical absorption studies. This may be due to the formation of intermediate energy levels created by the iodine doping. Even though iodine doping increases the carrier density of the polymer film, the enhancement of the conductivity is not so pronounced due to the low mobility of the carriers. It may also be possible that the doping induced defect states are not contributing much towards the electrical conductivity of the polymer.

2.4 Conclusions

Investigations on the electrical and optical properties of plasma polymerized pyrrole thin films in the pristine and the iodine doped forms are carried out. The electrical conductivity studies reveal that the dominant carrier transport mechanism in these films is space charge limited type conduction. An electric field induced enhancement of the conductivity is also observed. Considerable changes are observed in the structural, optical, and electrical properties of the iodine doped polypyrrole films, compared to the pristine ones. The decrease in band gap and the enhancement of electrical conductivity are explained on the basis of the decrease in binding energy by the incorporation of charged defects. The enhancement of defect levels by iodine doping is elucidated with the help of Urbach tail analysis. Iodine doping results in the creation of charged defects in the polymer chain. The additional levels created by doping modify the electronic structure of polypyrrole, which is clearly recognized at the band edges. From the Urbach tail analysis it is found that the disorders created by doping are more prominent in the visible region than in the NIR region.

References

[1] E. Ju, K. Sik, and A. G. Macdiarmid, High molecular weight soluble polypyrrole, Synth. Met., 125 (2002) 267–272

[2] Terje A. Skotheim, Handbook of Conducting Polymers, Marcel Decker, Inc , New York, (1986) Chapter 14

[3] C.O.Yoon, M. Reghu., D. Moses and A.J .Heeger, Transport near the metal-insulator transition: Polypyrrole doped with PF6, Phys.Rev. B, 49 (1994) 10851

[4] B Chapman, R.G. Buckley, N.T. Kemp, A.B Kaiser, D Beaglehole and H.J Trodahl, Low-energy conductivity of PF6-doped polypyrrole, Phys. Rev.B 60 (1999) 13479

[5] D Sakthi Kumar, Kenji Nakamura, Satoko Nishiyama, Shigeru Ishil, Hiromichi Noguchi, Kunihiro Kashiwagi, and Yasuhiko Yoshida, Optical and electrical characterization of plasma polymerized pyrrole films, J.Appl. Phys. 93 (2003), 2705- 2711

[6] Yasuda., Plasma polymerization, Academic press, New York, (1985)

[7] S Saravanan, C Joseph Mathai, M R Anantharaman, S Venkatachalam, Low k thin films based on rf plasma-polymerized aniline, New Journal of Physics 6 (2004) 64

[8] C Joseph Mathai, S Saravanan., M.R Anantharaman, S. Venkitachalam, S. Jayalekshmi, Characterization of low dielectric constant polyaniline thin film synthesized by ac plasma polymerization technique, J Phys.D: Appl Phys, 35 (2002) 240-245

[9] H Akther and A. H. Bhuiyan, Electrical and optical properties of plasma-polymerized N, N,3,5-tetramethylaniline thin films, New J. Phys. 7 (2005) 173

[10] I. K. Saito and A.J Ikushima, Absorption edge in silica glass, Phys. Rev. B, 62 (2000) 8584-8587

[11] J Tauc, A Menth, D.L Wood., Optical and Magnetic investigations of the Localized States in Semiconducting Glasses, Phys.Rev.Lett, 25 (1970) 749-752

[12] A Iribarren,. R.Castron –Rodriguez, V.Sosa, J.L. Pena, Band-tail parameter modeling in semiconducting materials, Phys. Rev. B, 58(4) (1998) 1907-1911

[13] Rajan K. John, D Sakthi Kumar, S Jayalekshmi, M R Anantharaman and M G Krishna Pillai, Structural studies on plasma polymerized pyrrole, Asian Chemistry Letters, 1 (1997) 27-30

[14] L.G. Paterno, S Manolache. and F. Denes., Synthesis of polyanniline-type thin layer structures under low-pressure RF-plasma conditions, Synthetic Metals, 130(1) (2002) 85- 97

[15] S. Eufunger, V. Ooij, T.H Ridgway, DC plasma-polymerization of pyrrole: Comparison of films formed on anode and cathode, J.Appl.Polymer. Sci., 61 (9) (1996) 1503-1514

[16] Wang, J.; Neoh, K.G.; Kang, E.T., Comparative study of chemically synthesized and plasma polymerized pyrrole and thiophene thin films, Thin Solid Films, 446(2) (2004) 205-217

[17] H Akther and A. H. Bhuiyan, Electrical and optical properties of plasma-polymerized N,N,3,5-tetramethylaniline thin films, New J. Phys. 7 (2005) 173

[18] J. Tauc, Amorphous and Liquid Semiconductors. Plenum Press, London & New York (1974)

[19] C. Joseph Mathai, S. Saravanan, M.R. Anantharaman, S. Venkitachalam, S. Jayalekshmi, Effect of iodine doping on the bandgap of plasma polymerized aniline thin films, J. Phys. D: Appl. Phys. 35 (17) (2002) 2206

[20] Paolo Coppo, Raoul Schroeder, Martin Grell, Michael L.Turner, Investigation of solution processed poly(4,4-dioctylcyclopentadithiophene) thin films as transparent conductors, Synthetic Metals,143(2) (2004) 203-206

[21] M.S.Silverstein, I-Visoly-Fisher, Plasma polymerized thiophene: Molecular structure and electrical properties, Polymer, 43(1) (2002) 11-20

[22] P.W.M.Blom, C.Tanase, D.M.deLeeuw, R.Coehoorn, Thickness scaling of the space-charge-limited current in poly(pp-phenylene vinylene), Appl.Phys.Lett, 86 (2005) 092105

[23] Mammen Samuel, C.S Menon, N.V Unnikrishnan, Electrical conduction processes in as-deposited indium phthalocyanine chloride thin films using gold and aluminium electrode combination, J. Phys: Cond. Mat. 18 (2006) 135-141

[24] P W M Blom, de Jong and J. J M Vleggaar, Electron and hole transport in poly (p-phenylene vinylene) devices, Appl.Phys.Lett, 68 (1996) 3308

[25] A.K.Bakshi, k. Tashio, Y. Minagave, Electrically conducting polymers: from fundamental to applied research, Bull. Mater.Sci, 18(5) (1995) 469-495

[26] B Xu., Jaewu Choi, A.N Carus. and P. A. Dowben, Band filling and depletion through the doping of polyaniline thin films Appl.Phys. Lett. 80(23) (2002) 4342-434

[27] M. Beaudoin, A.J.G.De Vries, S.R. Johnson, H. Laman, T. Tiedje, Optical absorption edge of semi-insulating GaAs and InP at high temperatures, Appl. Phys. Lett., 70 (1997) 3540-3542

[28] A. Iribarren, R. Castron –Rodriguez, V. Sosa and J.L Pena, Modelling of the disorder contribution to the band-tail parameter in semiconductor materials, Phys.Rev.B, 60(7) (1999) 4758

[29] M. Arif, M.Yun, S Gangopadhyay, K. Gosh, L. Fadiga, F. Galbrecht, U. Scherf and S Guha, Polyfluorene as a model system foe space-charge-limited conduction, Phys. Rev. B, 75 (2007) 195202

Chapter 3

DOPED POLYPYRROLE WITH APPRECIABLE SOLUBILITY, CRYSTALLINE ORDER AND ELECTRICAL CONDUCTIVITY SUITABLE FOR DEVICE APPLICATIONS

This chapter deals with the synthesis of polypyrrole with appreciable solubility and processability and the detailed structural, morphological, electrical and optical characterization of the polymer, synthesized using chemical oxidative polymerization technique with ammonium persulfate (APS) as the oxidant. Various dopants such as di (2-ethylhexyl) sulfosuccinic acid sodium salt (NaDEHS), dodecylbenzene sulfonic acid (DBSA) and dodecylbenzene sulfonic acid sodium salt (NaDBSA) are tried to improve the solubility in different solvents. Studies are carried out on doped polypyrrole in powder and spin coated thin film forms. The improved solubility of the doped PPy in different solvents makes it, by and large, a prospective candidate for various device applications.

3.1 Introduction

Interest in the development of conducting polymers such as polypyrrole, polyaniline and polythiophene has intensified tremendously during the last few decades on account of their tunable electrical and optical properties for applications in rechargeable batteries, functional electrodes, electrochromic devices, optical switching devices, and so on.

Conducting organic polymers have semiconductor properties because of their conjugated structure and have high potential for many applications in light emitting diodes, chemical and biological sensors, photovoltaic cells, corrosion inhibition devices, miroactuators, antielectrostatic coatings and functional membranes [1,2]. They conduct electricity and display good electrical and optical properties generally shown by inorganic systems [3]. Polypyrrole is a widely studied conjugated polymer endowed with interesting electrical transport properties, catalytic and sensor properties, environmental stability and biocompatibility [4,5]. However, the polymer, synthesized electrochemically, chemically or by plasma polymerization is insoluble in most solvents, which restricts its applications in device technology. The poor solubility of polypyrrole is due to the presence of long chain conjugated structure, the strong intramolecular interactions among polypyrrole chains, the crosslinking of the polypyrrole chains and the weak interactions of polypyrrole with the solvents, which limit its processability, characterizion and applications [6].

Reports show that early endeavours to synthesize water soluble conducting polymers were mainly focussed on chemical synthesis of polyaniline and the modification of polyaniline structure by treating with various polar group mediators [7]. It has been reported that polythiophene becomes soluble in common organic solvents by the attachment of an adaptable side chain such as an alkyl group with a carbon number of 4 or more on the third position of the thiophene unit which shows a somewhat high conductivity of about 30-100 S/cm after doping [8]. By adding fixed charges to the main chain conjugated polymer, self-doping and processability in polar solvents, including water, are conceivable [9].

Many efforts are being made to increase the solubility of polypyrrole by making functionalized pyrrole by N alkylation or C alkylation of heterocyclic groups by doping with anionic surfactants. Because of the flexibility of the alkyl group, the structural rigidity of the polymer can be diminished and the alkyl side chain in the polymer backbone prompts the loss of planarity in the aromatic rings, due to steric hindrance [10]. It is reported that Kwan Sik Jang and co-workers have synthesized a few water soluble polypyrroles by doping with different dopants containing alkyl chains. The synthesized polymers were made water soluble by making a chemical alteration with chlorosulfonic acid [11]. Introduction of counter-ions to the polymer backbone is found to improve the solubility of polypyrrole. Substituted monomers reduce the strong intermolecular interactions between polymer chains in the doped state. It has been reported by P. Jayamurugesan and co-workers that doping the polymers with organic acids like dodecylbenzene sulfonic acid (DBSA) and camphor sulfonic acid (CSA) emphatically influences their conductivity, morphology and thermal stability [12].

Even though efforts are being made to increase the solubility of polypyrrole, detailed structural, morphological and electrochemical studies of PPy doped with different dopants and soluble in various solvents have not been pursued widely The prime objective of the present work is the synthesis of polypyrrole using the dopants di (2-ethylhexyl) sulfosuccinic acid sodium salt (NaDEHS), dodecylbenzene sulfonic acid (DBSA) and dodecylbenzene sulfonic acid sodium salt

(NaDBSA), with appreciable solubility and processability suitable for device applications.

3.2 Materials and methods

Pyrrole monomer of 98% purity supplied by Aldrich Chemical Company was further purified by distillation. The other chemicals used for the synthesis of doped PPy were purchased from Sigma-Aldrich and were utilized without further purification.

3.2.1 Synthesis of polypyrrole (PPy) using chemical method

In the present work, polypyrrole (PPy) was synthesized by chemical oxidative polymerization with ammonium persulfate (APS) as the oxidant. In a typical synthesis, 0.3 molar pyrrole in 200 mL of distilled water was mixed with 0.1 molar APS in 100 mL distilled water, slowly under constant stirring for 30 minutes. The solution mixture was stirred for 24 hours in an ice bath maintained at a temperature of 0-5^{o} C. The resulting polypyrrole powder was filtered out and washed with distilled water several times and dried under vacuum for 24 hours.

3.2.2 Synthesis of polypyrrole with appreciable solubility

Polypyrrole with improved solubility was synthesized by doping with the dopants, NaDEHS, DBSA and NaDBSA. In a typical synthesis, 0.3 molar pyrrole and 0.15 molar NaDEHS, the dopant, in 200 mL distilled water were mixed under vigorous magnetic stirring. After a few minutes of stirring, 0.1 molar APS in 100 mL distilled water was added dropwise into the solution. The solution mixture was stirred for 24 hours

in an ice bath. The resultant precipitate thus obtained was filtered and washed with distilled water several times and dried under vacuum for 24 hours. The same procedure was adopted for synthesizing doped PPy, using the other dopants, DBSA and NaDBSA.

3.2.3 Characterization

The percentage of elements C, H, N and S in the doped polypyrrole samples was estimated utilizing CHNS analysis technique with the instrument Elementar Vario EL III. For the solubility studies, calculated quantities of doped PPy powder were dissolved by ultrasonification in various organic solvents for 24 hours and the extent of dissolution of the computed amount of the doped PPy powder in different solvents was observed. The DC electrical conductivity studies were carried out on the doped PPy pellets and the doped PPy films obtained by spin coating the solution of the doped PPy powders in various solvents, using the four probe method. The Fourier transform infrared (FTIR) spectral studies were conducted using Thermo Nicolete Avatar 370 DTGS model FTIR spectrometer in the wavenumber range of 400–4000 cm^{-1}. The X-Ray diffraction (XRD) patterns were obtained using the Rigaku Dmax C diffractometer with Cu Kα radiation of wavelength 1.54 Å. Ultraviolet-Visible (UV-Vis) optical absorption spectra of the pristine and doped PPy samples were recorded using Jasco V 570 UV-Vis-NIR spectrophotometer. The thermal studies were done from room temperature to 700 °C using Perkin Elmer, Diamond machine and the Differential Scanning Calorimetry (DSC) studies, by using Mettler Toledo DSC 822e, to understand the melting behaviour and

glass transition of the polymer samples. Raman spectra were recorded with a Horiba LabRam (800 mm) HR spectrometer equipped with a 514 nm Argon ion laser of 15 mW power. The field emission scanning electron microscopy (FESEM) images of the polymer samples were acquired using Carl-Zeiss Sigma 250 electron microscope and the transmission electron microscopy (TEM) patterns, utilizing Jeol/JEM 2100 model machine.

3.3 Results and Discussions

3.3.1 CHNS analysis

Table 3.1 CHNS analysis data of PPy and doped PPy samples

Sample No	Sample Name	C%	H%	N%	S%	C/N
1	PPy	46.22	3.00	13.74	1.26	3.36
2	PPy-NaDBSA	53.92	5.71	13.21	2.82	4.08
3	PPy-DBSA	70.27	8.34	7.56	4.98	9.29
4	PPy-NaDEHS	60.19	7.68	6.46	4.79	9.31

The results of elemental analysis of PPy and doped PPy samples are shown in Table 3.1. The high sulfur content in doped PPy samples indicates the presence of sulfonyl groups in the polymer. The increased C/N ratio of the doped samples indicates the incorporation of large sized surfactant anions into the polymer backbone [2].

3.3.2 Solubility and electrical conductivity

Table 3.2 Solubility of doped PPy in organic solvents.

Solvent	Solubility PPy-NaDEHS (wt% / vol.)	Solubility PPy-DBSA (wt% / vol.)	Solubility PPy-NaDBSA (wt% / vol	Conductivity PPy-NaDEHS (S/cm)	Conductivity PPy-DBSA (S/cm)	Conductivity PPy-NaDBSA (S/cm)
meta-Cresol (m-cresol)	≈ 8	≈ 9	≈ 7	3.4×10^{-1}	6.8×10^{-1}	1.2×10^{-1}
N-Methyl-2-pyrrolidone (NMP)	≈ 9	≈ 8	≈ 7	5.8×10^{-1}	4.6×10^{-1}	0.5×10^{-1}
Dimethylformamide (DMF)	≈ 7	≈ 6	≈ 7	0.6×10^{-1}	1.4×10^{-1}	1.8×10^{-1}
Dimethyl sulfoxide (DMSO)	≈ 7	≈ 8	≈ 7	0.5×10^{-1}	0.3×10^{-1}	0.6×10^{-1}
Dichloroethane	≈ 5	≈ 6	≈ 5	1.5×10^{-3}	1×10^{-2}	1.2×10^{-3}
Chloroform	≈ 4	≈ 5	≈ 6	1.4×10^{-3}	1.7×10^{-3}	1.5×10^{-2}

Table 3.3 Electrical conductivity of PPy and doped PPy samples in pelletized form

Sample No	Sample Name	Conductivity in S/cm
1	PPy	2.5×10^{-3}
2	PPy-NaDBSA	3.2×10^{-2}
3	PPy-DBSA	5.6×10^{-2}
4	PPy-NaDEHS	6.4×10^{-2}

The solubility and room temperature electrical conductivity of the synthesized PPy, doped with NaDEHS, DBSA and NaDBSA in various organic solvents are shown in Table 3.2. The solubility is checked by dissolving the doped polymer in various solvents. All the doped polymer samples show good solubility in m-cresol, NMP, DMF and DMSO because of the presence of long alkyl chain containing dopants which effectively reduce the intermolecular and intramolecular interactions and crosslinking among the PPy chains [13].

The increased solubility of the doped PPy samples in polar solvents like NMP, DMF and DMSO is due to the expanded coil conformation in which the doped PPy interacts with the polar solvent, thereby enhancing pi interaction along the chains and increasing the carrier mobility [4].

The conductivity of PPy and the doped samples in the form of pelletized powder is slightly lower compared to that of the PPy films cast from the solvents, as shown in Table 3.3. This is because of the various types of structural disorders in PPy chains which considerably influence the charge-carrier mobility and finally the conductivity of the polymer. The introduction of anionic surfactants into the backbone of polymer will enhance the conductivity because the surfactants modify the conducting network of PPy chains and introduce an ordered arrangement of the macromolecular chains [14].

3.3.3 FTIR spectroscopic studies

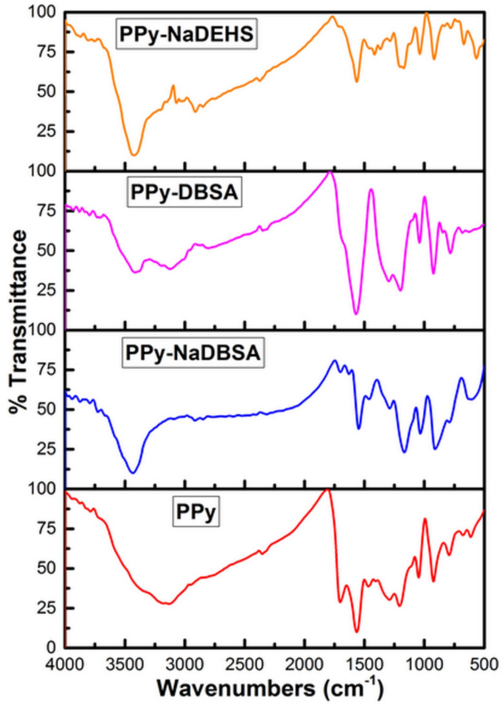

Figure 3.1 The FTIR spectra of PPy and doped PPy samples

The FTIR spectra of PPy and doped PPy samples are illustrated in figure 3.1. The peak at 3130 cm^{-1} in the spectrum of PPy corresponds to C-H stretching vibrations and the strong peaks at 3433 cm^{-1}, 3415 cm^{-1} and 3424 cm^{-1} in the spectra of PPy-NaDBSA, PPy-DBSA and PPy-NaDEHS respectively, are assigned to NH stretching vibrations [15]. The peak at 1702 cm^{-1} in PPy is shifted to the small peak at 1718 cm^{-1} in PPy-NaDEHS, indicating the presence of DEHS anions, which are responsible for the improved solubility of PPy in various solvents [16]. Low intensity peaks observed at 2934 cm^{-1} in PPy and at 2806 cm^{-1} and 2911 cm^{-1} in PPy- NaDBSA and PPy - DBSA can be ascribed to the

S=O and the aromatic C-H stretching vibrations of the benzenoid ring in the NaDBSA and DBSA dopants, respectively [17]. The absorption peaks at 1563 cm^{-1} for PPy and at 1547 cm^{-1}, 1559 cm^{-1} and 1562 cm^{-1} for the doped PPy samples, correspond to the fundamental vibrations of the polypyrrole ring .This shift to lower wavenumbers observed in the doped PPy samples may be caused by the ionic interaction of anionic surfactants with polypyrrole [18]. The bands at 1467 cm^{-1} in PPy and at 1450 cm^{-1} and 1414 cm^{-1} in the doped samples represent C-N stretching vibrations of the pyrrole ring [19]. The peak at 1718 cm^{-1} in PPy-NaDEHS related to C=O vibrations of the two ester groups in the dopant is diminished in intensity in view of the detachment of the anionic dopant molecules from the polymer due to the introduced sulfonate groups balancing the charges around the polymer chains [11]. The broad bands from 1414 to 1289 cm^{-1} in the pristine and the doped PPy samples are attributed to the C-H and C-N bending vibrations. The observed wide bands in the region of 1166 to 1032 cm^{-1} in the spectra of the doped PPy samples are related to the breathing vibrations of the pyrrole ring [13]. The S=O vibrations of sulfonate anions are indicated by the bands at 1171 cm^{-1}, 1198 cm^{-1} and 1166 cm^{-1} in the doped PPy samples. The peaks at 924 cm^{-1}, 909 cm^{-1} , 919 cm^{-1} in PPy and the doped samples are due to the =C-H out-of-plane vibrations [20] and those at 604 cm^{-1} and 681 cm^{-1} demonstrate the characteristic vibrations of DBSA. The bands at 565 cm^{-1} and 588 cm^{-1} in the doped samples represent the C–S stretching vibrations, indicating the attachment of the sulfonic acid groups into the polymer backbone.

3.3.4 XRD studies

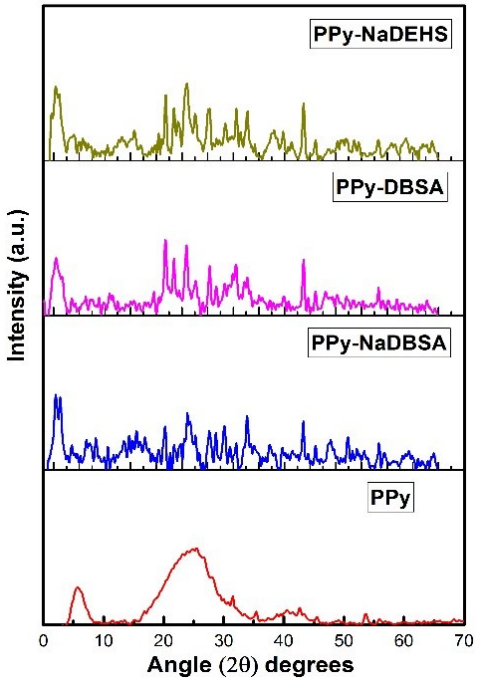

Figure 3.2 The XRD patterns of PPy and doped PPy samples

The XRD patterns of PPy and doped PPy samples are shown in figure 3.2. The plot of PPy shows broad peaks around 2θ values of 5.73^0 and 25.55^0 indicating amorphous structure [21]. The broad peaks at 5.5^o in PPy-NaDEHS, 5.4^o in PPy-DBSA and 5.3^o in PPy-NaDBSA indicate the layered structure of the polymer chains. The long alkyl chains of the dopants prevent the close packing of the individual polymer chains by acting as flexible spacers between PPy chains and solvate the polymer, prompting enhanced solubility in organic solvents [22]. In the region between 2θ values of 10^o to 20^o, no well-defined peaks are visible but small shoulders are found at 2θ= 11^o,13^o, 15^o and 18^o in all the doped samples. The appearance of the intense and narrow

peaks between 2θ = 20° to 50° in all the doped samples illustrates the presence of crystalline domains within the amorphous PPy [23]. The XRD peaks seen in pristine polypyrrole are feeble and wide, contrasted to the sharp and narrow diffraction peaks observed in the doped samples. It is obvious from the XRD patterns of the doped samples that the intensity of the diffraction peaks increases due to the semi-crystalline nature of the resulting doped PPy compositions. These observations are additionally in high concurrence with the morphological changes observed in the doped PPy samples, as per the FESEM and TEM investigations, described in the accompanying sections.

3.3.5 Raman studies

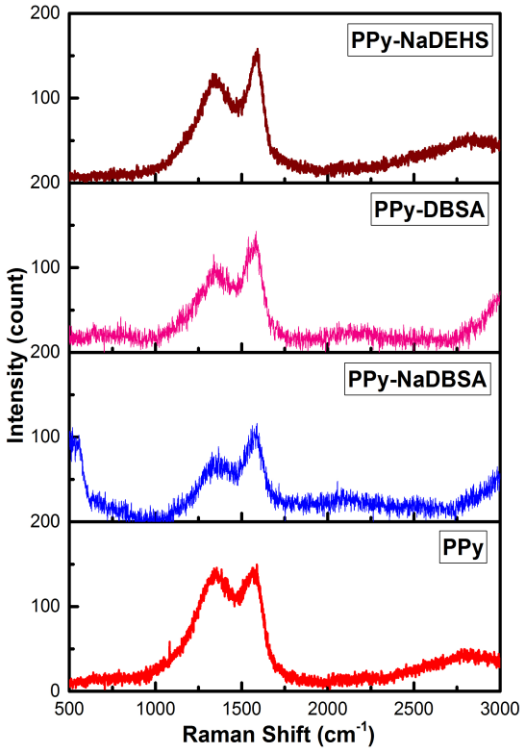

Figure 3.3 Raman spectra of PPy and doped PPy samples

The Raman spectra pf PPy and doped PPy samples are shown in figure 3.3. The peaks at 1573, 1583 and 1587 cm^{-1} in PPy and doped samples represent the C=C backbone stretching of PPy [21]. The peaks at 1348, 1361, 1354 and 1340 cm^{-1} in the samples can be ascribed to the ring-stretching mode of PPy. The small peak at 1051 cm^{-1} in PPy is assigned to the C-H in plane deformation vibration [24]. The sharp peaks from 1340 to 1361 cm^{-1} and 1573 to 1587 cm^{-1} observed in all the doped samples indicate the slight increase in the crystallinity of the doped samples leading to the increase in electrical conductivity which supports the inferences from the XRD and the morphological studies.

3.3.6 Thermo-gravimetric analysis (TGA)

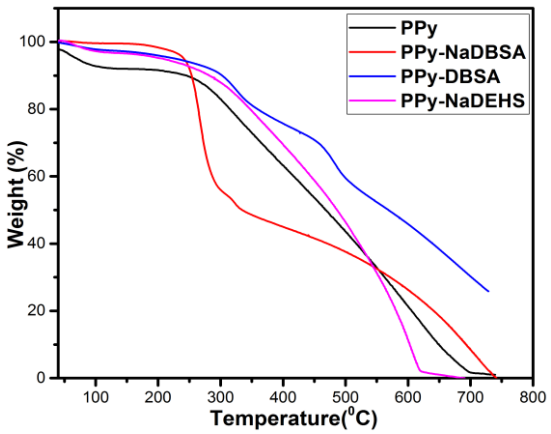

Figure 3.4 The TG curves of PPy and doped PPy samples

The thermal degradation curves of PPy and doped PPy samples are shown in figure 3.4 The initial degradation processes of PPy and the doped PPy samples occur at temperatures between 47 °C to 135 °C

which correspond to the elimination of moisture, solvents, oligomers and unreacted monomers [25]. The second weight loss starts at around 230 ^{o}C for PPy, PPy-NaDBSA and PPy-NaDEHS and at 313 ^{o}C for PPy-DBSA. This corresponds to the evaporation and degradation of $DEHS^-$ and $DBSA^-$ dopant components of PPy which occur due to the destruction of the columbic attraction between the dopants and the polymer backbone [4]. The complete decomposition occurring at 239 ^{o}C, 261 ^{o}C, 275 ^{o}C and 460 ^{o}C for PPy, PPy-NaDBSA, PPy-NaDEHS and PPy-DBSA respectively, represents the breaking of the PPy chains. Polypyrrole doped with DBSA shows higher thermal stability, compared to the other doped PPy compositions. The increase in thermal stability of the doped samples is attributed to the enhanced crystallinity of these samples, as evidenced from the XRD and TEM analysis.

3.3.7 DSC studies

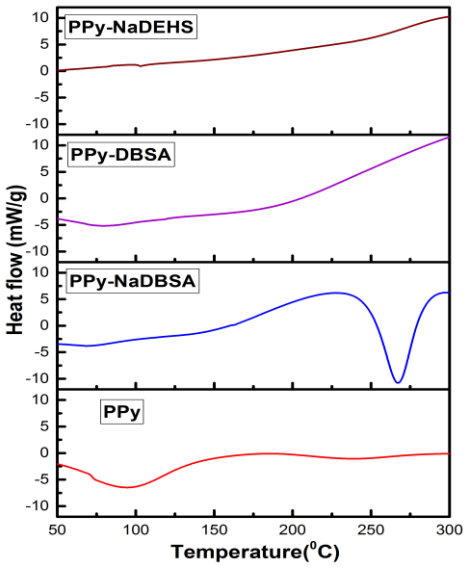

Figure 3.5 The DSC curves of PPy and doped PPy samples

The curves showing heat flow (w/g), at different temperatures, termed as the DSC curves, related to PPy and doped PPy samples are given in figure 3.5. The glass transition temperature T_g and the melting point T_m of PPy respectively are 98 ^oC and 240 ^oC. The doped samples, PPy-NaDBSA , PPy-DBSA and PPy-NADEHS show the values of T_g at 131 ^oC, 134 ^oC and 142 ^oC respectively . The T_m value of the PPy-NaDBSA is 267 ^oC and a higher value of T_m is observed for the other doped samples. The increase in the values of T_g and T_m of the doped samples supports the enhanced crystallinity of these samples as observed in the XRD studies [24].

3.3.8 UV - Visible absorption studies

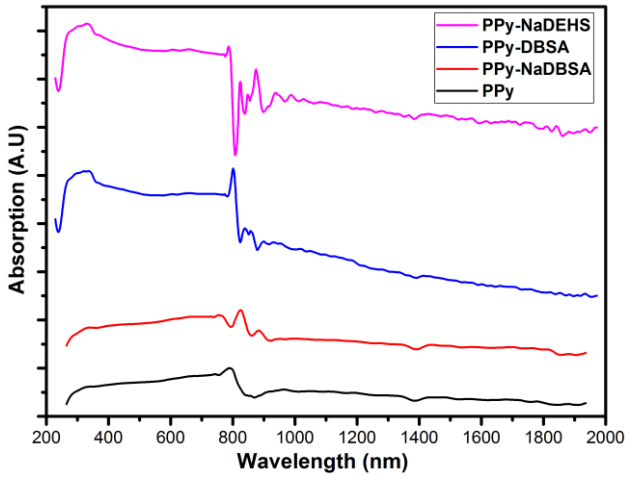

Figure 3.6 UV-Visible absorption spectra of PPy and doped PPy samples

The optical absorption spectra in the UV-Visible region, for PPy and doped PPy samples in the solvent m-cresol, are shown in figure 3.6

The weak peak at 453 nm in PPy is blue shifted to lower wavelength region around 338 nm to 372 nm, in the doped samples, which is an indication of the strong interaction of PPy with the dopants [26]. The solutions of doped PPy show weak absorption peaks from 338 nm to 372 nm corresponding to the π-π^* transition and stronger absorption around 930 nm to 960 nm, associated with the bipolaron states of PPy [27]. These protonation stages of PPy due to the introduction of polaron and bipolaron states will enable the easier transition of electrons due to the small energy gap, which in turn increases the conductivity [1]. The small peaks observed in the wavelength region 319 nm to 605 nm are due to the localized states in PPy. The strong free carrier tail bands observed at 1429 nm and 1576 nm of the doped samples are related to the delocalization of electrons in the polaron bands and provide a qualitative measure of the carrier mobility in the polymer chain and the high degree of conjugation achieved in the polymer structure a result of doping, which result in the enhancement of electrical conductivity [22].

3.3.9 FESEM studies

Typical FESEM images of PPy and doped PPy are shown in figure 3.7. The image of PPy in figure 3.7 (a) shows the usual, regular globular morphology and the individual granules observed are nearly spherical [28]. In the image of the doped sample, PPy-NaDBSA, shown in figure 3.7 (b), the globular structure disappears and the granules have fused together to form a smooth single layer.

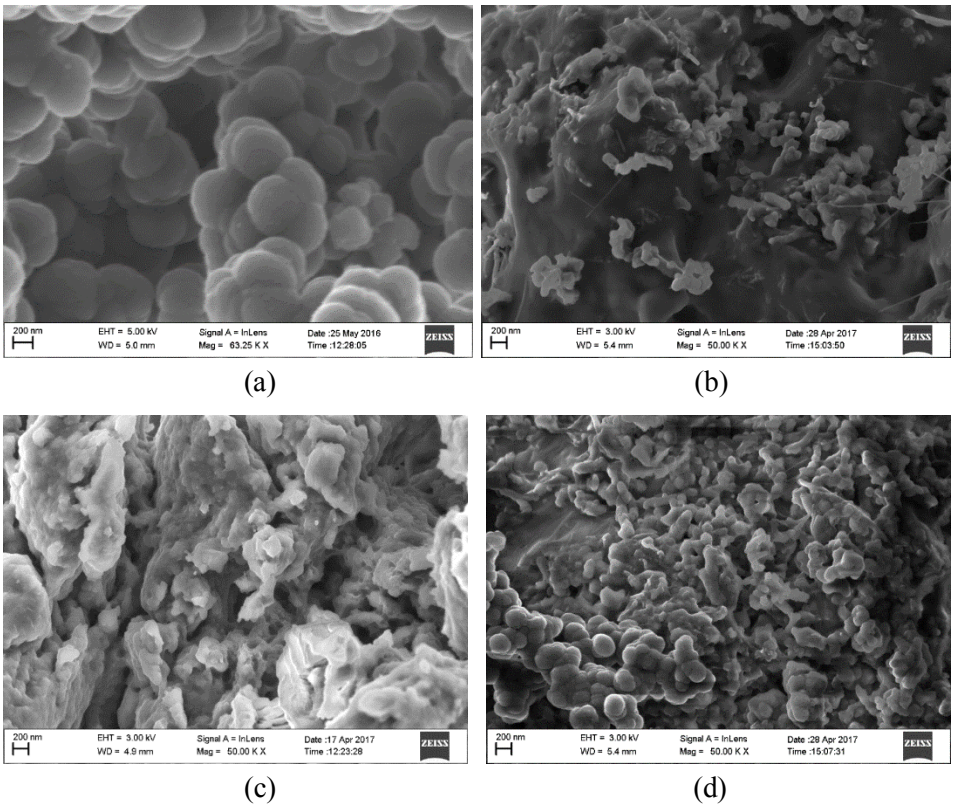

Figure 3.7 FESEM images of (a) PPy (b) PPy-NaDBSA (c) PPy-DBSA (d) PPy-NaDEHS

The image given in figure 3.7 (c) shows that the globular structure of pristine PPy is lost and the DBSA doped PPy is seen like having a layered structure with a slightly rougher surface, compared to PPy doped with NaDBSA. The FESEM image in figure 3.7 (d) of PPy doped with NaDEHS also shows that the globules fuse together to form single layered, continuous structure, which enhances the electrical conductivity. No phase separation is observed in figures 3.7 (c) and 3.7 (d), confirming good compatibility of the components in the doped samples [29].

3.3.10 TEM analysis

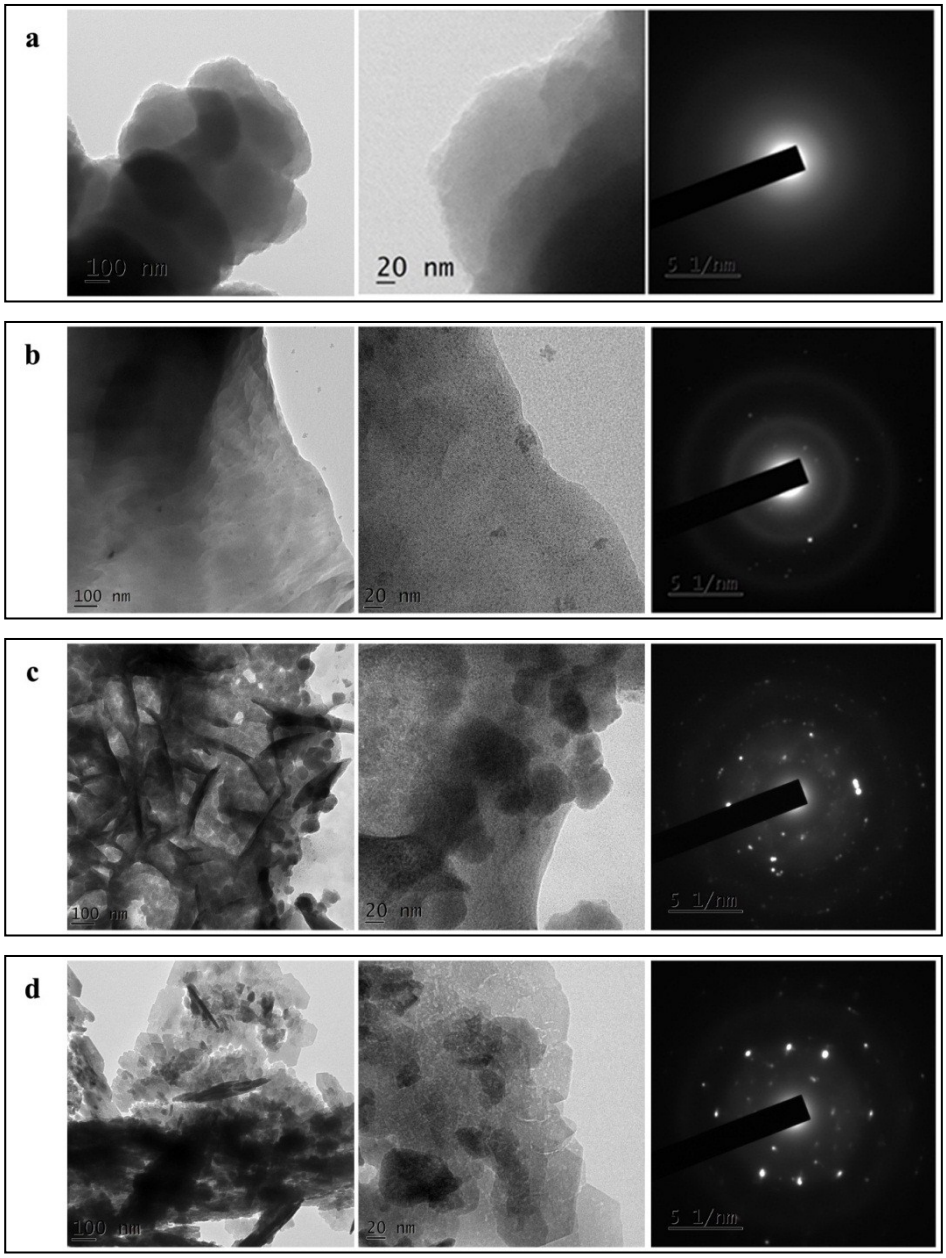

Figure 3.8 TEM images of (a) PPy (b) PPy-NaDBSA (c) PPy-DBSA (d) PPy-NaDEHS

The TEM images and the selected area electron diffraction patterns at 100 nm and 20 nm of PPy and doped PPy samples are shown in figure 3.8. The typical polymeric nature of PPy is clearly seen in figure 3.8 (a) and the TEM image and the SAED pattern demonstrate amorphous nature without any extent of crystallinity. The presence of dopant is obviously seen in the 100 nm and 20 nm scale images given in figure 3.8 (b). The globular structure of PPy has almost disappeared and it has acquired a sheet like structure. The SAED pattern shows some extent of crystallinity. that it has less crystallinity contrasted with [figures 3.8 (c) and (d)]. The TEM images at 100 nm and 20 nm scales along with SAED pattern given in figure 3.8 (c) of DBSA doped PPy shows that its structure has been much affected by doping. The globular structure of PPy has totally vanished and now a finlet like structure is visible over the sheets. The SAED pattern shows some crystalline spots along with the amorphous rings of PPy. The TEM images shown in figure 3.8 (d) of NaDEHS doped PPy likewise demonstrate that the globular structure has vanished totally. The impact of dopant has resulted in the creation of fragmented sheets or petals like structure for PPy and furthermore the presence of dopant is visible in the images at 100 nm and 20 nm scales. The dark region in the TEM images corresponds to the dopant present in PPy [30]. The bright spots in SAED pattern show that NaDEHS doping has imposed significantly the extent of crystallinity of doped PPy. These observations support the inferences obtained from the XRD and FESEM analysis.

3.4 Conclusions

Doped polypyrrole compositions with appreciable solubility in organic solvents are synthesized by chemical oxidative polymerization using ammonium persulfate as the oxidant and di (2-ethylhexyl) sulfosuccinic acid sodium salt (NaDEHS), dodecylbenzene sulfonic acid (DBSA) and dodecylbenzene sulfonic acid sodium salt (NaDBSA) as the dopants. The doped PPy powders show good solubility in m-cresol, NMP, DMF and DMSO and moderate solubility in dichloroethane and chloroform. The appreciable extent of solubility and processability acquired through doping and the enhanced crystalline order and electrical conductivity achieved consequently make the chemically synthesized polypyrrole, a prospective candidate for various device applications. The elemental analysis and FTIR spectroscopy studies demonstrate that dopants are effectively incorporated into the PPy structure. The significant degree of crystallinity achieved through doping by the amorphous PPy structure is evident from the XRD studies. The TGA results indicate the improved thermal stability of the doped PPy samples. The increase in the glass transition temperature and the melting temperature of the doped PPy samples, compared to pristine PPy, revealed by the DSC studies indicates the increased structural order in the doped PPy compositions. The FESEM and TEM studies confirm the significant impact of the dopants in modifying the morphology of PPy structure and the SAED patterns support the enhanced crystalline order of the doped PPy compositions. The present studies highlight the superb power of appropriate dopants to control the structural and morphological features of chemically synthesized polypyrrole and to offer means of

designing doped polypyrrole compositions with desired structural, electrical and optical characteristics suitable for different types of device applications.

References

[1] S. Bilal, M. Sohail, and A. A. Shah, Synthesis and Characterization of Soluble and Thermally Stable Polypyrrole-DBSA Salts, J.Chem. Soc. Pak., 36(6) (2014), 976–982

[2] N. Suhada, M. Tahiruddin, R. Daik, and B. Selangor, Synthesis and characterization of anionic surfactants doped polypyrrole, Der Pharma Chemica, 7(6) (2015) 159–162

[3] M. Gerard, A. Chaubey, and B. D. Malhotra, Application of conducting polymers to biosensors, Biosens. Bioelectron., 17(5) (2002) 345–359

[4] E. Ju, K. Sik, and A. G. Macdiarmid, High molecular weight soluble polypyrrole, Synth. Met., 125 (2002) 267–272

[5] C. Basavaraja, W. J. Kim, D. G. Kim, and D. S. Huh, Synthesis and characterization of soluble polypyrrole–poly(ε-caprolactone) polymer blends with improved electrical conductivities, Mater. Chem. Phys., 129(3) (2011) 787–793

[6] Y. Shen and M. Wan, Soluble Conductive Polypyrrole Synthesized By In Situ Doping with β-Naphthalene Sulphonic Acid, Polymer Chemistry, 35(17) (1997) 3689–3695

[7] J. Yue and A. J. Epstein, Synthesis of self-doped conducting polyaniline, J. Am. Chem. Soc., 112() (1990) 2800–2801

[8] S. Chen, L. Chien-Shiun, and How-an, Conductivity Relaxation and Chain Motions in Conjugated Conducting Polymers: Neutral Poly(3-alkylthiophenes), Macromolecules, 26 (1993) 2810–2816

[9] E. Zeglio, M. Vagin, C. Musumeci, F. N. Ajjan, R. Gabrielsson, X. T. Trinh, N. T. Son, A. Maziz, N. Solin, and O. Inganäs, Conjugated Polyelectrolyte Blends for Electrochromic and Electrochemical Transistor Devices, Chem. Mater., 27(18)(2015) 6385–6393

[10] W. Wang, D. Yu, and F. Tian, Photoluminescence of a soluble polypyrrole based on N-vinylpyrrole, J. Lumin., 130(3) (2010) 494–497

[11] K. S. Jang, H. Lee, and B. Moon, Synthesis and characterization of water soluble polypyrrole doped with functional dopants, Synth. Met., 143(3) (2004) 289–294

[12] P. Jayamurgan, V. Ponnuswamy, S. Ashokan, and T. Mahalingam, The effect of dopant on structural , thermal and morphological properties of DBSA-doped polypyrrole, Iranian Polymer Journal, 22(3) (2013). 219–225

[13] H. K. Lim, S. O. Lee, K. J. Song, S. G. Kim, and K. H. Kim, Synthesis and properties of soluble polypyrrole doped with dodecylbenzenesulfonate and combined with polymeric additive poly(ethylene glycol), J. Appl. Polym. Sci., 97(3) (2005) 1170–1175

[14] M. Trchova and J. Kova, Synthesis and structural study of polypyrroles prepared in the presence of surfactants, Synth. Met., 138(3) (2003) 447–455

[15] S. Deivanayaki, V. Ponnuswamy, R. Mariappan, and P. Jayamurugan, Synthesis and characterization of polypyrrole/TiO2 composites by chemical oxidative method, Optik (Stuttg)., 124(12) (2013) 1089–1091

[16] M. Taunk and S. Chand, Chemical synthesis and charge transport mechanism in solution processed flexible polypyrrole films, Mater. Sci. Semicond. Process., 39 (2015) 659–664

[17] H. K. Chitte, Synthesis of Polypyrrole Using Ammonium Peroxy Disulfate (APS) as Oxidant Together with Some Dopants for Use in Gas Sensors, Mater. Sci. Appl., 2(10) (2011) 1491–1498

[18] Ghalib, H.; Abdullah, I.; Daik, R., Electrical Conductivity of Anionic Surfactant- Doped Polypyrrole Nanoparticles Prepared via Emulsion Polymerization, Pertanika Journal of Science and Technology 21(2) (2013) 459-472

[19] M. A. Chougule, S. G. Pawar, P. R. Godse, R. N. Mulik, S. Sen, and V. B. Patil, Synthesis and Characterization of Polypyrrole (PPy) Thin Films, Soft Nanosci. Lett., v 1(1) (2011) 6–10

[20] T. Ishak, T. Kudin, M. Zu, and A. Yahya, Synthesis and Characteristics of Conducting Polymer- Based Polypyrrole in Different Solvents, Journal of Materials Science and Engineering, 2(2) (2012) 190–195

[21] N. Su, Synthesis and characterization of polypyrrole doped with anionic spherical polyelectrolyte brushes, Express Polym. Lett., 6(9) (2012) 697–705

[22] H.-W. R. Jang, Kwan SikMin-Kyu Songa, Young-Taek Kima, Bum-Seok Kimb, Jinhwan Kimc, Kookheon Chard, A, H. Lee, and B. Moon, Synthesis and characterization of soluble polypyrrole doped with alkylbenzenesulfonic acids , Synth. Met., 141(3) (2004) 315–319

[23] S. Bilal, F. Perveen, and A. A. Shah, Chemical synthesis of polypyrrole doped with dodecyl benzene sulfonic acid, Journal of Scientific and Innovative Research, 4(1) (2015 33–42

[24] Pullarkat P. Jeeju, Sreekanath J. Varma, S. Jayalekshmi, Novel polypyrrole films with excellent crystallinity and good thermal stability, Materials Chemistry and Physics, 134(2-3) (2012) 803-808

[25] M. Sohail, S. Bilal, and A. A. Shah, Synthesis and characterization of completely soluble polypyrole salts via inverse emulsion polymerization using a mixture of chloroform and 2- butanol as a dispersing medium, JPMS Conference Issue Materials, (2011) 12–15

[26] S. T. Navale, A. T. Mane, A. A. Ghanwat, A. R. Mulik, and V. B. Patil, Camphor sulfonic acid (CSA) doped polypyrrole (PPy) films : Measurement of microstructural and optoelectronic properties, Measurement, 50 (2014) 363–369

[27] A. Reung-u-rai, A. Prom-jun, and W. Prissanaroon-ouajai, Synthesis of Highly Conductive Polypyrrole Nanoparticles via Microemulsion Polymerization, Journal of Metals, Materials and Minerals, 18(2) (2008) 27–31

[28] S. Shrikrushna and J. A. K. Milind V Kulkarni, Influence of Dodecylbenzene Sulfonic Acid Doping on Structural, Morphological, Electrical and Optical Properties on Polypyrrole/3C-SiC Nanocomposites, J. Nanomed. Nanotechnol., 6(5) (2015) 3–7

[29] P. Jayamurugan, V. Ponnuswamy, S. Ashokan, R. N. Jayaprakash, and N. Ashok, DBSA doped polypyrrole blended with Poly (4-styrenesulfonic acid) by mechanical mixing , Materials Science-Poland, 32(4) (2014) 648–651

[30] C. Basavaraja, W. J. Kim, P. X. Thinh, and D. S. Huh, Electrical conductivity studies on water-soluble polypyrrole-graphene oxide composites, Polym. Compos., 32(12) (2011) 2076–2083

…..ꕥ…..

Chapter 4

STUDIES ON DBSA DOPED POLYPYRROLE/GRAPHENE NANOCOMPOSITE FILMS GROWN BY SPIN COATING AND ELECTRO-SPRAYING

This chapter illustrates the studies on DBSA doped, polypyrrole/graphene nanocomposite films coated on glass substrates by spin coating and electro-spraying. The solutions of the doped polymer/graphene nanocomposite are obtained in different solvents including dimethylformamide (DMF), dimethyl sulfoxide (DMSO), N-Methyl-2-pyrrolidone (NMP) and meta-cresol (m-cresol). Thin films of DBSA doped, PPy/graphene nanocomposites are obtained on glass substrates by spin coating using the solutions in different solvents. Attempts are made to improve the solubility of the doped PPy/graphene composite in m-cresol, by subjecting the solution in m-cresol to electro-spraying for two different concentrations of graphene. The structural, morphological, optical, and electrical properties of spin coated and electro-sprayed films of doped PPy/graphene nanocomposite are investigated in detail.

4.1 Introduction

Polypyrrole, as explained earlier is a conjugated polymer, widely studied in bulk and thin film forms and is endowed with many meritorious properties suitable for device applications in many arenas of technology [1]. Additionally, polymer blends based on PPy can be used as protective covers to shield metals from corrosion. Because of the solid

bonding of PPy to iron or steel treated with nitric acid, it can be used to make good adhesives [2]. In order to improve the mechanical strength and the electrical transport properties of PPy to make it suitable for specific applications, different composites of PPy with metals, metal oxide nanoparticles and various carbon nanostructures have been developed and are being subjected to extensive studies [3]. A major limitation in pragmatic utilizations of PPy comes from the lack of solubility in common solvents. In order to improve the solubility of PPy. suitable dopants like dodecylbenzenesulfonic acid, camphor sulfonic acid and sodium dodecyl sulphate can be used, as explained in the previous chapter [4].

The composites of PPy with graphene, endowed with the meritorious properties of both PPy and graphene are quite interesting materials for many technological applications [5]. The work presented in this chapter is related to the studies on the nanocomposite films of DBSA doped PPy/graphene, grown on glass substrates using spin coating and electro-spraying techniques.

Spin coating technique is widely utilized in the making of integrated circuits, optical mirrors, color television screens and magnetic disks for data storage and the quality of the resulting films depends on the spin speed and the viscosity of the precursor solutions [6,7]. The solubility of DBSA doped PPy/graphene composite in m-cresol is found to be much better compared to that in other solvents. Hence, thin films of DBSA doped PPy/graphene composite are also grown by electro-spraying its solution in m-cresol and this method is expected to generate

narrow size distributions of sub-micrometric particles, with restricted agglomeration of particles [8] and good reproducibility of the growth conditions.

4.2 Materials and methods

Pyrrole monomer of 98% purity, purchased from Aldrich Chemicals was purified by distillation before use. Graphene and the other chemicals used for the synthesis of doped PPy and doped PPy/graphene composite were purchased from Sigma-Aldrich and were used without further purification.

4.2.1 Synthesis of DBSA doped PPy

Polypyrrole, doped with DBSA, having appreciable solubility in organic solvents was synthesized, employing chemical oxidative polymerization method using the oxidant, ammonium persulfate (APS), as explained in the previous chapter. The DBSA doped polypyrrole in the form of dried powder was used to make the composite with graphene.

4.2.2 Synthesis of DBSA doped, PPy/graphene nanocomposite and the film growth by spin coating

The DBSA doped, PPy powder of quantity around 4 weight % was blended with 2 weight % of graphene and dissolved in various solvents like DMSO, DMF, NMP and m-cresol and all the solutions were kept under continuous stirring for 48 hours until homogeneous compositions were formed. These homogeneous solutions were used for spin coating of the nanocomposite films on glass substrates using the

HO-THS-05 Holmarc Opto-Mechatronics spin coating machine, at a spin speed of 1000 rpm with acceleration of 600 rpm/s and total spin time around 30 seconds at room temperature.

4.2.3 Coating of DBSA doped, PPy/graphene nanocomposite films by electro-spraying

From the homogeneous solutions of DBSA doped, PPy/graphene composite in four different solvents, it was found that better dispersion of the nanocomposite was obtained in m-cresol. Two ideal concentrations of graphene of 1 weight % and 2 weight % were used to make the composite with DBSA doped PPy and these composite samples were labelled as PPyE1 and PPyE2. The solutions of these composites in m-cresol were subjected to sonication for 48 hours for acquiring consistency. The solutions of PPyE1 and PPyE2 composites in m-cresol were electro-sprayed at 28°C and 40 % relative humidity in an electro-spinning chamber. A nozzle with inner diameter of 14.5 mm was set horizontally on a syringe pump of model HO-SPLF-04 against a HO-MR-01 mandrel rotator. Glass substrates were attached to the grounded target to collect the electro-sprayed nanocomposite films.

The infrared spectra of the spin coated and electro-sprayed nanocomposite films were recorded using Thermo Nicolete Avatar 370 DTGS model Fourier transform IR (FTIR) spectrometer in the wavenumber range of 400–4000 cm^{-1}. The XRD patterns were obtained using the Rigaku Dmax C diffractometer with Cu Kα radiation of wavelength 1.54 Å. Ultraviolet-visible absorption spectra of the films were recorded using Jasco V 570 UV-Vis-NIR spectrophotometer. The DC

electrical conductivity studies were done utilizing four probe method. Raman spectra were recorded using the Horiba LabRam (800 mm) HR spectrometer equipped with a 514 nm Argon ion laser of 15 mW power. The FESEM images of the nanocomposite samples were obtained using Carl-Zeiss Sigma 250 electron microscope and the TEM patterns, using Jeol/JEM 2100 model.

4.3 Results and discussions

4.3.1 FTIR spectral analysis

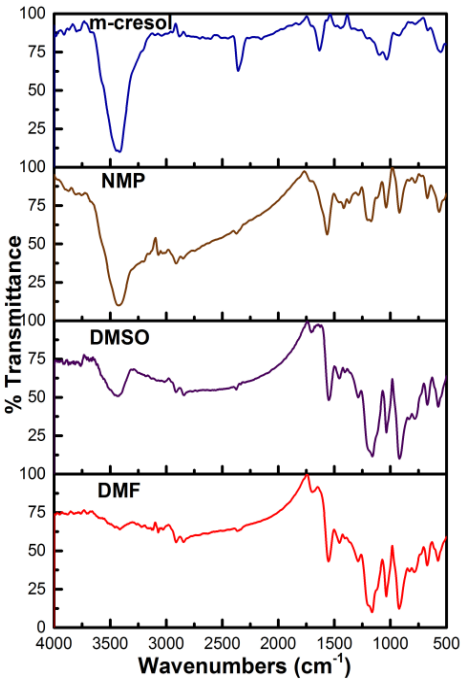

Figure 4.1. (a) FTIR spectra of spin coated, DBSA doped PPy//graphene composite films using different solvents

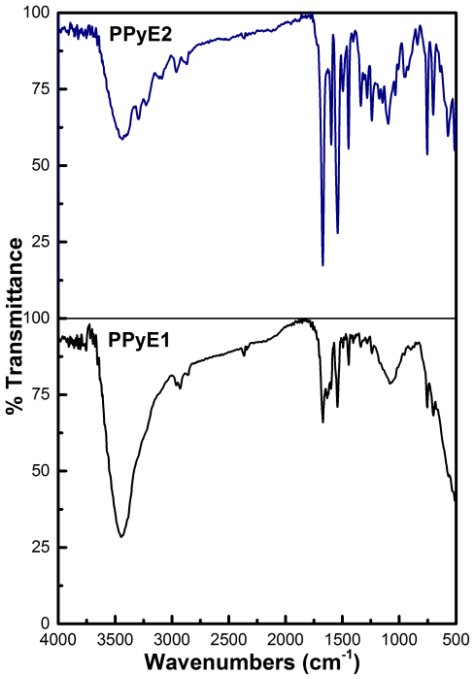

Figure 4.1. (b) FTIR spectra of electro-sprayed, DBSA doped PPy/graphene composite films using m-cresol

The FTIR spectra of spin coated films of DBSA doped PPy/graphene nanocomposite using different solvents like DMF, DMSO, NMP and m-cresol are shown in figure 4.1 (a) and those of the electro-sprayed films using m-cresol in figure 4.1 (b) respectively. For the spin coated films, all the characteristic peaks of DBSA doped PPy are observed in agreement with the results on the FTIR spectral analysis of the DBSA doped PPy, discussed in the previous chapter [9, 10, 11, 12, 13, 14, 15]. The presence of graphene in the DBSA doped PPy/graphene composite results in the slight shifting of the characteristic peaks of the DBSA doped PPy to lower wavenumbers. This is an indication of the association of graphene to the NH functional group of PPy backbone [16,17].

Compared with the spin coated films, more broad peaks are seen in the electro-sprayed films with two different graphene concentrations. The peaks at 3444 cm^{-1} in PPyE1 and at 3436 cm^{-1} in PPyE2 represent the N-H stretching vibrations of polypyrrole. The new peaks at 3293 cm^{-1}, 3219 cm^{-1} and 3084 cm^{-1} seen in PPyE2 are related to the homogeneous dispersion of graphene in the solvent. These peaks are not appearing in PPyE1, because of the reduced graphene concentration. The presence of new frequencies, changes in frequency positions and band expansion in PPyE2 can be ascribed to the increased interaction of polypyrrole with graphene in this composite [18] sample. The broad peak at 1672 cm^{-1} in PPyE2 and the narrow peak at 1670 cm^{-1} in PPyE1 represent the carbonyl C=O stretching vibration. The peaks from 1097 cm^{-1} to 1404 cm^{-1} in PPyE2 and the one at 1080 cm^{-1} in PPyE1 are related to COH/COC (epoxy) functional group vibrations [17]. All the characteristic peaks of

the spin coated films of DBSA doped PPy/graphene composite also appear in the electro-sprayed films but with shifts in peak positions and with more peak intensity. The characteristic peaks of polypyrrole can be distinguished in both the spin coated and electro-sprayed films, which is an indication that the completed polymerization process is retained in the presence of graphene, without structural disorders for PPy. The FTIR spectral studies of both types of the composite films confirm the effective incorporation of graphene within the polypyrrole structure [19].

4.3.2 XRD analysis

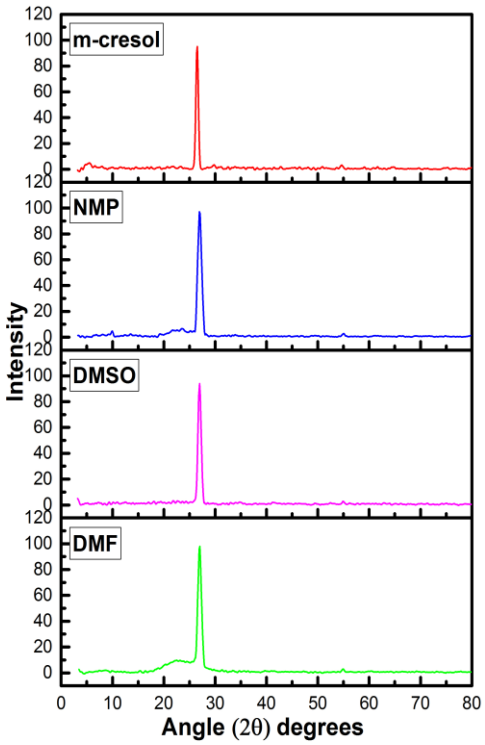

Figure 4.2. (a) XRD patterns of spin coated, DBSA doped, PPy/graphene composite films

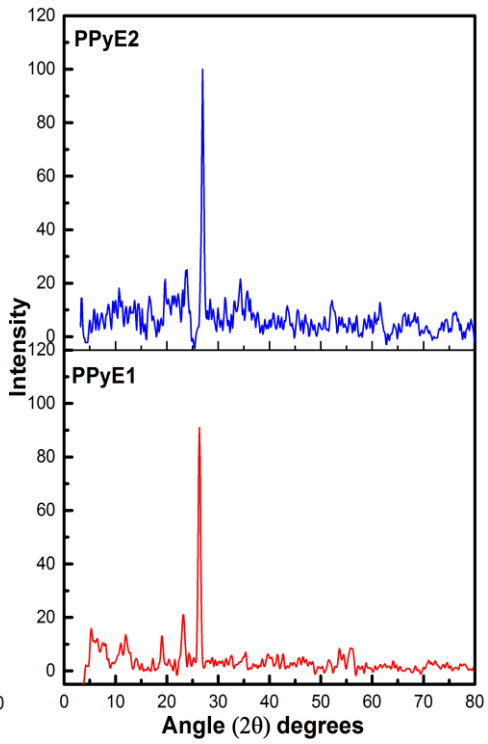

Figure 4.2. (b) XRD patterns of electro-sprayed films of DBSA doped, PPy/graphene composite

The XRD patterns of spin coated and electro-sprayed films of DBSA doped, PPy/graphene composite are shown in figures 4.2 (a) and (b) respectively All the four spin coated films demonstrate very intense and narrow peak at 26.9^0 with additional intense diffraction peaks at 44.7^0 and 54.8^0 matching the (002), (101) and (004) planes of hexagonal system which is a clear indication of the presence of graphene in the composite films [20]. The d spacing values for the peaks at 26.9^0, 44.7^0 and 54.8^0 are 3.32 A^o, 2.03 A^o and 1.67 A^o respectively. The sharp peaks at 31.8^0 and 32.7^0 are also due to the presence of graphene indicating a highly ordered structure for the nanocomposite [21]. The presence of the narrow and sharp peaks between 30^o to 60^o in all the four spin coated films illustrates the presence of crystalline domains within the amorphous PPy structure. The uniform incorporation of the dopant DBSA within the PPy matrix can also be confirmed from the presence of these crystalline phases [22].

The XRD patterns of the electro-sprayed films of the nanocomposite with two different graphene concentrations also show crystalline nature. The strong and sharp diffraction peaks at 26.4^0 in PPyE1 and at 26.9^0 in PPyE2 can be assigned to the high crystalline structure of graphene [23]. The sharp peaks from 12.2^o to 23.4^o in PPyE1 and from 10.8^o to 23.9^o in PPyE2 reveal the crystalline nature of DBSA doped polypyrrole films [24]. The peaks at 23.4^o and 43^o in PPyE1 and at 23.9^o and 43.3^o in PPyE2 represent the broad reflection peaks of graphene [25].The XRD patterns of the electro-sprayed films are similar to those of the spin coated films, but the intensity of the diffraction peaks is higher in the

former case compared to the latter. The peak intensity also increases with the increase in graphene concentration in the composite films due to the enhanced semi-crystalline nature of the resulting doped PPy composition. The XRD studies of the DBSA doped, PPy/graphene nanocomposite films indicate that by doping amorphous PPy with DBSA and making composites with graphene by ex situ polymerization, polypyrrole based nanocomposites films with appreciable crystalline nature can be grown on suitable substrates.

4.3.3 UV-Visible absorption studies

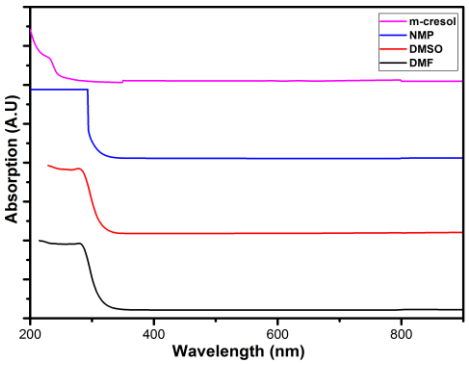

Figure 4.3. (a) UV-visible absorption spectra of spin coated, DBSA doped PPy/grapheme composite films using different solvents

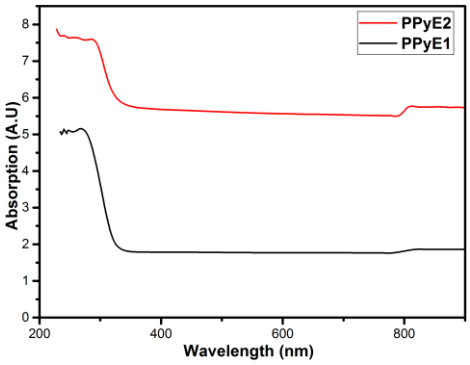

Figure 4.3. (b) UV-visible absorption spectra of electro-sprayed, DBSA doped, Py/graphene composite films using m-cresol

The UV-Visible absorption spectra of spin coated and electro-sprayed films of DBSA doped, PPy/graphene nanocomposite films are shown in figures 4.3(a) and (b) respectively. The small shoulder peaks seen at 218 nm and 239 nm for the spin coated films in DMF and DMSO

are attributed to π-π* transition of the benzenoid ring in PPy chain [26]. The shoulder peaks displayed at 382 nm in DMF, DMSO and NMP and at 350 nm in m-cresol are ascribed to the polaronic transition and the peaks observed at 810 nm, 789 nm, 799 nm and 797 nm in DMF, DMSO, NMP and m-cresol respectively are attributed to the bipolaronic transitions [27]. Both these transitions are associated with the doping level of PPy which represents the protonation stages of PPy chain. The doped state of PPy facilitates easier electron transport due to the small energy gap and thus the electrical conductivity increases. The presence of charge carriers like polarons and bipolarons in DBSA doped, PPy/graphene composite is an affirmation that PPy has been effectively doped with DBSA. The enhanced conductivity of doped polypyrrole is a consequence of band gap reduction due to the formation of polaron and bipolaron levels within the band gap [28].

The electro-sprayed films with two different graphene concentrations demonstrate more absorption bands and new absorption shoulders with slight increase in intensity. The UV-visible absorption spectra of the electro-sprayed films of DBSA doped, PPy/graphene composite show UV absorption peak at 240 nm in PPyE1 and at 259 nm in PPyE2 which correspond to the π-π* transition of the benzenoid ring in PPy chain. The polaronic and bipolaronic transitions can be observed at 376 nm and 378 nm and at 788 nm and 813 nm in PPyE1 and PPyE2 respectively. This indicates the characteristic red shift of PPyE2 peaks compared to PPyE1 peaks, observed in the polaron and bipolaron ranges on increasing the graphene concentration which can be attributed to the extended

conjugation length resulting from the π-π* stacking between the polymer backbone and graphene [25].

4.3.4 Solubility and Conductivity

Table 4.1 Solubility and conductivity of spin coated, DBSA doped, PPy/graphene composite films using various solvents

Solvents	Solubility (weight % per volume)	Conductivity (S/cm)
m-cresol	≈ 9	7.4×10^{-1}
NMP	≈ 8	3.2×10^{-1}
DMSO	≈ 8	1.5×10^{-1}
DMF	≈ 7	0.9×10^{-1}

Table 4.2 Solubility and conductivity of electro-sprayed, DBSA doped, PPy/graphene composite films using m-cresol

Samples	Solubility (weight % per volume)	Conductivity (S/cm)
PPyE2	≈ 10	4.2
PPyE1	≈ 9	2.5

The solubility of the synthesized DBSA doped, PPy/graphene nanocomposite was checked by dissolving it in various common organic solvents. The solubility of the nanocomposite in DMF, DMSO, NMP and m-cresol solvents and the room temperature conductivity of the spin coated films of the nanocomposite are shown in Table 4.1 The DBSA doped, PPy/graphene nanocomposite shows good solubility in the four solvents because of the presence of long alkyl chain-containing dopant

which sufficiently diminishes the intermolecular and intramolecular interactions and the crosslinking among the PPy chains [29].The solubility of DBSA doped, PPy/graphene nanocomposite in m-cresol for two different graphene concentrations, PPyE1 and PPyE2 and the room temperature conductivity of the electro-sprayed films of the two nanocomposite samples are shown in Table 4.2. The incorporation of the dopant DBSA in the polymerization process of PPy to form DBSA doped PPy and the DBSA doped PPy/graphene composite increases the solubility of the composites, significantly. The good solubility of the nanocomposite in polar solvents is mainly because of the high polarity indices ranging from 6.7 to 7.4 which help to develop strong hydrogen bonds with the polymer [30].

From Tables 4.1 and 4.2, one can see that the spin coated and electro-sprayed films of the nanocomposite dissolved in m-cresol show the highest electrical conductivity compared to the films of the composite dissolved in other solvents. Results also indicate that the room temperature electrical conductivity of the electro-sprayed films of the composite is higher compared to the spin coated films of the composite. In the electro-sprayed films of the composite, the conductivity increases with increase in the concentration of graphene and the maximum conductivity of 4.2 S/cm has been obtained for the film, PPyE2. The role of graphene in enhancing the electrical conductivity of the spin coated and the electro-sprayed films of the DBSA doped, PPy/graphene composite is in facilitating π– π^* interactions among graphene and the DBSA doped PPy which improve the probable conductive pathways for the electrical charges. The

enhanced electrical conductivity attained by the incorporation of graphene into DBSA doped PPy, is, related to the expansion of conjugation chain length induced due to the presence of graphene [27].

4.3.5 Raman spectroscopy studies

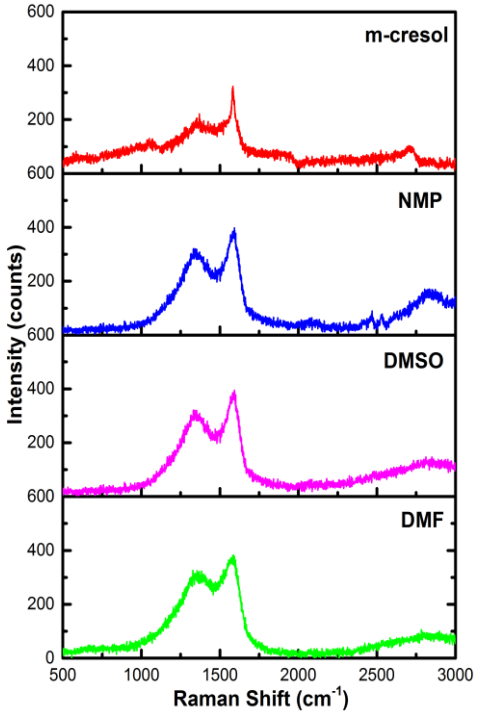

Figure 4.4 (a) Raman spectra of spin coated films of DBSA doped,, PPy/graphene composite

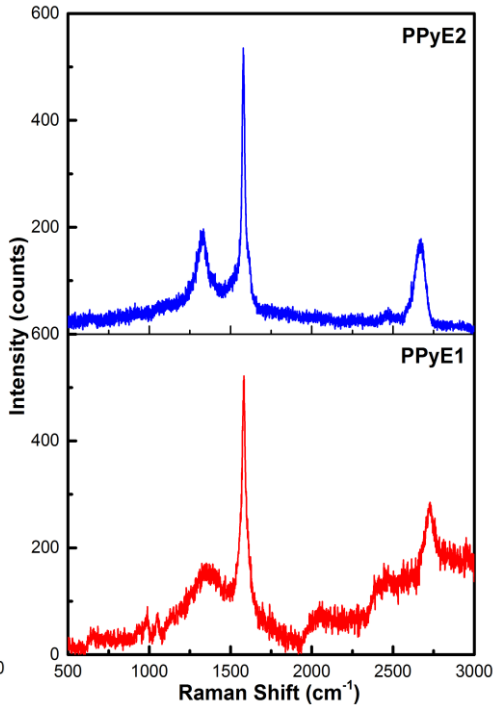

Figure 4.4 (b) Raman spectra of electro-sprayed, DBSA doped, PPy/graphene composite films

Raman spectra of spin coated films of the DBSA doped, PPy/graphene composite dissolved in various solvents and the spectra of electro-sprayed films of the composite dissolved in m-cresol are shown in figures 4.4 (a) and 4.4 (b) respectively. The characteristic Raman peaks of spin coated films are observed as the G bands appearing at

1591 cm^{-1}, 1582 cm^{-1}, 1586 cm^{-1} and 1597 cm^{-1} related to the solvents, DMF, DMSO, NMP and m-cresol, respectively. The disorder-induced D bands can be seen at 1373 cm^{-1}, 1365 cm^{-1}, 1345 cm^{-1} and 1354 cm^{-1} related to the solvents, DMF, DMSO, NMP and m-cresol respectively [31]. The G band is a direct result of the bond stretching of all pairs of sp^2 carbon atoms in both the rings and the chains. The D band is related to deformities, edge impacts and dangling sp^2 carbon atoms that break the symmetry [32]. Raman spectra of spin coated films show variations in relative intensities of the G and D bands, produced by changing the solvents. The intensities of the G band marginally increase and the intensities of the D band diminish by changing the solvent from DMF to m-cresol while no 2D range peaks have been observed. The intensity ratio of the D and G bands appraises the imperfections of graphene based samples where a higher proportion guarantees more deformities on graphene. The intensity ratio of D to G bands in the spin coated films from DMF, DMSO, NMP and m-cresol are calculated to be 0.848, 0.823, 0.807 and 0.647 respectively. The decrease in the I_D/I_G when the solvent is changed from DMF to m-cresol is a clear indication of the improvement in the conjugated structure of PPy, extension of the molecular chains and the decrease in the level of imperfections subsequent to the doping of PPy with DBSA and the forming of the DBSA doped, PPy/graphene composite [33,34].

The spectra of the electro-sprayed films of PPyE1 and PPyE2 shown in figure 4.4(b) clearly exhibit the awesome G bands with high intensity and typically weak D bands. Additionally, the presence of 2D band is frequently utilized as an affirmation for a high quality, defect

free graphene sample and also is a confirmation for the presence of graphene in the DBSA doped,PPy/ghaphene nanocomposite. In PPyE1 and PPyE2 films the peaks at 1593 cm^{-1} and 1577 cm^{-1} correspond to the G bands and the ones at 1364 cm^{-1} and 1325 cm^{-1} to the D bands respectively. The peaks observed at 2742 cm^{-1} and 2676 cm^{-1} in PPyE1 and PPyE2 films respectively represent the 2D bands or the overtones of the D band. The 2D band appears as a strong band in graphene and it does not represent defects [35]. The presence of PPy in the composite is revealed by the small peaks at 1059 cm^{-1}, 1027 cm^{-1} , 988 cm^{-1}, 983 cm^{-1}, 950 cm^{-1} , 938 cm^{-1} and 928 cm^{-1}. The peaks at 928 cm^{-1}, 938 cm^{-1}, 950 cm^{-1}, 983 cm^{-1} and 988 cm^{-1} are related to the bipolaron and polaron structure of PPy [33].

The I_D/I_G for the electro-sprayed film, PPyE2 is 0.363 and that for PPyE1 is 0.297.The increase of the I_D/I_G for the former is due to the increase in the concentration of graphene in that film, which leads to the more ordered arrangement of extended conjugation length of the PPy backbone [27]. In other words, the electro-sprayed films become structurally more ordered with increase in graphene concentration. This conclusion based on the Raman spectral analysis of the electro-sprayed films of the nanocomposite supports the earlier observations on the basis of the XRD studies and the observed improvement in electrical conductivity of the electro-sprayed films.

4.3.6 Microstructure analysis-FESEM studies

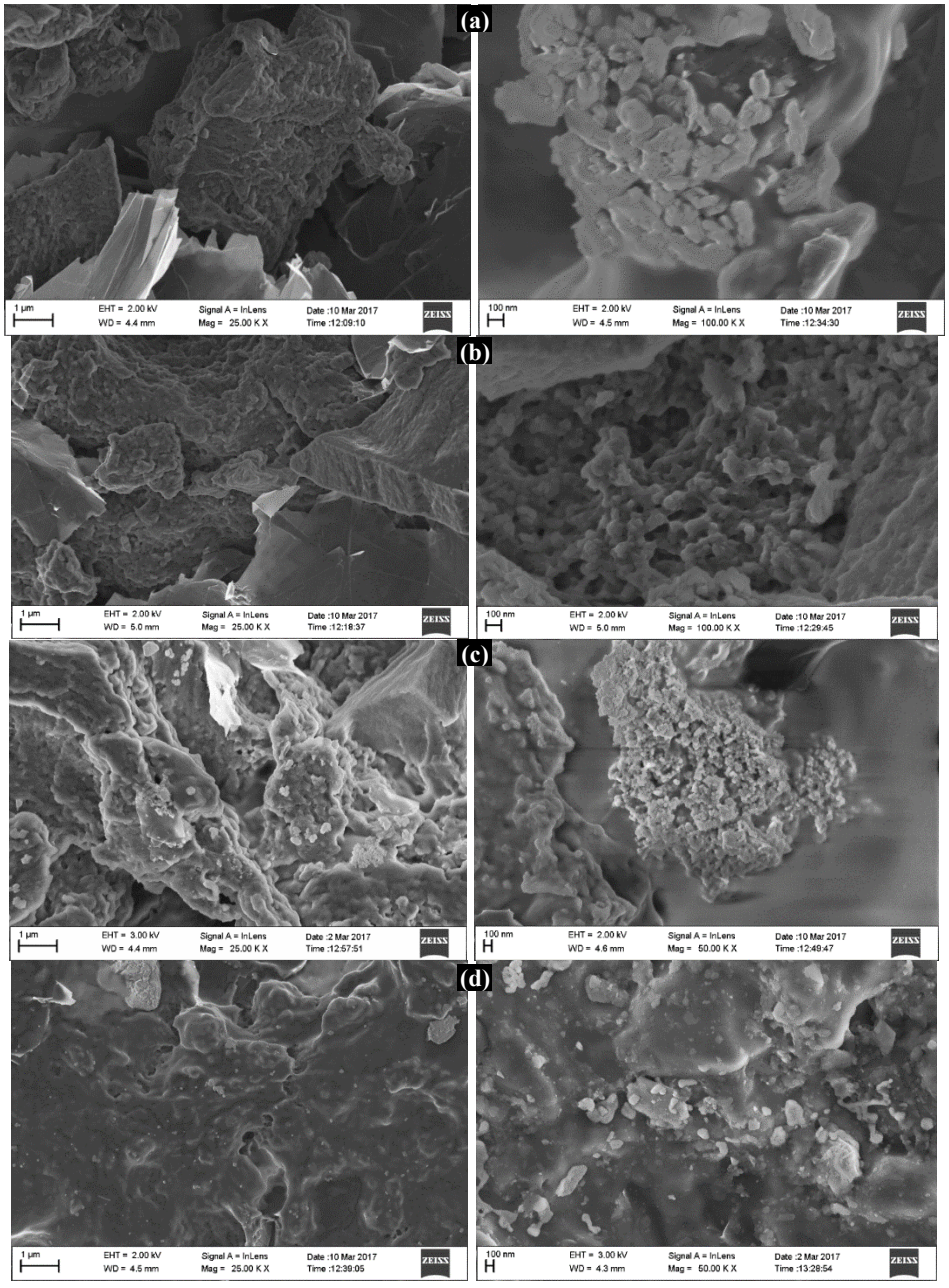

Figure 4.5 FESEM images of the spin coated films of the DBSA doped, PPy/graphene nanocomposite dissolved in (a) DMF (b) DMSO (c) NMP and (d) m-cresol

The FESEM images of the spin coated and electro-sprayed films of the DBSA doped, PPy/graphene nanocomposite, grown using different solvents are shown in figures 4.5 and 4.6 respectively. Surface morphology of the spin coated films prepared from the solvents DMF, DMSO, NMP and m-cresol seems to be quite different, depending upon the solvents used. Both graphene and DBSA doped PPy are seen separately without effective blending in figure 4.5(a) which points towards the non-uniform dispersion of graphene and DBSA doped PPy in DMF. In figure 4.5. (b), the presence of doped PPy and graphene can be clearly seen. Granular form of PPy due to the dopant DBSA [36] and the layered graphene structure are noticeable independently. FESEM images of the film of the composite dissolved in NMP, shown in figure 4.5 (c) demonstrate that graphene sheets coated with PPy can be clearly observed from the magnified image of this film. Increased dissolution of PPy and uniform dispersion of graphene in NMP has resulted in the development of a superior composite in contrast with the situations of the films cast from the solvents DMSO and DMF. The formation of a fine composite of graphene and DBSA doped PPy can be visualized in the images shown in figure 4.5 (d) which belong to the films of the nanocomposite cast from the solvent, m-cresol. Graphene layers are noticeable within the DBSA doped PPy matrix. The composite formation is in such a way that graphene is covered with doped PPy. The increased dissolution of doped PPy in m-cresol and the uniform dispersion of graphene in it are the favourable factors for the formation of well blended composite. The wrinkled graphene sheets related with the coverage of PPy are

observed in all the FESEM images of the polymer composite [37]. The FESEM studies additionally propose that on the addition of graphene to the DBSA doped PPy, the doped polymer can steadily hold onto the surface of graphene on account of the electrostatic attraction between doped PPy and graphene [38].

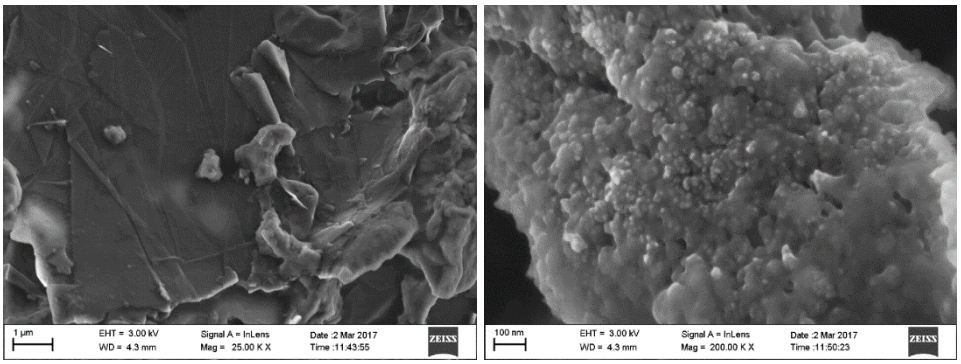

(a)

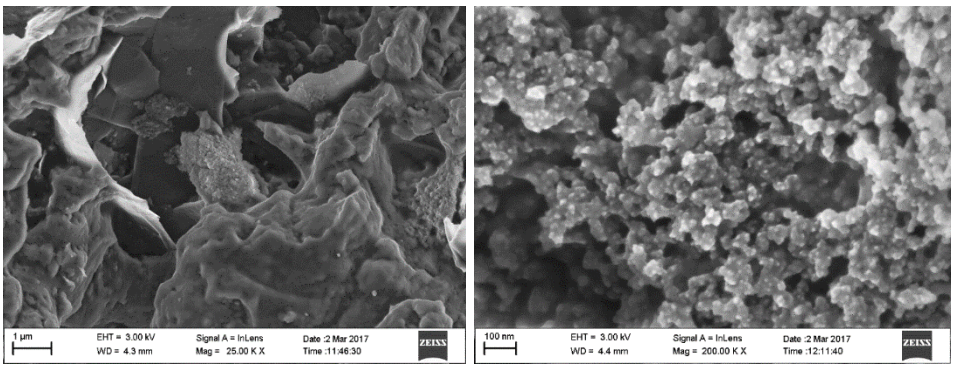

(b)

Figure 4.6 FESEM images of the electro- sprayed films of DBSA doped, PPy/graphene composite, dissolved in m-cresol (a) PPyE1 (b) PPyE2

In the images at 1 μm scale of both the films, the presence of DBSA doped PPy and graphene is clearly perceptible. The formation of a perfectly blended composite relies upon the solubility and dispersivity of the components in the solvent. Through the procedure of electro-spraying, it is feasible to get uniform beaded nano structures by optimizing the solution properties. In the present case, m-cresol is used to dissolve the DBSA doped, PPy/graphene composite. The presence of DBSA enhances the dissolution of PPy in the solvent. In the low resolution images at 1um scale of both PPyE1 and PyYE2, the formation of PPy/graphene composite is clearly visible. The globular structure of both the film samples can be found in the 100 nm scale images. In the image at 100 nm scale of PPyE1, it is seen that a bead like structure of the composite has been formed [39]. The beads are somewhat uniform and distinct. The image at 100 nm scale of PPyE2 clearly shows the formation of interconnected bead like structure of the doped PPy/graphene composite. This high resolution image shows, doped PPy in the form of nanobeads, being uniformly embedded on the surface of graphene [40].

4.3.7 Microstructure analysis-TEM studies

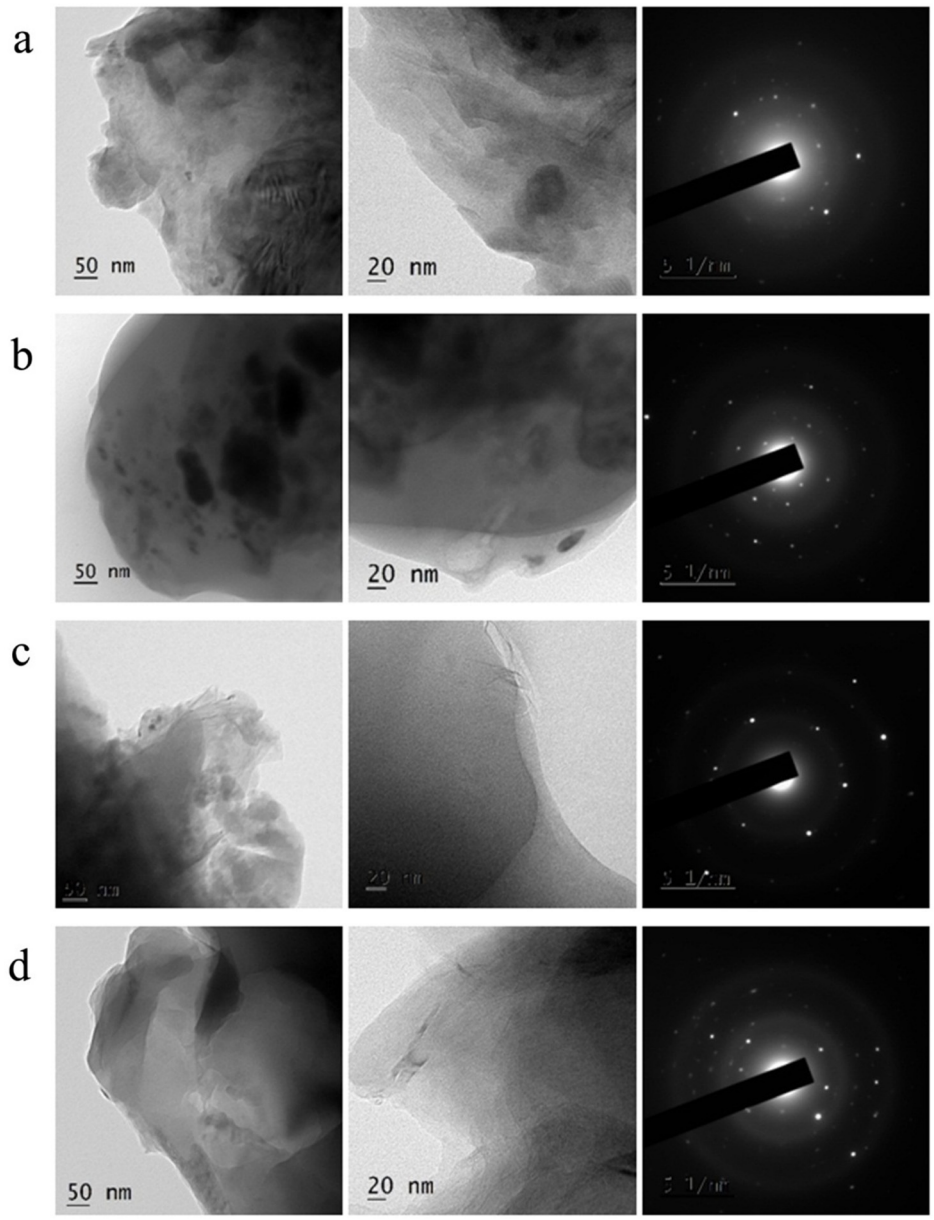

Figure 4.7 TEM images and SAED patterns of the spin coated films of the DBSA doped, PPy/graphene composite dissolved in (a) DMF (b) DMSO (c) NMP and (d) m-cresol

The TEM images and the selected area electron diffraction patterns at 50 nm and 20 nm of the spin coated films of the doped PPy/graphene composite, dissolved in various solvents are shown in figure 4.7. The images of the spin coated films show the presence of graphene sheets and an interconnection between graphene and the doped polymer [41]. The TEM images of the films of the nanocomposite dissolved in DMF, shown in figure 4.7 (a), illustrate that the composite formation is not so fine. The graphene layers are visible inside the doped PPy matrix. The surface morpholgy is not uniform, due to low dispersion of the doped PPy and graphene in the solvent.The SAED pattern also shows the presence of both grpahene and PPy. It is evident from the 20 nm scale image of the film of the nanocomposite dissolved in DMSO, shown in figure 4.7.(b) that graphene and the doped PPy have been blended into a fine composite. The SAED pattern contains bright spots, illutrating the presence of crystalline graphene. The diffused rings seen in the SAED pattern confirm the presence of amorphous PPy. The layers seen in the 20 nm scale image of the film of the nanocomposite dissolved in NMP,shown in figure 4.7 (c) are those of graphene. The bright spots along with diffused rings in the SAED pattern of the film are due to the presence of graphene and the doped polymer PPy in the composite. From the TEM images of the films of the nanocomposite dissolved in m-cresol,shown in figure 4.7 (d) , the fine blending of the components, graphene and the DBSA doped PPy in the nanocomposite can be established. The graphene layers inside the doped PPy are clearly visible in the 20 nm scale image. With the addition of graphene to the DBSA doped PPy dissolved in the four solvents, the doped polymer can

steadily hold onto the surface of graphene due to the electrostatic attraction between the doped PPy and graphene [38]. The bright spots and the diffused rings present in the SAED patterns support the findings.

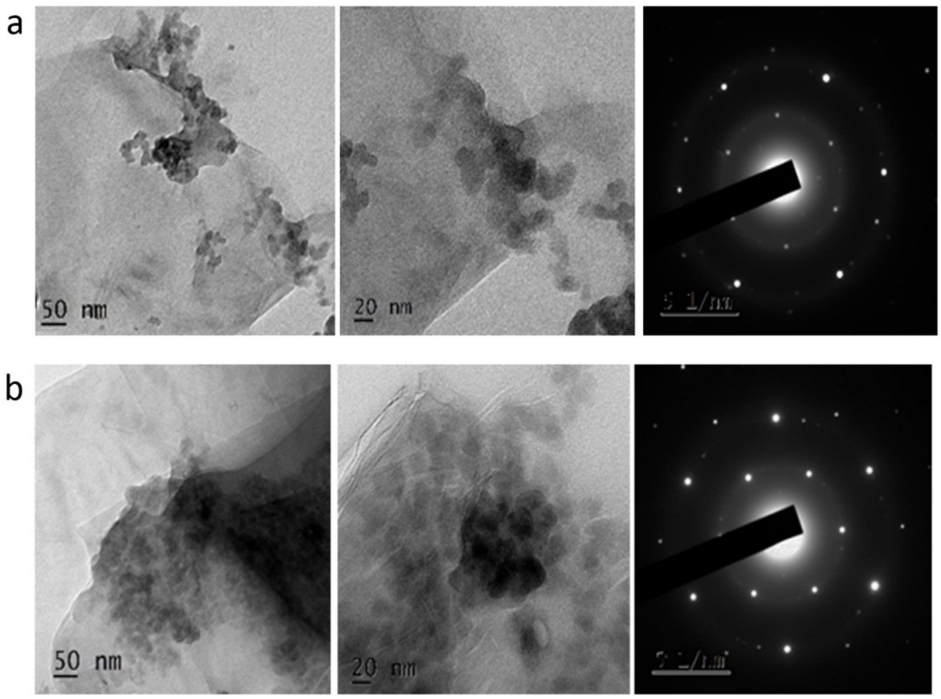

Figure 4.8 TEM images and SAED patterns of the electro-sprayed films of the DBSA doped, PPy/graphene nanocomposite dissolved in m-cresol (a) PPyE1; (b) PPyE2

The TEM images and the selected area electron diffraction patterns at 50 nm and 20 nm of the electro-sprayed films of the doped PPy/graphene nanocomposite, dissolved in m-cresol are shown in figure 4.8. The graphene layers are clearly visible and doped PPy is seen covering the graphene layers in the images shown in figure 4.8 (a). In the SAED patterns, the bright spots represent the presence of graphene and the diffused rings, that of doped PPy. The TEM images of the

electro-sprayed film of PPyE2 shown in figure 4.8.(b), obviously demonstrate that the mixing of graphene and the doped PPy has happened quite effectively in the formation of the composite PPyE2. The graphene layers are visible inside the doped PPy matrix. The selected area electron diffraction patterns of the electro-sprayed films show more crystalline nature than those of the spin coated films and the extent of crystallinity of PPyE2 sample is higher than that of PPyE1 because of the higher concentration of graphene.

4.4 Conclusions

Polypyrrole (PPy) with appreciable solubility in organic solvents was synthesized by chemical oxidative polymerization with dodecylbenzene sulfonic acid (DBSA) as dopant and ammonium persulfate (APS) as oxidant. The synthesized, DBSA doped PPy was used to make the nanocomposite with graphene using various solvents like DMF, DMSO, NMP and m-cresol. The FTIR spectroscopic investigations of the spin coated and electro-sprayed films of the DBSA doped, PPy/graphene nanocomposite reveal the bond formation of doped polypyrrole with graphene. The XRD studies indicate the partially crystalline nature of the nanocomposite films. Strong impact of the solvents on the optical absorption has been observed in the UV-Visible absorption studies. The electro-sprayed films of the nanocomposite dissolved in m-cresol, show maximum electrical conductivity around 4.2 S/cm, .which is much higher than that of the spin coated films. Raman spectroscopy studies of the electro-sprayed films of the doped PPy/graphene nanocomposite illustrate the presence of the G bands of

graphene with quite high intensity and that of the D bands with much less intensity, indicating the overall defect free nature of the nanocomposite. The investigations on the morphological features of the spin coated and electro-sprayed films of the doped PPy/graphene nanocomposite by the FESEM and TEM studies reveal that, in the nanocomposite, the graphene layers are covered by the DBSA doped PPy matrix. The doped PPy can steadily hold onto the surface of graphene due to the electrostatic attraction between the doped PPy and graphene. The presence of the dopant DBSA and graphene brings more structural order to the DBSA doped, PPy/graphene nanocomposite and enhances the crystalline nature of the nanocomposite to a significant extent.

References

[1] A. Kassim, Z. B. Basar, and H. N. M. E. Mahmud, Effects of preparation temperature on the conductivity of polypyrrole conducting polymer, J. Chem. Sci., 114(2) (2002) 155–162

[2] S. Sakthivel and A. Boopathi, Synthesis and Characterization of Polypyrrole (PPY) Thin Film by Spin Coating Technique, J. Chem. & Chemi.Sci.,4(3) (2014) 150-155

[3] A. Liu, C. Li, H. Bai, and G. Shi, Electrochemical Deposition of Polypyrrole / Sulfonated Graphene Composite Films, J. Phys. Chem. C., 114(51) (2010) 22783–22789

[4] P. Jayamurugan, V. Ponnuswamy, Y.V. Subba Rao, S. Ashokan, S. Meenakshisundar, Influence of spin coating rate on the thickness, surface modification and optical properties of water dispersed PPy composite thin films, Mater. Sci. Semicond. Process., 39 (2015) 205–210

[5] K. Singh, A. Ohlan, and S. K. Dhawan, Polymer-Graphene Nanocomposites : Preparation, Characterization, Properties, and Applications, Nanocomposites Farzad Ebrahimi, IntechOpen, (2012) https://www.intechopen.com/books/nanocomposites

[6] B. Parija and S. Panigrahi, Fundamental understanding and modeling of spin coating process : A review, Indiasn Journal of Physics, 83(4) (2009) 493–502

[7] S. D. Sathaye, K. R. Patil, S. D. Kulkarni, P. P. Bakre, S. D. Pradhan, B. D. Sarwade, and S. N. Shintre, Modification of spin coating method and its application to grow thin films of cobalt ferrite, Journal of Materials Science, 38(1) (2003) 29–33

[8] N. Bock, M. A. Woodruff, D. W. Hutmacher, T. R. Dargaville, Electrospraying, a Reproducible Method for Production of Polymeric Microspheres for Biomedical Applications, Polymers, 3(1) (2011) 131–149

[9] S. Deivanayaki, V. Ponnuswamy, R. Mariappan, and P. Jayamurugan, Synthesis and characterization of polypyrrole/TiO2 composites by chemical oxidative method, *Optik (Stuttg).*, 124(12) (2013) 1089–1091

[10] V. K. Gade, D. J. Shirale, P. D. Gaikwad, K. P. Kakde, P. A. Savale, H. J. Kharat, B. H. Pawar, and M. D. Shirsat, Synthesis and characterization of Ppy-PVS, P (NMP) -PVS and their co-polymer Ppy-P (NMP) -PVS films by galvanostatic method,Int. J. Electrochem. Sci., 2 (2007) 270–277

[11] S. Bilal, F. Perveen, and A. A. Shah, Chemical synthesis of polypyrrole doped with dodecyl benzene sulfonic acid, Journal of Scientific and Innovative Research, 4(1) (2015) 33–42

[12] S. Bose, T. Kuila, E. Uddin, N. Hoon, A. K. T. Lau, and J. Hee, In-situ synthesis and characterization of electrically conductive polypyrrole / graphene nanocomposites, Polymer (Guildf)., 51(25) (2010) 5921-5928

[13] S. Li, X. Lu, Y. Xue, J. Lei, T. Zheng, and C. Wang, Fabrication of Polypyrrole / Graphene Oxide Composite Nanosheets and Their Applications for Cr (VI) Removal in Aqueous Solution, Plos One, 7(8) (2012) e43328

[14] K. S. Jang, H. Lee, and B. Moon, Synthesis and characterization of water soluble polypyrrole doped with functional dopants, Synth. Met., 143(3) (2004) 289–294

[15] R. Hu and X. Wang, Graphene oxide/polypyrrole composites for highly selective enrichment of U(VI) from aqueous solutions, Polym. Chem., 5 (2014) 6207–6215

[16] R.N.Singh, Madhu and R Awasthi, Polypyrrole Composites: Electrochemical Synthesis, Characterizations and Applications, Electropolymerization, Ewa Schab-Balcerzak, Intech Open (2011)

[17] X. Feng, R. Li, Z. Yan, X. Liu, R. Chen, Y. Ma, and X. Li, Preparation of Graphene / Polypyrrole Composite Film via Electrodeposition for Supercapacitors, IEEE Transactions on Nanotechnology, 11(6) (2012) 1080–1086

[18] M. T. Ramesan, Synthesis, Characterization, and Conductivity Studies of Polypyrrole / Copper Sulfide Nanocomposites, Applied Polymer, 128(3) (2013) 1540–1546

[19] Helinando P. de Oliveria, Stefanie A. Sydlik and Timothy M. Swager, Supercapacitors from Free-Standing Polypyrrole / Graphene Nanocomposites, J. Phys. Chem. C., 117(20) (2013) 10270-10276

[20] S. Konwer and S. K. Dolui, Synthesis and characterization of polypyrrole / graphite composites and study of their electrical and electrochemical properties, Mater. Chem. Phys., 124(1) (2010) 738–743

[21] M. K. Pati, P. Pattojoshi, and G. S. Roy, Synthesis of Graphene-Based Nanocomposite and Investigations of Its Thermal and Electrical Properties, Journal of Nanotechnology, 2016 (2016) 1-9

[22] S. Shrikrushna and J. A. K. Milind V Kulkarni, Influence of Dodecylbenzene Sulfonic Acid Doping on Structural, Morphological, Electrical and Optical Properties on Polypyrrole/3C-SiC Nanocomposites , J. Nanomed. Nanotechnol., 6(5) (2015) 3–7

[23] F. T. Thema, M.J. Moloto, E.D. Dikio, N.N. Nyangiwe, L. Kotsedi, M. Maaza and M. Khenfouch, Synthesis and Charactrization of Graphene Thin Films by Chemical Reduction of Exfoliated and Intercalated Graphite Oxide, Journal of Chemistry 2013 (2013) 1-6

[24] P. Jayamurugan, V. Ponnuswamy, S. Ashokan, and T. Mahalingam, Investigation on Optical , Morphological and Thermal Properties of Spray Coated Polypyrrole Film, Int. J. Thin Film Sci. Tec., 2(3) (2013) 261–266

[25] C. Bora, R. Pegu, B. J. Saikai, S.K. Dolui, Synthesis of polythiophene/graphene oxide composites by interfacial polymerization and evaluation of their electrical and electrochemical properties, Polymer International, 63(12) (2014) 2061-2067

[26] M. basheer A. K Deshmukh, Highly dispersible graphene oxide reinforced polypyrrole/polyvinyl alcohol blend nanocomposits with high dielectric constant and low dielectric loss, RSC Adv., 5(76) (2015) 61933-61945

[27] M. Shafiqur, W. A. Hammed, R. Yahyah, H. Nabi, and M. Ekramul, Optoelectrical and photoluminescence quenching properties of poly (N-vinyl carbazole)- polypyrrole/reduced graphene oxide nanocomposites, Synthetic Metals, 226 (2017) 188-194

[28] W. A. Hammed, M. S. Rahman, H. N. M. E. Mahmud, R. Yahya, K. Sulaiman, M. S. Rahman, H. N. M. E. Mahmud, R. Yahya, and K. Sulaiman, Processable dodecylbenzene sulfonic acid (DBSA) doped poly (N-vinyl carbazole) -poly (pyrrole) for optoelectronic applications, Des. Monomers Polym., (20)(1) (2017) 1–10

[29] H. K. Lim, S. O. Lee, K. J. Song, S. G. Kim, and K. H. Kim, Synthesis and properties of soluble polypyrrole doped with dodecylbenzenesulfonate and combined with polymeric additive poly(ethylene glycol), J. Appl. Polym. Sci., 97(3) (2005) 1170–1175

[30] K. T. Song, J. Y. Lee, H. D. Kim, D. Y. Kim, S. Y. Kim, and C. Y. Kim, Solvent effects on the characteristics of soluble polypyrrole, Synthetic Metals, 110(1) (2000) 57–63

[31] A. A. Dubale, W. Su, A. G. Tamirat, and C. Pan, The synergetic effect of graphene on Cu_2O nanowire arrays as highly efficient hydrogen evolution photocathode in water splitting, J. Mater. Chem. A, 2 (43) (2014) 18383-18397

[32] A. C. Ferrari, Raman spectroscopy of graphene and graphite : Disorder, electron – phonon coupling, doping and nonadiabatic effects, Solid State Communications, 143(1-2) (2007) 47–57

[33] X. Tang, T. Liu, H. Li, D. Yang, and L. Chen, Notably enhanced thermoelectric properties of lamellar polypyrrole by doping with β -naphthalene sulfonic acid, RSC Adv., 7 (2017) 20192–20200

[34] T. Palaniselvam, H. B. Aiyappa and S. Kurungot, An efficient oxygen reduction electrocatalyst from graphene by simultaneously generating pores and nitrogen doped active sites, J. Mater. Chem., 22(45) (2012) 23799-23805

[35] A. C. Ferrari, J. C. Meyer, V. Scardaci, C. Casiraghi, M. Lazzeri, F. Mauri, S. Piscanec, D. Jiang, K. S. Novoselov, S. Roth, and A. K. Geim, Raman Spectrum of Graphene and Graphene Layers, Phys. Rev. Lett. 97 (18) (2006) 187401

[36] P. Jayamurgan, V. Ponnuswamy, S. Ashokan, and T. Mahalingam, The effect of dopant on structural , thermal and morphological properties of DBSA-doped polypyrrole, Iranian Polymer Journal, 22(3) (2013) 219–225

[37] G. G. Kumar, C. J. Kirubaharan, S. Udhayakumar, K. Ramachandran and K. S. Nahm, Synthesis, Structural, and Morphological Characterizations of Reduced Graphene Oxide-Supported Polypyrrole Anode Catalysts for Improved Microbial Fuel Cell Performances, ACS Sustainable Chem. Eng., 2(10) (2014) 2283-2290

[38] J. Zhu, Y. Xu, J. Wang, J. Wang, Y. Bai, and X. Du, Morphology controllable nano-sheet polypyrrole – graphene composites for high-rate supercapacitor, Phys. Chem. Chem. Phys., 17(30) (2015) 19885–19894

[39] Eva kostakova, Eva Zemanova, Petr Mikes, Julie Soukupova, Hana Matheisova, Karel Kloud, Electrospinning and electrospraying of polymer solutions with spherical fullerenes, Nanocon., 23. - 25. 10. 2012, Brno, Czech Republic, EU, 10 (2012) 23-25

[40] A. R. Sadrolhosseini, S. A. Rashid, A. S. M. Noor, A. Kharazmi, H. N. Lim, and M. A. Mahdi, Optical Band Gap and Thermal Diffusivity of Polypyrrole-Nanoparticles Decorated Reduced Graphene Oxide Nanocomposite Layer, Journal of Nanomaterials, 2016(2) (2016) 1-8

[41] S. Sahoo, G. C. Nayak, and C. K. Das, Synthesis and Electrochemical Characterization of Modified Graphene / Polypyrrole Nanocomposites, Macromolecular Symposia, 315(1) (2012) 177–187

.....ooo.....

Chapter 5

STUDIES ON THE STRUCTURAL AND ELECTROCHEMICAL PROPERTIES OF LITHIUM SUBSTITUTED POLYPYRROLE AS A PROSPECTIVE CATHODE MATERIAL FOR FLEXIBLE LITHIUM-ION CELLS

This chapter gives an account of the studies carried out on the structural and electrochemical performance of Li-ion cells, assembled using Li-substituted polypyrrole as the cathode active material. Chemical oxidative polymerization method is employed to synthesize polypyrrole (PPy) using anhydrous ferric chloride ($FeCl_3$) as the oxidant and it is dedoped using NH_4OH solution in the fully reduced state. The dedoped polypyrrole is treated with n-butyllithium in hexanes (n-BuLi) in an argon (99.999% purity) filled glove box to get the lithiated form of polypyrrole (PPyL). Concentration of n-BuLi is varied to improve metalation and the lithium content in the lithiated samples is estimated using ICP-AES analysis. The lithiated PPy is characterized by FTIR spectroscopy, XRD, FESEM and TEM techniques to understand the structural and the morphological details. The thermal studies using the TGA technique show that the lithiated polypyrrole has good thermal stability. Coin cells are assembled in the argon filled glove box using Li-substituted polypyrrole as the cathode, lithium metal foil as the anode and lithium hexaflurophosphate ($LiPF_6$) as the electrolyte. The electrochemical capabilities of the assembled cells are characterized using voltage sweep cyclic voltammetry and charge-discharge cycling techniques. The cells are found to show an open circuit voltage of 3.3 V and maximum specific capacity of 30.03 $mAhg^{-1}$. All the assembled cells show stable charge discharge cycling behaviour up to 60 cycles and coulombic efficiency of around 85 %. The prime advantage of using n-Buli as a dopant for the synthesis of the lithiated polypyrrole is the much reduced material cost involved, compared to the cost of the conventional materials used for lithiation, like $LiPF_6$ or $LiBF_4$. The specific capacity of the cells can be further improved by optimizing the Li-doping concentration.

5.1 Introduction

The development of conducting polymer based rechargeable Li-ion cells with high energy density, long life span and low cost is being extensively pursued among research and development groups, worldwide [1]. Polymers have been attracting much attention as electrode materials due to their advantages of good electrochemical performance, high stability, structural tenability and design flexibility [2]. Polymers like polypyrrole (PPy), polythiophene (PTh) and polyanniline (PANI) are being widely examined as active electrode materials for lithium-ion cells, because they can be easily switched between the oxidized and the reduced states [3]. Because of their environmentally favourable nature and the conceivable development adaptability, recent focus is on developing rechargeable cells based on different types of electrically conducting polymers. Among the conducting polymers, polypyrrole is specially promising for commercial applications because of its good environmental stability, interesting structural and electrical properties and promising electrochemical characteristics [4].

Polypyrrole is electrochemically active and permits penetration of the electrolyte into the polymer mass [5], which makes it a prospective electrode material for rechargeable batteries. Due to the insertion and extraction of lithium ions into the polypyrrole, it is observed to be electrochemically active in the voltage range of 2.0-4.5 V versus Li/ Li+ with a theoretical capacity of 72 mAh/g [6]. In addition to the electrochemical activity of polypyrrole, it has an added benefits due to its conductivity, and hence the inert weight related with the preparation

of the cathode materials can be reduced considerably. [7]. It has also attracted much consideration as the effective additive material to enhance the performance of anode materials in lithium-ion cells [8]. As a conducting polymer, it shows good compatibility with sulphur and organic electrolytes. The morphology of polypyrrole is ideal to enrich the electrochemical behaviour of the sulphur cathode [9]. Nanosized PPy particles synthesized by chemical polymerization method and uniformly coated on the exterior of elemental sulphur, are found to enhance the conductivity, cycling stability and capacity of the sulphur cathode. It can play numerous roles in the electrode, as an active material, conducting additive and adsorbing agent [10]. It has been effectively utilized for synthesizing sulphur-polymer composites on account of its ease of synthesis, relatively high electrical conductivity, and good stability. Nanostructured polypyrrole can act as a conductive matrix in sulphur-polypyrrole composite, synthesized by chemical polymerization method and also as a dispersing agent to enable the formation of small sulphur particles during the in-situ deposition [11]. Conducting polypyrrole can serve as a stable wrapping layer during the charge-discharge process for some promising cathode materials such as $LiFePO_4$ and $LiMn_2O_4$ [12].

Rechargeable lithium-ion cells with high capacity, energy density and excellent cycling characteristics are presently ruling the battery market for powering electric vehicles and compact electronic gadgets [13]. These cells utilizing cathode active materials like $LiCoO_2$, $LiMn_2O_4$ and $LiFePO_4$ have amazing charge storage capacity with minimum limit of charge leakage when not being used. Nonetheless, material toxicity, chance of cell explosion and the absence of effective cell recycling

mechanism pose hazards which are to be addressed seriously. The cells, likewise, need adaptability in their design because of the structural characteristics of the electrode materials [14, 15]. In the designing of rechargeable Li ion cells with polymer-based cathode active materials, the key issue is to establish the ideal lithiation of the polymer cathode which can guarantee the highest electronic conductivity and specific charge capacity possible [16, 17]. However, many of the cathodes so far developed, using PPy have several problems related to the generally low capacity and the sloping charge –discharge curves which have constrained the functional utilization of PPy in energy storage devices [18].

In the present work, attempts have been made to accomplish lithium substitution in polypyrrole and study the electrochemical performance of the Li-ion cells assembled using the Li substituted polypyrrole as the cathode active material, lithium foil as the anode and lithium hexaflurophosphate ($LiPF_6$) as the electrolyte. The lithiation (metalation) has been effected by treating polypyrrole with n-butyllithium (n-BuLi) in hexane, which is a novel way to accomplish lithium substitution in polypyrrole. The prime advantage of this technique is the much reduced material cost involved in the synthesis of the lithiated polypyrrole, compared to the cost of the conventional materials used for lithiation, like $LiPF_6$ or $LiBF_4$. The structural and morphological investigations on Li-substituted polypyrrole, along with the detailed electrochemical characterization have not been pursued widely. The present work is mainly focussed on assembling rechargeable Li-ion cells with lithiated polypyrrole as cathode active material, capable of offering good performance characteristics.

5.2 Materials and methods

5.2.1 Synthesis

Chemical oxidative polymerization method was employed to synthesize polypyrrole using anhydrous ferric chloride as the oxidant and the polymer obtained was de-doped using NH_4OH solution to get the reduced form of the polymer. The de-doped polymer was treated with n-butyllithium in hexanes (n-BuLi) in an argon filled glove box to get the lithiated form of polypyrrole and the amount of n-BuLi was varied in four different volume concentrations to improve the metalation. The resultant, lithiated polypyrrole samples were named as PPyL4, PPyL8, PPyL12, and PPyL16 respectively and were subjected to detailed structural characterization. The electrodes based on the lithiated poypyrrole for assembling the Li ion cells were prepared by mixing 80 % of the active material, the lithiated polypyrrole, with 10 weight % of acetylene black as conducting medium and 10 weight % of polyvinylidene difluoride (PVDF) in N-methyl pyrrolidinone (NMP) solvent. The homogeneous slurry obtained was coated on a thin aluminum foil by spray coating and the coated foil was dried at 60^o C under vacuum overnight to get the NMP evaporated off. Circular disc, electrodes were cut from the aluminum foil with the active material content of 0.8 to 1.6 mg. The Li ion coin cells were assembled in the argon filled glove box using the lithiated polypyrrole based electrode as the cathode, lithium metal foil as the anode, porous polyethylene film as the separator and 1 M $LiPF_6$ in the 1:1 mixture of ethylene carbonate (EC) and dimethyl carbonate (DMC) as the electrolyte. The assembled cells were characterized to access their electrochemical capabilities.

5.2.2 Characterizations

The amount of lithium content in the samples was estimated using ICP-AES analysis with Thermo Electron IRIS INTREPID II XSP DUO spectrometer. The infrared spectra of the lithiated polypyrrole samples were recorded using Thermo Nicolete Avatar 370 DTGS model Fourier transform IR (FTIR) spectrometer in the wavenumber range of 400–4000 cm^{-1} . The XRD patterns were obtained using the Rigaku Dmax C diffractometer with Cu Kα radiation of wavelength 1.54 Å. The FESEM images of the samples were recorded using Carl-Zeiss Sigma 250 electron microscope and the TEM patterns, using Jeol/JEM 2100 model machine. The d.c. electrical conductivity values of the lithiated polypyrrole samples, obtained using the four probe method are in the range of 10^{-3} S/cm and are in the expected range for cathode active materials. The thermal studies were done from room temperature to 700 °C using Perkin Elmer, Diamond machine, which show that the lithiated samples have good thermal stability. The electrochemical properties of the assembled cells were analyzed by the voltage sweep cyclic voltammetry studies using the Bio-Logic SP-300 potentiostat at a scanning rate of 0.1 mV/s. The charge–discharge test of the cells was carried out between 2 V and 4 V using the 8 channel battery analyser (5 V, 1 mA-MTI Corporation USA) at C/10 current rate.

5.3 Results and discussion

5.3.1 Inductively coupled plasma atomic emission spectroscopic (ICP-AES) studies

In this technique, the atomic emission spectrum given out by a sample is used to determine its elemental composition .The wavelength

at which emission occurs identifies the element, while the intensity of the emitted radiation quantifies its concentration. The four lithiated polypyrrole samples were digested using 5 mL HNO_3 and made up to 100 mL using HPLC grade water and were analysed using ICP-AES technique. The results obtained are given in Table 5.1 and indicate that the lithium substitution in PPy increases with increase in the concentration of n-BuLi and reaches a maximum metalation of 21.56%. The variation of lithium content with the concentration of n-BuLi is shown in figure 5.1.

Table 5. 1 ICP-AES data of lithiated PPy samples

Sample Name	Lithium content (%)
PPyL4	10.25
PPyL8	13.52
PPyL12	16.49
PPyL16	21.56

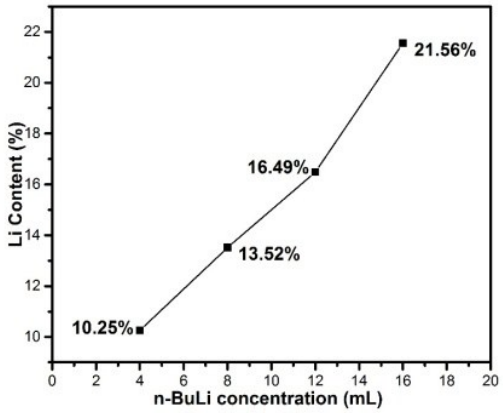

Figure 5.1 Variation of lithium content with n-BuLi concentration

5.3.2 FTIR spectroscopic studies

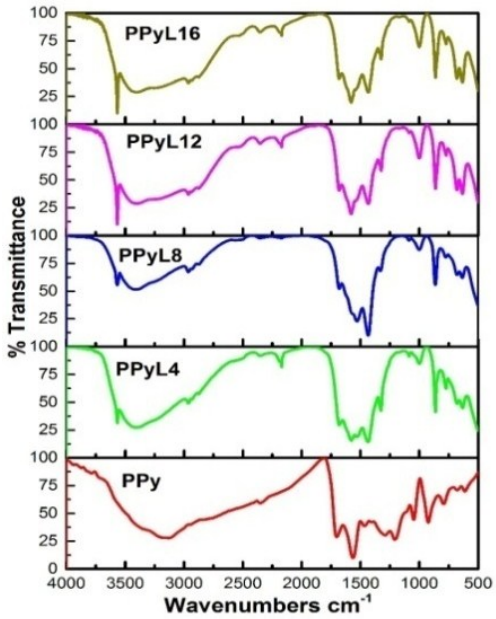

Figure 5.2 The FTIR transmission curves of PPy and lithiated PPy samples

The FTIR spectra of PPy and lithiated PPy samples are illustrated in figure 5.2. The absorption peaks at 1563 cm^{-1} for PPy and 1577 cm^{-1} for the lithiated PPy samples correspond to the C=C stretching vibrations in the pyrrole ring [19]. The peaks at 1290 cm^{-1} for PPy and at around 1326 cm^{-1} for the lithiated samples are attributed to the C-H in-plane deformation vibrations [20]. Low intensity peaks observed at around 2962 cm^{-1} to 2868 cm^{-1} can be attributed to the aromatic C-H stretching vibrations [21]. The bands from 1046 cm^{-1} to 1090 cm^{-1}, present in all the samples are assigned to the in-plane deformation vibrations of C-H and N-H [22] and the bands observed from 924 cm^{-1} to 998 cm^{-1} are due to the C-C out-of-plane ring deformation vibrations [23]. The peak due to the N-H stretching mode is present at 3130 cm^{-1} in the spectrum of PPy

[24] and for the lithiated samples, the intensity of this peak gets decreased and another peak appears at 3566 cm^{-1} for all the lithiated samples along with the characteristic peaks of PPy, which is a strong evidence for the lithium substitution in PPy. The intensity of the peak at 3566 cm^{-1} gets enhanced with the increase in the concentration of *n*-BuLi, indicating the successful lithium substitution in PPy. The origin of this peak is attributed to the formation of a hydrogen bond between the lithium ions and the amine group. During lithiation, this hydrogen bond formation leads to variations in the intensity and shape of the NH vibrational band. This explains the enhancement of the NH vibrational peak intensity with the increase in the Li doping concentration. The hydrogen bond formation also supports the observed partial lithium substitution in PPy.

5.3.3 X-ray diffraction studies

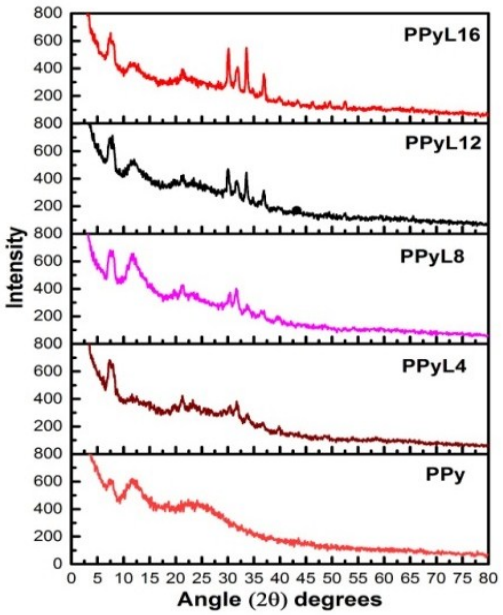

Figure 5.3 The XRD patterns of PPy and lithiated PPy samples

The XRD patterns of PPy and lithiated PPy are shown in figure 5.3. The PPy shows broad peaks around 2θ values of 9.4^0 and 16.3^0 indicating amorphous structure and are due to the scattering from PPy chains at the inter-planar spacing [25], which agrees well with the already reported data. Instead of broad peaks indicating amorphous nature, the lithiated samples show intense and narrow peaks at 28^0 and 39^0 with additional diffraction peaks at 30.25^0, 31.8^0, 33.6^0, 36.8^0 and 37.12^0. The presence of these additional peaks is a clear evidence of the lithium substitution in PPy. It is also observed that the lithiated samples have a more crystalline and ordered structure compared to pure PPy which maintains the structural integrity during the substitution of lithium ions in PPy. The XRD peaks seen in polypyrrole are weak and broad compared to the sharp and narrow diffraction peaks in the lithiated samples. It is clear from the XRD patterns of the lithiated samples that the intensity of the diffraction peaks increases with the increase in lithium concentration due to the semi-crystalline nature of the resulting Li doped PPy compositions. These results are also in good agreement with the morphological changes observed in the lithiated samples, as per the FESEM and TEM analysis, described in the following sections.

5.3.4 Microstructure analysis-FESEM studies

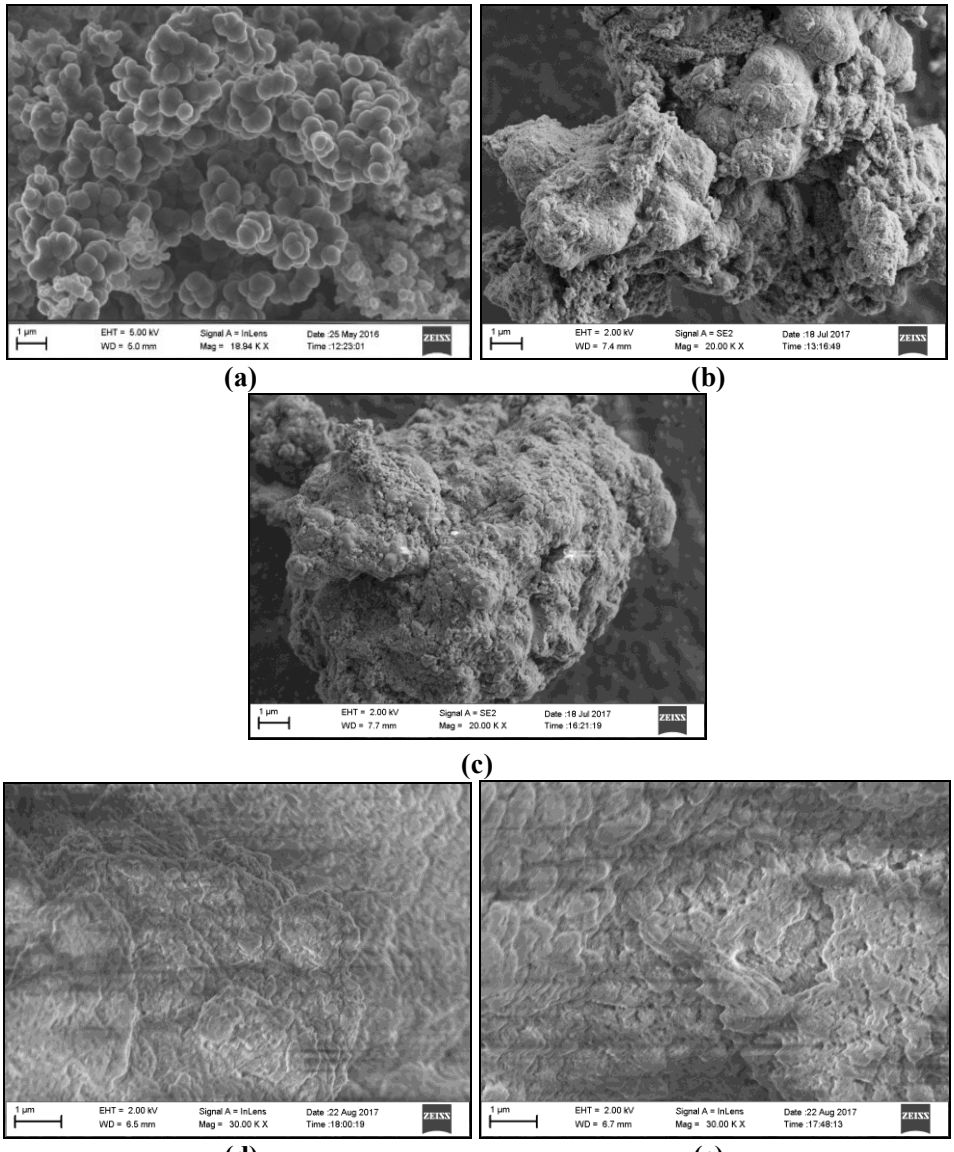

Figure 5.4 FESEM images of (a) PPy (b) PPyL4 (c) PPyL8 (d) PPyL12 (e) PPyL16

The structural morphology of PPy and the four lithiated PPy samples has been investigated by FESEM studies and the FESEM

images are shown in figure 5.4. Polypyrrole has a granular structure and agglomerates with an average diameter of 0.6 micrometer are created when chemical polymerization is carried out with $FeCl_3$ as the oxidant. The individual granules observed are nearly spherical and the PPy surface has a dense packing [26]. The denser surface morphology of PPy results in lower conductivity, compared to the lithiated samples, due to the limited range available for the charge carrier hoping between the agglomerates [27]. Surface morphology of the lithiated samples is considerably modified by increasing the n-BuLi concentration. For the lithiated sample with the lowest n-BuLi concentration, the surface morphology presents globular structures. As the concentration increases to the medium level, the morphology of the samples changes considerably from that of PPy. Upon lithiation, it is observed that the particles seem to merge together and become embedded with the adjacent particles forming a much agglomerated structure which can be seen from the FESEM images of the lithiated samples at the medium level of lithiation. On increasing the Li doping concentration to the highest level, bigger flake like structures are observed indicating uniformity in lithium distribution with in the PPy matrix. This type of more ordered structure assists the arrangement of electrically conductive network within the PPy chain leading to enhanced electron transport amongst the flakes, thus contributing to a high level of electrical conductivity. The FESEM analysis shows that the samples become structurally more ordered with the increase in n-BuLi concentration. The formation of these ordered structures supports the earlier conclusions on the basis of the XRD studies.

5.3.5 Microstructure analysis-TEM studies

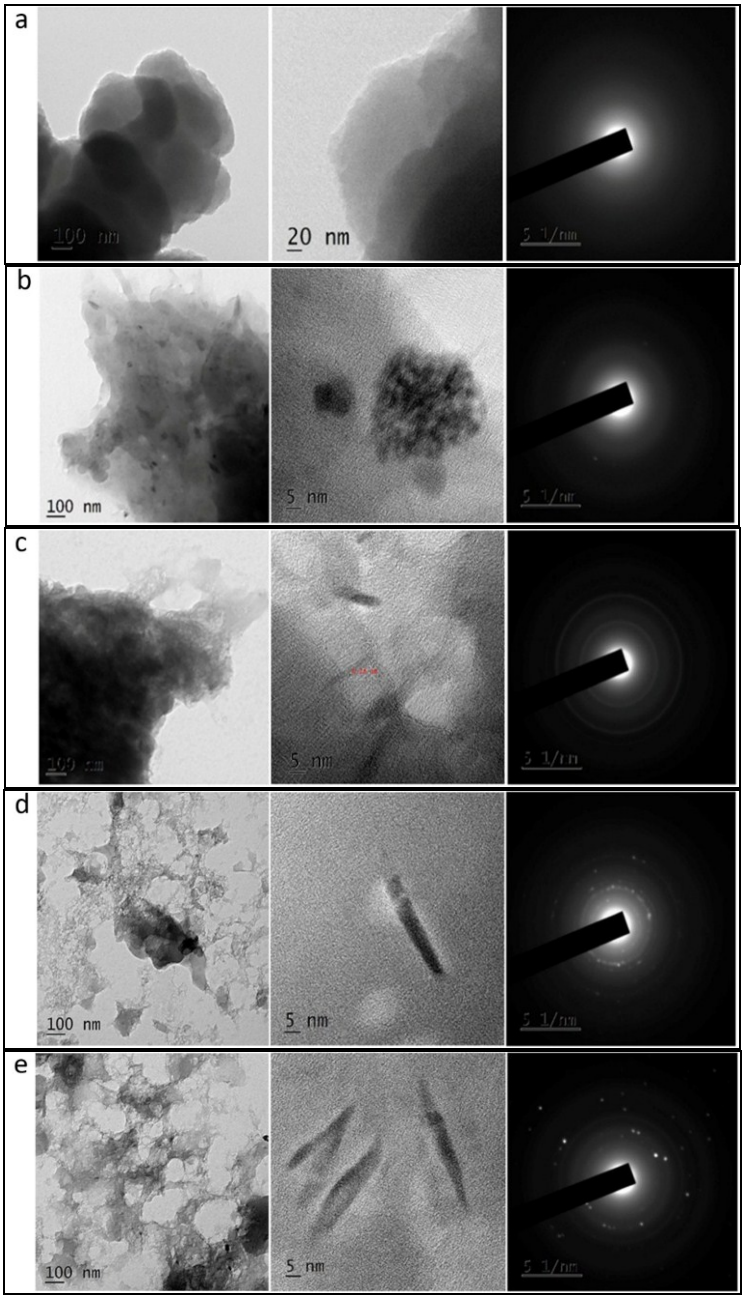

Figure 5.5 TEM images of (a) PPy (b) PPyL4 (c) PPyL8 (d) PPyL12 (e) PPyL16

The TEM images and the selected area electron diffraction (SAED) patterns of PPy and the four lithiated samples at 100 nm and 5 nm scales are shown in figure 5.5. The TEM image and the SAED pattern of PPy confirm its amorphous nature. Generally, PPy acts as an electrically conducting medium and takes part in lithiation and delithiation processes. The TEM images at 100 nm reveal that upon doping with n-BuLi, the individual PPy particles get clustered into agglomerates and lithium is distributed within the PPy matrix. The high resolution images at 5 nm scale show the lattice fringes obtained in the lithiated PPy due to the encapsulation of lithium within the matrix of PPy. The electrical conductivity of the lithiated samples were seen to have improved due to the decrease in the particle-to-particle contact resistance of the lithium encapsulated PPy matrix. The selected area electron diffraction patterns of the lithiated samples show crystalline nature which confirms the presence of lithium. The encapsulation of lithium inside PPy enhances its electrical conductivity. Polypyrrole being a conducting polymer acts as a backbone to form a conductive matrix with the lithium encapsulation. The polymer can also act as a protective layer to reduce the dissolution of ions [28].

5.3.6 Electrical conductivity studies

Table 5.2 The DC electrical conductivity values of PPy and lithiated PPy samples

Sample Name	Electrical conductivity (S/cm)
PPy	2.41×10^{-4}
PPyL4	2.72×10^{-3}
PPyL8	3.85×10^{-3}
PPyL12	4.05×10^{-3}
PPyL16	7.14×10^{-3}

The DC electrical conductivity of the samples was measured using the KEITHLEY 236 source measurement unit at room temperature and the results obtained are given in Table 5.2. The room temperature conductivity of PPy doped with $FeCl_3$ is 2.41×10^{-4} S/cm. The conductivity of the lithiated samples at room temperature is strongly dependent on the concentration of n-BuLi and continues to increase in the order of 10^{-3} S/cm with increase in n-BuLi concentration. The enhanced crystalline order associated with the lithiated PPy samples results in the increase in conductivity.

5.3.7 Thermo-gravimetric analysis

The thermal stability of PPy and the lithiated PPy samples was analysed by the thermo-gravimetric (TG) studies. The corresponding thermal curves of the samples are shown in figure 5.6**.** The TG plots of PPy and the lithiated PPy samples show good thermal stability. All the samples are observed to exhibit three distinct weight loss regions. The first weight loss occurs at temperatures between 65 ^{o}C to 167 ^{o}C for PPy and between 55 ^{o}C to 160 ^{o}C for the lithiated samples due to the loss of water molecules upon heating as reported by many authors [29]. The second weight loss occurring between 230 ^{o}C to 340 ^{o}C for PPy and 190 ^{o}C to 300 ^{o}C for the lithiated samples represents the evaporation of the dopant, n-BuLi, leading to the degradation process and the third one at still higher temperatures represents the breaking of the PPy chains [30]. All the samples are thermally stable in the temperature range of 55 ^{o}C to 340 ^{o}C and beyond that, the decomposition process becomes faster.

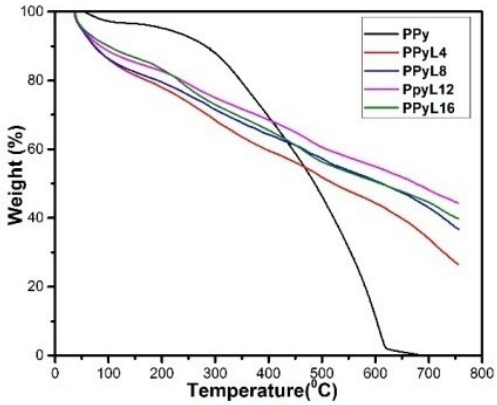

Figure 5.6 TG curves of PPy and lithiated PPy samples

5.3.8 Cyclic voltammetry (CV) studies

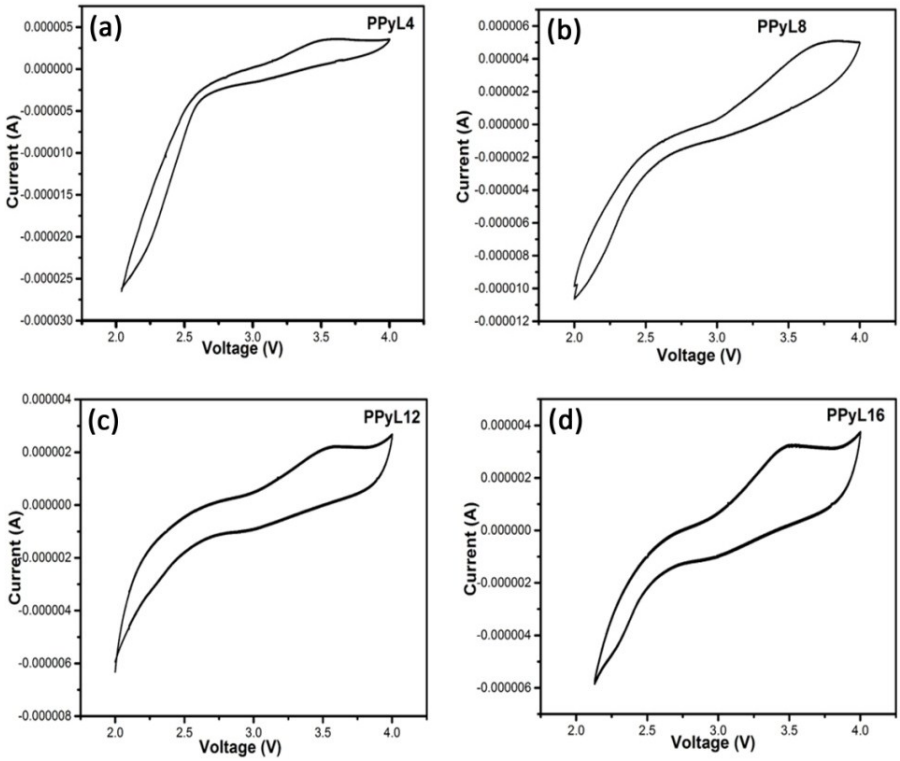

Figure 5.7 The CV curves of (a) PPyL4 (b) PPyL8 (c) PPyL12 (d) PPyL16 based coin cells

The cyclic voltammetry (CV) studies were carried out on coin cells assembled in the argon filled glove box using lithiated polypyrrole as cathode and Li metal as anode. The cells are found to show stable open circuit voltage around 3.3 V. The CV curves of PPy and the lithiated PPy samples at a sweep rate of 0.1 mV/s and voltage scan between 2 V to 4 V are shown in figure 5.7. The response curves show reversible characteristics corresponding to cathodic and anodic scans. The oxidation potential lies in the range of 3.3 V to 3.8 V which corresponds to the removal of Li from the lithiated PPy cathode, through the electrolyte to the anode and the reduction falls between 2.3 V to 2.8 V corresponding to the intercalation of Li back to the cathode from the anode .The approximately symmetrical peaks of the four lithiated samples with relative increase in the narrow peak-to-peak separation of the anodic and the cathodic potential, imply the good oxidation/reduction reversibility of the lithiated polypyrrole active material as the cathode. The cathodic and the anodic peaks turn out to be more prominent and resolved as the percentage of lithiation increases. The area of the CV curve also increases with increase in the percentage of lithiation. The increase in the area under the anodic and cathodic peaks with increase in the lithium concentration is mainly related to the electrochemical activity of Li^+ ions in polypyrrole and the enhancement of the electronic conductivity of the lithium substituted polypyrrole electrode material, which facilitate faster electron shuttling, an important factor in electrochemical battery cycling**.** It is also evident from the charge discharge studies, detailed in the next section, that the specific capacity of the lithiated samples increases with increase in the percentage of lithiation.

5.3.9 Charge- discharge cycling studies

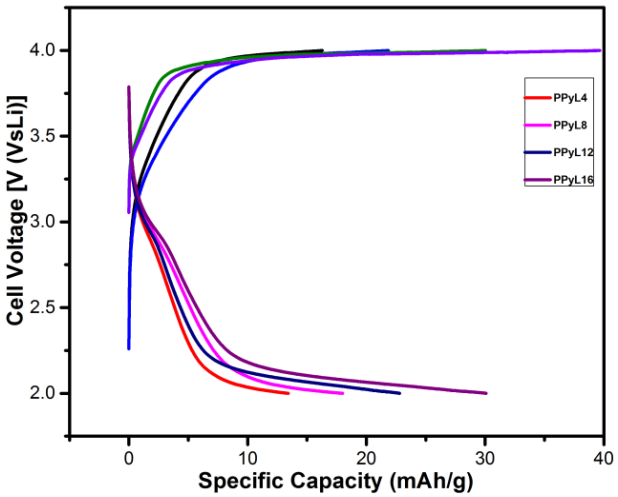

Figure 5.8 Charge-discharge curves of PPyL4, PPyL8, PPyL12 and PPyL16 based coin cells

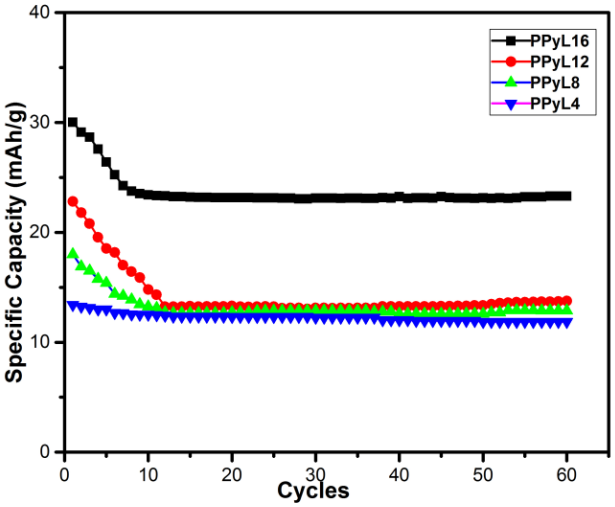

Figure 5.9 Specific capacity versus cycle number curves of PPyL4, PPyL8, PPyL12 and PPyL16 based coin cells

The charge–discharge curves of the four assembled coin cells, studied between 2 V and 4 V are shown in figure 5.8 and the cycling performance is illustrated in figure 5.9. The cell based on PPyL16, which is the lithium substituted PPy with maximum Li substitution around 21.56 %, shows the maximum specific capacity of 30.03 $mAhg^{-1}$ for the first cycle and afterwards shows a diminishing nature up to the 7^{th} cycle. After the 7^{th} cycle onwards, the capacity remains the same till the 60^{th} cycle and exhibits a stable capacity around 22.89 $mAhg^{-1}$. Studies on lithiated polypyrrole based Li-ion cells with good specific capacity close to the theoretical capacity, high coulombic efficiency and fantastic cycling stability have not been reported earlier. The theoretical capacity of lithiated polypyrrole is 72 $mAhg^{-1}$ [6,31,32]. In the present work, the maximum lithiation accomplished is only 21.56 % for the sample PPyL16 and consequently the theoretical capacity is much higher than the experimentally obtained value. The samples PPyL12, PPyL8 and PPyL4 show initial discharge capacities of 22.81 $mAhg^{-1}$, 17.99 $mAhg^{-1}$ and 13.40 $mAhg^{-1}$ respectively at initial cycles and thereafter there is a fall in capacity till the 12^{th} cycle. The retained stable capacities of these three samples are 13.85 $mAhg^{-1}$, 12.95 $mAhg^{-1}$ and 11.77 $mAhg^{-1}$ respectively after 60 cycles. The increase in specific capacity with increase in lithium concentration could be due to the increase in electrical conductivity of the samples. These results also support the fact that the area of the CV curve increases with the increase in the percentage of lithiation. As seen from the curves in figure 5.9, after the 7^{th} and 12^{th} charge - discharge cycles, all the four samples show better capacity retention and stable cycling behaviour. The initial coulombic efficiency of the four samples lies between 76 % and 80 % and after the 10^{th}

cycle onwards, the coulombic efficiency of all the samples, retains a steady value between 82 % and 85 % for all the charge discharge cycles.

5.4 Conclusions

The present work introduces a relatively less expensive lithium salt, n-butyllithium in hexanes (n-BuLi) as a dopant for synthesizing lithium substituted polypyrrole to be used as the cathode active material in rechargeable Li ion cells. The amount of lithium content in the lithiated PPy samples is estimated using ICP-AES technique which reveals that the lithium content increases by increasing the n-BuLi concentration. Studies using FTIR spectroscopy, XRD, FESEM and TEM techniques strongly support successful lithium substitution in PPy and the increase in the crystalline order of the polymer structure, with increase in the extent of lithiation. The conductivity of the lithiated samples continues to increase in the order of 10^{-3} S/cm with increase in the n-BuLi concentration. The TG plots of PPy and the lithiated PPy samples show good thermal stability. The coin cells assembled using the lithiated PPy as the cathode, lithium metal as the anode and lithium hexaflurophosphate ($LiPF_6$) as the electrolyte show an open circuit voltage of 3.3 V. The features of the CV curves of the coin cells indicate that the lithiated PPy based Li ion cells are electrochemically active. All the four cells show stable charge discharge cycling behaviour up to 60 cycles and coulombic efficiency around 85 %. The present studies highlight the meritorious features of the n-BuLi doped polypyrrole as a promising cathode active material to develop conducting polymer based Li ion cells with the inherent advantages of flexibility in cell design, reduced material cost and environmental friendliness.

References

[1] Bruno Scrosati, Jusef Hassoun and Yang-Kook Sun, Lithium-ion batteries. A look into the future. Energy Environ. Sci., 4 (2011) 3287–3295

[2] X. Zhao, Z. Zhao, M. Yang, H. Xia, T. Yu, and X. Shen, Developing Polymer Cathode Material for the Chloride Ion Battery, ACS Appl Mater.Interfaces, 9(3) (2017) 2535-2540

[3] L. Qie, L. Yuan, W. Zhang, W. Chen, and Y. Huang, Revisit of Polypyrrole as Cathode Material for Lithium-Ion Battery, Journal of the Electrochemical Society, 159(10) (2012) 1624–1629

[4] A. Kassim, Z. B. Basar, and H. N. M. E. Mahmud, Effects of preparation temperature on the conductivity of polypyrrole conducting polymer, J. Chem. Sci., 114(2) (2002) 155–162

[5] G.-X. W. Jia-Zhao Wanga,*, Shu-Lei Choua, Jun Chenb, Sau-Yen Chewa et.al, Paper-like free-standing polypyrrole and polypyrrole–LiFePO4 composite films for flexible and bendable rechargeable battery, Electrochem. Commun., 10 (2008) 1781–1784

[6] G. X. Wang, L. Yang, Y. Chen, J. Z. Wang, S. Bewlay, and H. K. Liu, An investigation of polypyrrole-LiFePO4 composite cathode materials for lithium-ion batteries, Electrochim. Acta, 50 (2005) 4649–4654

[7] R. P. Ramasamy, B. Veeraraghavan, B. Haran, and B. N. Popov, Electrochemical characterization of a polypyrrole / Co 0.2 CrO x composite as a cathode material for lithium ion batteries, Journal of Power Sources 124 (2003)197–203

[8] X. Gao1, Z. S., Wenbin Luo, Chao Zhong, David Wexler et.al, Novel Germanium/Polypyrrole Composite for High Power Lithium-ion Batteries, Sci. Rep.,4 (2014) 6095

[9] X. Liang, Y. Liu, Z. Wen, L. Huang, X. Wang, and H. Zhang, A nano-structured and highly ordered polypyrrole-sulfur cathode for lithium – sulfur batteries , J. Power Sources 196 (2011) 6951–6955

[10] P. Xin, B. Jin, H. Li, X. Lang, C. Yang, W. Gao, Y. Zhu, W. Zhang, S. Dou, and Q. Jiang, Facile Synthesis of Sulfur–Polypyrrole as Cathodes for Lithium–Sulfur Batteries, Chemelectrochem, 4 (2017) 115-121

[11] Y. Fu, Y. Su, and A. Manthiram, Sulfur-Polypyrrole Composite Cathodes for Lithium-Sulfur Batteries, Electrochem. Soc., 159 (2012) A1420–A1424

[12] X. Gao, Y. Deng, D. Wexler, G. Chen, S. Chou, H. Liu, Z. Shi, and J. Wang, Improving the electrochemical performance of the LiNi0.5Mn1.5O4 spinel by polypyrrole coating as a cathode material for the lithium-ion battery, J. Mater. Chem. A., 3 (2014.) 404–411

[13] X. Du, T. Yang, J. Lin, T. Feng, J. Zhu, L. Lu, Y. Xu, and J. Wang, Microwave-Assisted Synthesis of SnO 2 @ polypyrrole Nanotubes and Their Pyrolyzed Composite as Anode for Lithium-Ion Batteries, ACS Appl. Mater. Interfaces 8 (2016) 15598–15606

[14] Masaki Yoshio, Ralph J. Brodd, Akiya Kozawa, Lithium-Ion Batteries, Science and Technologies, Springer XXVI .,452 (2009) 279

[15] Bo Xu, Danna Qian, Ziying Wang, Ying Shirley Meng, Recent progress in cathode materials research for advanced lithium ion batteries, Materials Science and Engineering 73 (2012) 51–65

[16] K. Ghanbari, M. F. Mousavi, M. Shamsipur, H. Karami, Synthesis of polyaniline/graphite composite as a cathode of Zn-polyaniline rechargeable battery, J. PowerSources 170 (2) (2007) 513-519

[17] W.-M. Chen, L. Qie, L.-X. Yuan, S.-A. Xia, X.-L. Hu, W.-X. Zhang,Y.-H. Huang, Polymer Nanocomposites Based on Inorganic and Organic Nanomaerials. Electrochim. Acta., 56 (2011) 2689

[18] C. Su, L. Wang, L. Xu, and C. Zhang, Synthesis of a novel ferrocene-contained polypyrrole derivative and its performance as a cathode material for Li-ion batteries. Electrochim. Acta., 104 (2013) 302–307

[19] C. Basavaraja, W. J. Kim, D. G. Kim, and D. S. Huh, Synthesis and characterization of soluble polypyrrole–poly(ε-caprolactone) polymer blends with improved electrical conductivities, Mater. Chem. Phys., 129 (2011) 787–793

[20] M. Trchova and J. Kova, Synthesis and structural study of polypyrroles prepared in the presence of surfactants, Synth. Met., 138 (2003) 447–455

[21] H. K. Chitte, Synthesis of Polypyrrole Using Ammonium Peroxy Disulfate (APS) as Oxidant Together with Some Dopants for Use in Gas Sensors, Mater. Sci. Appl., 2 (2011) 1491–1498

[22] S. Bilal, M. Sohail, and A. A. Shah, Synthesis and Characterization of Soluble and Thermally Stable Polypyrrole-DBSA Salts, J Chem. Soc.Pak., 36(6) (2014) 976–982

[23] Ghalib, H., Abdullah, et al., Electrical Conductivity of Anionic Surfactant-Doped Polypyrrole Nanoparticles Prepared via Emulsion Polymerization, Science and Technology 21(2) (2013) 459–471

[24] X. Ma, Æ. G. Li, and Æ. M. Wang, Oxidative polymerization of pyrrole in the presence of a poly (sodium-p-styrenesulfonate) and its gas-responses, J Mater.Sci 41 (2006) 7604–7610

[25] M. A. Chougule, S. G. Pawar, P. R. Godse, R. N. Mulik, S. Sen, and V. B. Patil, Synthesis and Characterization of Polypyrrole (PPy) Thin Films, Soft Nanosci. Lett., 1(1) (2011) 6–10

[26] H. K. Chitte, N. V Bhat, V. E. Walunj, and G. N. Shinde, Synthesis of Polypyrrole Using Ferric Chloride (FeCl 3) as Oxidant Together with Some Dopants for Use in Gas Sensors, Journal of Sensor Technology, 1 (2011) 47–56

[27] T. Ishak, T. Kudin, M. Zu, and A. Yahya, Synthesis and Characteristics of Conducting Polymer- Based Polypyrrole in Different Solvents, Journal of Material Science and Engineering 2(2) (2012) 190–195

[28] C. Li, H. P. Zhang, L. J. Fu, H. Liu, Y. P. Wu, E. Rahm, R. Holze, and H. Q. Wu, Cathode materials modified by surface coating for lithium ion batteries, Electrochimica Acta., 51 (2006) 3872–3883

[29] K. S. Jang, H. Lee, and B. Moon, Synthesis and characterization of water soluble polypyrrole doped with functional dopants, Synth. Met., 143 (2004) 289–294

[30] Y. Shen and M. Wan, Soluble Conducting Polypyrrole Doped with DBSA – CSA Mixed Acid, Journal of Applied Polymer Scienc, 68 (1997) 1277–1284

[31] P. Novdk and W. Vielstich, Performance of the Low-Current-Density-Synthesized Polypyrrole in Lithium Cells Containing Propylene Carbonate, J.Electrochem. Soc., 37(6) (1990) 1681-1689

[32] T. Osaka, T. Mamma, K. Nishimura, S. Kakuda, and T. Ishii, Application of Solid Polymer Electrolyte to Lithium / Polypyrrole Secondary Battery System, J.Electrochem. Soc., 141(8) (1994) 1994–1998

.....ooo.....

Chapter 6

ON THE IMPROVEMENT OF THE ELECTROCHEMICAL BEHAVIOUR OF LITHIUM SUBSTITUTED POLYPYRROLE FOR APPLICATIONS IN LITHIUM-ION CELLS

The present chapter deals with the efforts undertaken to improve the electrochemical performance of lithium substituted polypyrrole as the cathode active material in Li-ion based cells. The improvement in the electrochemical performance is achieved by synthesizing polypyrrole by chemical oxidative polymerization strategy using ammonium persulfate (APS) as the oxidant. The previous chapter deals with the studies on chemically synthesized PPy, in which $FeCl_3$ has been used as the oxidant. Polypyrrole synthesized using the modified approach is subjected to lithiation by treating with n-butyllithium in hexanes (n-BuLi).The Li enriched PPy is used as the cathode active material to assemble Li ion cells and the assembled cells are subjected to detailed electrochemical characterization. The cells are found to show significant improvement in the electrochemical performance compared to the performance of the cells, discussed in the previous chapter.

6.1 Introduction

Rechargeable lithium ion cells dominate the market as the most favoured energy sources for powering portable electronic devices and hybrid electric vehicles due to the high energy density, excellent cycling stability and decreasing material cost, offered by them. One of the challenges associated with Li ion cells is that their capacity is constrained by the amount of lithium that can be stored in the electrodes [1]. Extensive research efforts have been devoted for the development of novel types of electrode materials with excellent electrochemical performance [2]. Conducting polymer based rechargeable Li-ion cells with high specific capacity, high energy density, excellent cycling characteristics and long life span [3,4] are being widely investigated as novel types of devices for developing flexible energy storage systems.

Electrically conducting polymers are materials that conduct electricity and have electronic band structure with pi conjugated delocalized electrons spread along the polymer backbone [5]. As explained earlier, conducting polymers have assumed high significance in the development of flexible type display devices, solar cells, gas sensors, chromic devices, rechargeable batteries and sensors [6]. Polypyrrole has received a great deal of attention than any other conducting polymer owing to its remarkable environmental stability, high electrical conductivity, promising electrochemical attributes and biocompatibility [7]. Conducting polymers can act as conductive matrices for the electrode materials, thereby improving the performance of cathode and anode materials in lithium-ion cells [8].They can also

serve as stable wrapping layers, for potential cathode materials like $LiFePO_4$ and $LiMn_2O_4$ during the charge-discharge processes [9]. Researchers mainly focus on polypyrrole because of its excellent physicochemical and environmental stability, remarkable electrochemical features biocompatibility and moderately low cost [10].

Polypyrrole can assume various roles in the electrode material as an active material, conducting additive and adsorbing agent [11]. Incorporation of polypyrrole into the cathode active materials will improve the electrical conductivity, which in turn results in higher specific capacity [12]. Polypyrrole has also been used in the making of modified sulphur cathodes for applications in Li—S cells [13]. The introduction of polypyrrole into the sulphur/graphene composite electrode enhances the discharge capacity and cycling stability of Li-S cells [14]. Despite the fact that polypyrrole is one of most comprehensively used cathode materials for applications in rechargeable cells, the PPy based cathodes have a few limitations related to the generally low capacity and the sloping charge – discharge curves, which have constrained the functional utilization of PPy in energy storage devices [15].

In the previous chapter, structural, morphological and electrochemical conduct of lithiated polypyrrole as a forthcoming cathode material for Li ion cells has already been discussed. The previous chapter deals with the synthesis of polypyrrole by chemical oxidative polymerization using $FeCl_3$ as the oxidant, followed by detailed structural, morphological and electrochemical characterization of the Li enriched PPy [16]. The present chapter features the improved electrochemical performance and

the structural and morphological changes brought about by synthesizing polypyrrole using APS as the oxidant. The electrochemical performance of the Li-ion cells assembled using the Li substituted polypyrrole as the cathode active material, lithium foil as the anode and lithium hexaflurophosphate ($LiPF_6$) as the electrolyte is assessed. A remarkable improvement in the discharge capacity and rate capability has been achieved. The lithiation (metalation) has been effected by treating polypyrrole with n-butyllithium (n-BuLi) in hexanes, which is a novel and cost effective method to achieve lithium substitution in polypyrrole, as explained earlier.

6.2 Materials and methods

The chemicals used for the synthesis of lithiated PPy are of analytical grade. As explained earlier, pyrrole monomer of 98% purity was purchased from Aldrich Chemicals and was purified by distillation to remove impurities before use. The oxidant, ammonium persulfate (APS) and n-butyllithium in hexanes (n-BuLi) were used as received.

6.2.1 Synthesis of polypyrrole (PPy)

Polypyrrole (PPy) was synthesized by chemical oxidative polymerization with ammonium persulfate (APS) as the oxidant, as explained earlier in chapter 5. The synthesized polypyrrole was de-doped using NH_4OH solution to get the reduced form of the polymer.

6.2.2 Synthesis of lithiated polypyrrole

The lithiated polypyrrole or the Li substituted PPy, was obtained by treating PPy with n-butyllithium in hexanes (n-BuLi) in an argon

filled glove box and the concentration of n-BuLi was varied in four distinct volume concentrations to improve the metalation. The lithiated polypyrrole samples are named as LiPPy 1, LiPPy 2, LiPPy 3 and LiPPy 4.

6.2.3 Sample characterization

The amount of lithium content in the lithiated PPy samples was assessed utilizing ICP-AES analysis with Thermo Electron IRIS INTREPID II XSP DUO spectrometer. The infrared spectra of the lithiated polypyrrole samples were recorded using Thermo Nicolete Avatar 370 DTGS model Fourier transform IR (FTIR) spectrometer in the wavenumber range of 400–4000 cm^{-1} . The XRD patterns were obtained using the Rigaku Dmax C diffractometer with Cu Kα radiation of wavelength 1.54 Å. The FESEM images were acquired using Carl-Zeiss Sigma 250 electron microscope and the TEM patterns, using Jeol/JEM 2100 model machine. The d.c. electrical conductivity of the lithiated polypyrrole samples, obtained by the four probe method is in the range of 10^{-2} S/cm, which is suitable for cathode active materials. The thermal studies were done from room temperature to 700 °C using Perkin Elmer, Diamond machine, which demonstrate that the lithiated samples have good thermal stability.

6.2.4 Electrochemical measurements

The cathode electrodes based on the lithiated polypyrrole for assembling the Li ion cells were prepared by mixing 80 % of the active material, the lithiated polypyrrole with 10 weight % of acetylene black as the conducting medium and 10 weight % of polyvinylidene difluoride (PVDF) in N-methyl pyrrolidone (NMP) solvent as the binder. The

homogeneous slurry obtained was coated on a thin aluminium foil by spray coating and was allowed to dry at 60 °C, overnight under vacuum. Circular disks were cut from the coated foil and used as the cathode active material. The mass of cathode material on each circular disc was approximately 1.6 mg. Stainless steel Swagelok cells were assembled in an argon filled glove box for the electrochemical characterizations, utilizing the lithiated polypyrrole based electrode as the cathode, lithium metal foil as the anode, porous polyethylene film as the separator and 1 M $LiPF_6$ in the 1:1 mixture of ethylene carbonate (EC) and dimethyl carbonate (DMC) as the electrolyte. The cyclic voltammetry (CV) studies were carried out using the Bio-Logic SP-300 potentiostat at a scanning rate of 0.1 mV/s between the voltage window of 2-4 V. The galvanostatic charge-discharge test of the assembled cells was carried out between 2 V and 4 V using the 8 channel battery analyser (5 V, 1 mA-MTI Corporation, USA) at C/10 current rate.

6.3 Results and discussion

6.3.1 Inductively coupled plasma atomic emission spectroscopic (ICP-AES) studies

Table 6.1 ICP-AES data of lithiated PPy samples

Sample name	Lithium content (%)
LiPPy 1	13.4
LiPPy 2	17.6
LiPPy 3	20.7
LiPPy 4	25.8

The amount of lithium content in the lithiated PPy samples was analysed using ICP-AES technique and the results are shown in Table 6.1.

It is seen that the maximum metalation or lithium substitution obtained for the sample LiPPy 4 is 25.8 % and also the extent of lithiation increases with increase in the concentration of n-BuLi. The variation of lithium content with the concentration of n-BuLi is shown in figure 6.1.

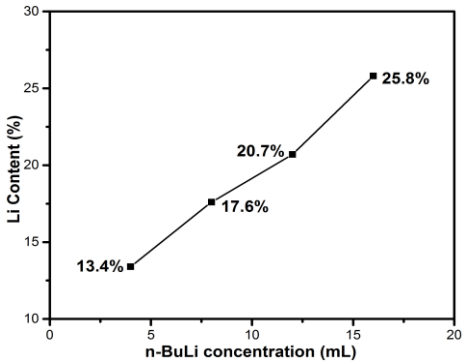

Figure 6.1 Variation of lithium content with n-BuLi Concentration

6.3.2 FTIR spectroscopic studies

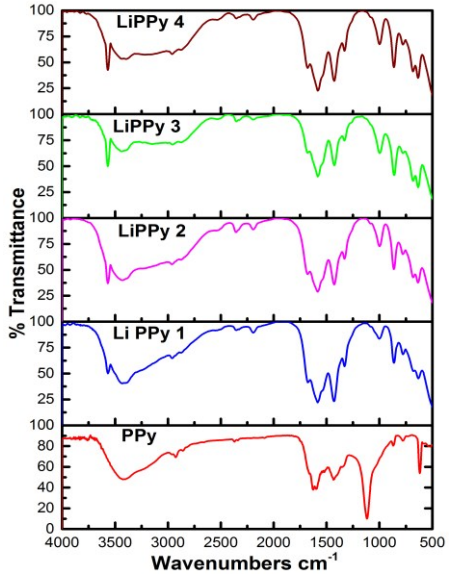

Figure 6.2 The FTIR transmission curves of PPy and lithiated PPy

The FTIR spectra of polypyrrole and lithiated PPy samples are shown in figure 6.2. The peaks at 1539 cm^{-1} , 1583 cm^{-1} , 1581 cm^{-1} 1429 cm^{-1} and 1434 cm^{-1} observed in every sample can be ascribed to C-N and C-C asymmetric and symmetric ring-stretching vibrations [17]. The band at 1112 cm^{-1} in PPy and the ones at 1326 cm^{-1} and 1330 cm^{-1} in the lithiated PPy samples are attributed to C–H and C–N in-plane deformation vibrations [18]. The peak at 998 cm^{-1} in all the samples can be related to the C-C out-of-plane ring deformation vibrations [19]. The low intensity absorption bands at 2924 cm^{-1} in PPy and at 2955 cm^{-1} and 2958 cm^{-1} in the lithiated PPy can be related to the aromatic C-H stretching vibrations [20]. The NH stretching vibration of polypyrrole appears at 3417 cm^{-1} as a broad peak and for the lithiated PPy samples, the intensity of this peak gets diminished. The lithiated PPy samples show a new peak at 3569 cm^{-1} and the intensity of this peak is getting enhanced with the increase in the concentration of *n*-BuLi, which is a strong indication of the successful lithium substitution in PPy. The increase in the NH vibrational peak intensity with the increase in Li doping concentration is a result of the formation of the hydrogen bond between lithium and the amine group.

6.3.3 X-ray diffraction studies

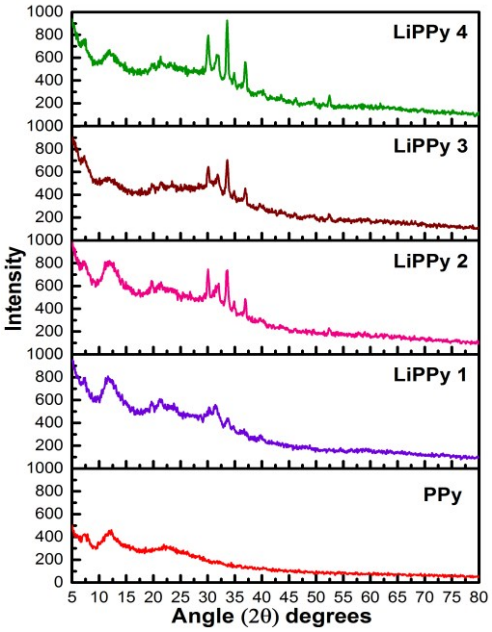

Figure 6.3 The XRD patterns of PPy and lithiated PPy

The XRD patterns of PPy and lithiated PPy are depicted in figure 6.3. The broad peaks at 2θ values of 7.8^0 and 12.2^0 are the characteristic peaks of amorphous polypyrrole [21] . The lithiated PPy samples show semi-crystalline peaks at 30.07^0, 33.58^0 and 36.87^0 instead of the broad peaks of PPy and the extra diffraction peaks observed at 21.4^0, 23.7^0, 34.8^0, 44.5^0 and 52.4^0 provide ample proof of the lithium substitution in PPy. The presence of the narrow and sharp peaks in all the four lithiated PPy samples is a consequence of the lithium substitution in PPy. The increase in the intensity of the diffraction peaks with the increase in lithium concentration is because of the semicrystalline nature of the resulting Li doped PPy compositions. The sharp and narrow diffraction

peaks observed in the lithiated PPy samples compared to the weak and broad peaks seen in PPy illustrate the presence of crystalline domains in the amorphous PPy with Li substitution.

6.3.4 Microstructure analysis-FESEM studies

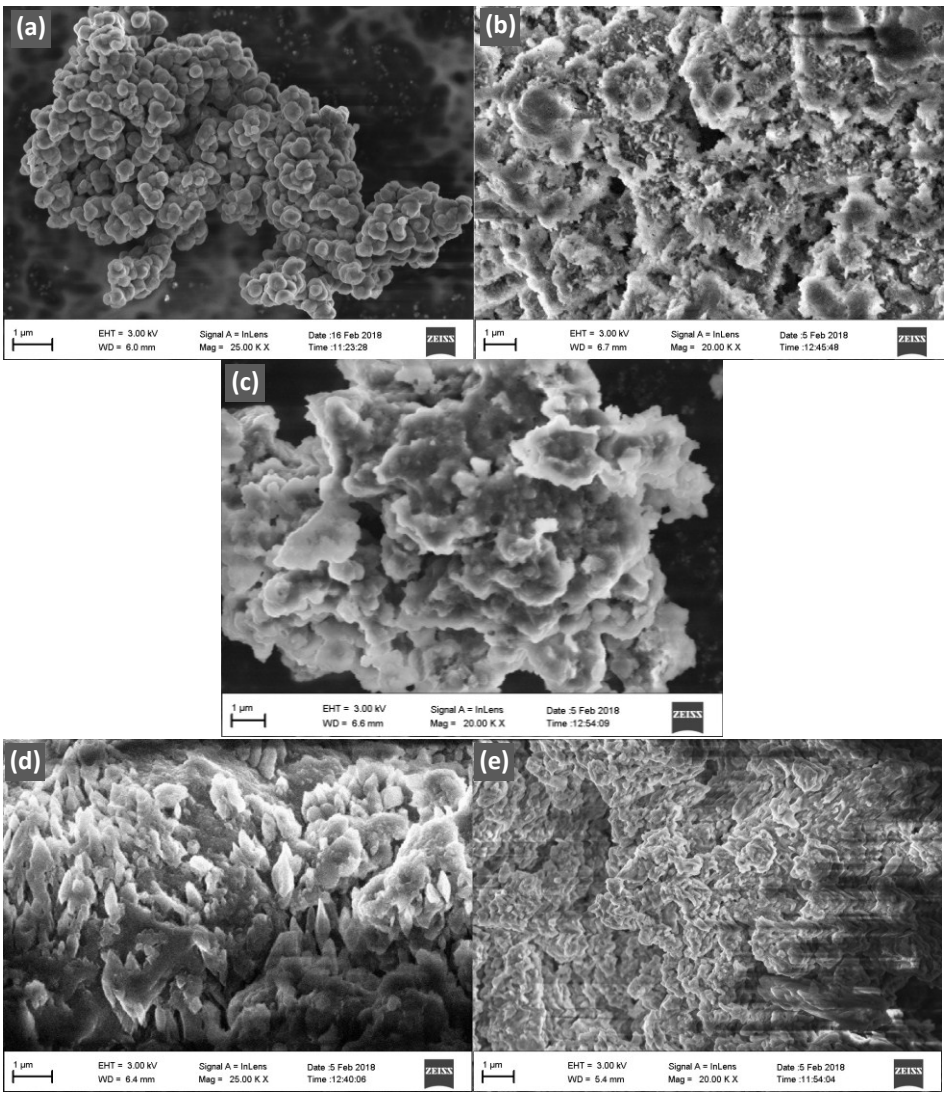

Figure 6.4 FESEM images of (a) PPy (b) LiPPy 1 (c) LiPPy 2 (d) LiPPy 3 (e) LiPPy 4

The FESEM images of pure PPy and lithiated PPy samples are shown in figure 6.4. When the polymerization of pyrrole is done using APS, the surface morphology is globular and the agglomerated PPy structure with singular granules having spherical shape can be observed. The FESEM image of unlithiated PPy clearly reveals the most commonly observed structure of PPy. The impact of lithiation on the morphology of PPy is clear from the FESEM images of the lithiated PPy samples. The spherically shaped globules start spreading as of pressed, using a hydraulic press or as smashed with a hammer. Upon increasing the amount of lithiation the distinct PPy globules start to fuse together, tending to get shaped into a layered structure as seen in the figures 6.4 (b), (c) and (d). From these images, it can be inferred that the individual particles seem to combine and become embedded with the adjacent particles, forming an agglomerated structure, as observed from the FESEM images of the lithiated PPy samples. At maximum lithiation the globular structure totally vanishes and the lithiated PPy acquires an almost uniform layered structure. This uniform layered structure helps in the arrangement of electrically conductive path ways inside the lithiated PPy chains [22]. The process of lithiation has much impact on the surface morphology of PPy, since it changes from a spherical or globular structure having minimum surface area to a layered structure with more surface area, upon lithiation, which is a better choice for applications in Li ion cells. The FESEM analysis shows that the lithiated PPy compositions turn out to be structurally more ordered with the increase in n-BuLi concentration. The formation of these ordered structures supports the earlier conclusions arrived at on the basis of the XRD studies.

6.3.5 Microstructure analysis-TEM studies

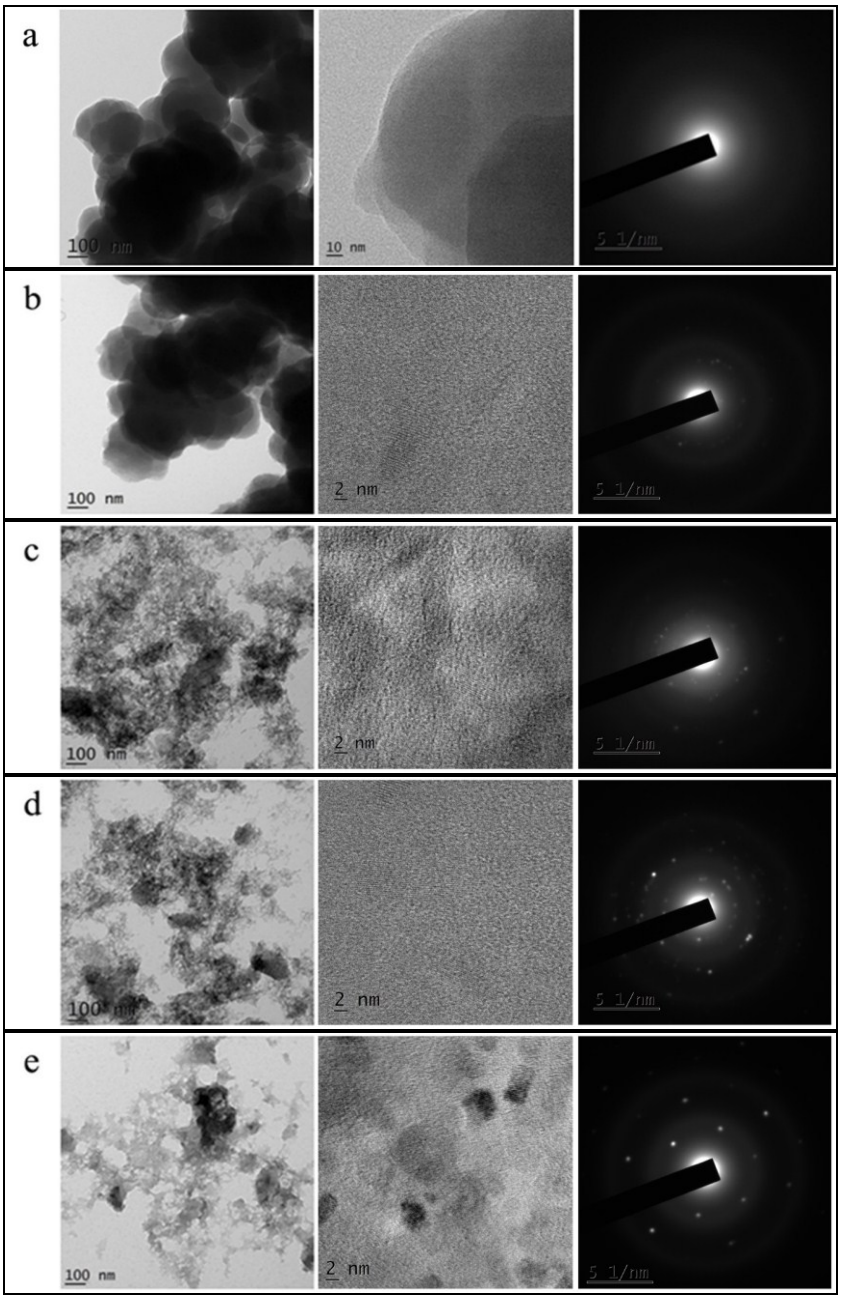

Figure 6.5 TEM images and SAED patterns of (a) PPy (b) LiPPy 1 (c) LiPPy 2 (d) LiPPy 3 (e) LiPPy 4

The TEM images and the selected area electron diffraction (SAED) patterns of PPy and the four lithiated PPy compositions in two magnification levels are shown in figure 6.5. The TEM images of PPy show nearly uniform spherical particles and the amorphous nature of pure PPy can be confirmed from the TEM images and the SAED pattern, in which there are no crystalline spots [10]. Significant changes are observed in the structure of PPy upon lithiation. In the sample LiPPy1, in which lithiation is least, one can see that the globular structure of PPy is not much affected and only the outer surface has been affected due to lithiation. In the samples LiPPy 2, LiPPy 3 and LiPPy 4, in which the extent of lithiation is higher, the globular structure is totally lost and it starts to form a porous, layered structure. With lithiation, PPy starts to show crystalline nature, which is evident from the SAED patterns, showing crystalline spots along with amorphous rings. In the sample LiPPy 4, in which lithiation is the highest, the SAED pattern shows the highest extent of crystalline nature. In the high resolution images at 2 nm scale of each sample, the presence of lattice fringes supports the presence of lithium within the PPy matrix. It is clear that as the degree of lithiation increases, the visibility of fringes is also increasing. Lattice fringes are found to be maximum in the sample LiPPy 4 while for sample LiPPy1 the lattice fringe visibility is reduced. It is also inferred that upon doping with n-BuLi, to achieve Li substitution, the individual PPy particles get grouped into agglomerates and lithium is distributed within the PPy matrix. The encapsulation of lithium inside PPy is clear from the lower magnification images of all the lithiated samples.

6.3.6 Electrical conductivity studies

Table 6.2 The DC electrical conductivity of PPy and lithiated PPy samples

Sample code	Electrical conductivity (S/cm)
PPy	3.52×10^{-4}
LiPPy 1	2.35×10^{-2}
LiPPy 2	4.69×10^{-2}
LiPPy 3	6.46×10^{-2}
LiPPy 4	7.15×10^{-2}

The DC electrical conductivity data of PPy and the lithiated PPy compositions at room temperature, measured using the Keithley 236 source measurement unit is summarized in Table 6.2. The conductivity of the lithiated samples relies upon the concentration of the n-BuLi dopant and keeps on increasing in the order of 10^{-2} S/cm with increase in the n-BuLi concentration. It has been observed that the conductivity depends on the doping level and the relative increase in conductivity of the lithiated samples with doping can be attributed to the creation of more extended conjugation lengths and the ordered arrangement of the polymer chains [23]. Increase of conductivity is consistent with the enhancement of crystallinity of the lithiated PPy compositions, observed in the XRD data and SAED patterns. The maximum electrical conductivity obtained for the lithiated PPy with maximum Li substitution shows 10 times enhancement compared to that of the lithiated PPy with maximum Li content, synthesized using $FeCl_3$ as the oxidant.

6.3.7 Thermo-gravimetric(TG) analysis

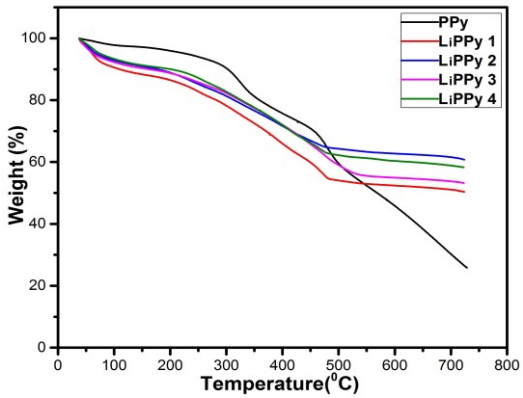

Figure 6.6 TG curves of PPy and lithiated PPy

Polypyrrole and the lithiated PPy compositions show good thermal stability and exhibit three distinct weight loss regions as per the thermo gravimetric (TG) curves shown in figure 6.6 The first weight loss occurs at temperatures between 70 ^{o}C to 130 ^{o}C for PPy and between 50 ^{o}C to 175 ^{o}C for the lithiated PPy samples due to the evaporation of the residual water [24]. The second weight loss occurring between 235 ^{o}C to 308 ^{o}C for PPy and 205 ^{o}C to 321 ^{o}C for the lithiated PPy compositions corresponds to the polymer degradation which is mainly due to the loss of the dopants from the polymer chain [25]. The final degradation occurs at 326 ^{o}C for PPy and approximately at 342 ^{o}C for all the lithiated PPy samples which represents the breaking of the PPy chains [19]. Moderate enhancement in thermal stability has been observed for the lithiated PPy samples.

6.3.8 Cyclic voltammetry (CV) studies

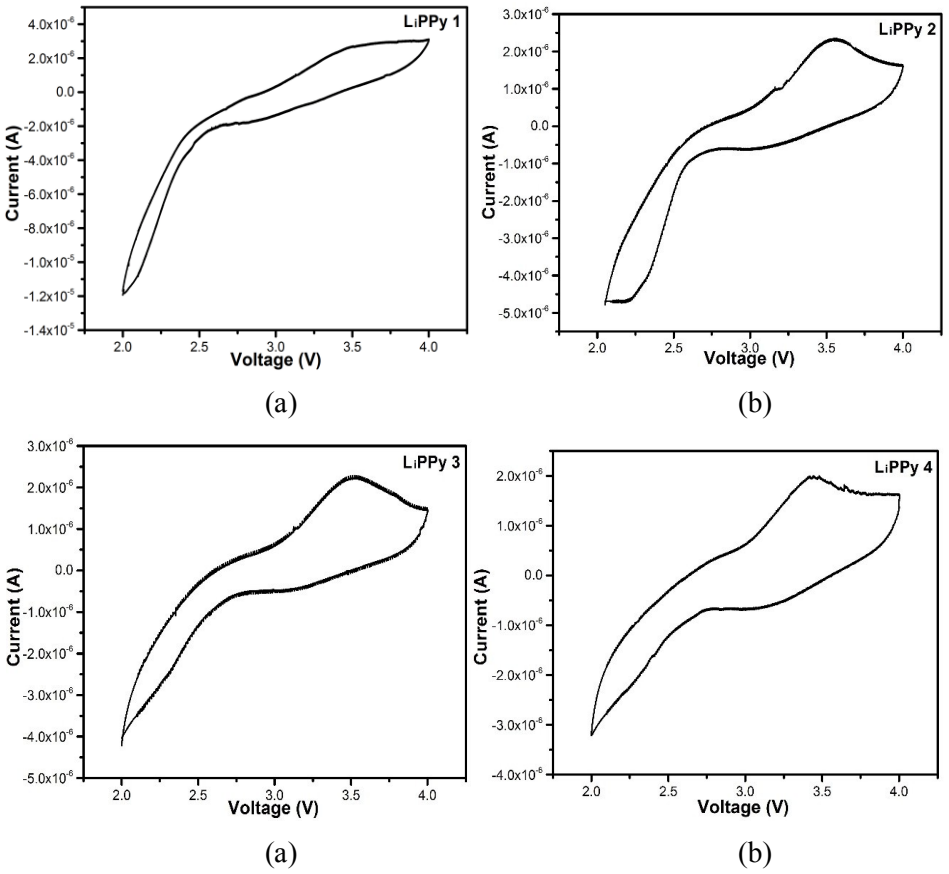

Figure 6.7 CV curves of (a) LiPPy 1 (b) LiPPy 2 (c) LiPPy 3 and (d) LiPPy 4 based Li ion cells

Cyclic voltammetry (CV) curves of Li ion cells assembled using lithiated PPy samples at a sweep rate of 0.1 mV/s and between 2 V to 4 V are shown in figure 6.8. The cells are found to indicate stable open circuit voltage around 3.8 V. All the CV curves show oxidation potential at 3.5 V and reduction potential at 2.7 V. The anodic scan peak at 3.5 V is related to

the removal of Li from the lithiated PPy cathode, through the electrolyte to the anode and the cathodic scan peak at 2.7 V corresponds to the intercalation of Li back to the cathode from the anode [26]. The good oxidation/reduction reversibility of the lithiated polypyrrole cathode is revealed by the symmetrical peaks in the CV curves corresponding to the four lithiated samples with relative increment in the narrow peak-to-peak separation of the anodic and the cathodic potential. The excellent electrochemical activity of Li ions in lithium substituted polypyrrole is revealed by the increase in the area under the anodic and cathodic peaks with increase in lithium substitution. [4].

6.3.9 Charge- discharge studies

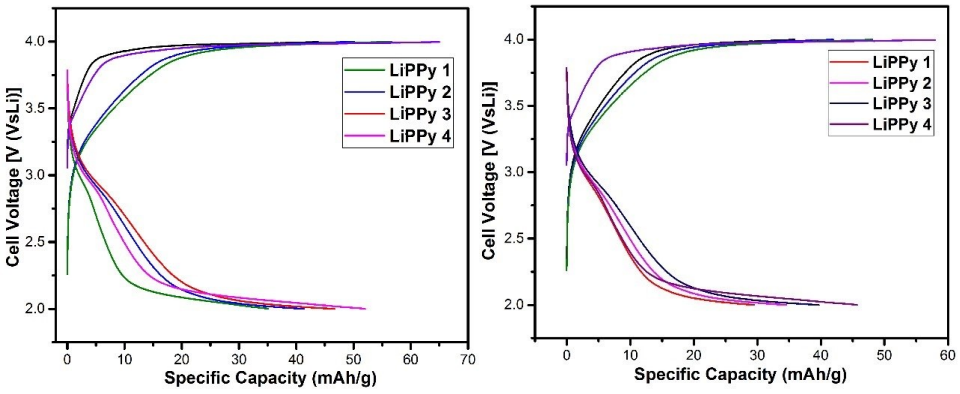

Figure 6.8 Charge-discharge profiles of LiPPy 1, LiPPy 2, LiPPy 3 and LiPPy 4 based Li ion cells at (a) 0.1 C and (b) 0.2 C

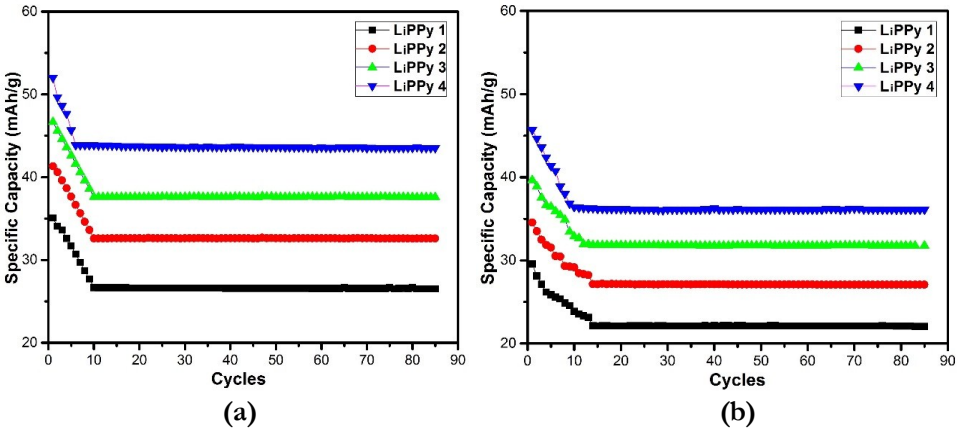

Figure 6.9 Cycling performance of LiPPy1, LiPPy 2, LiPPy 3 and LiPPy 4 based Li ion cells at (a) 0.1 C and (b) 0.2 C

The charge-discharge profiles of the four assembled cells between 2 V and 4 V are shown in figures 6.8 (a) and (b) for two different current rates and the cycling performance of the cells is illustrated in figures 6.9 (a) and (b). The cell based on LiPPy 4 (maximum lithium content of 25.8 %) shows the first discharge capacity of 52.02 $mAhg^{-1}$ and 45.70 $mAhg^{-1}$ at 0.1 C and 0.2 C respectively with a slight fading of capacity upto the 7^{th} cycle and the 9^{th} cycle respectively. Thereafter the discharge capacity at 0.1 C and 0.2 C remains stable at 43.6 $mAhg^{-1}$ and 36.8 $mAhg^{-1}$ respectively till the 85^{th} cycle corresponding to the capacity retention of about 83.8 % and 82.7 %. The theoretical capacity of lithiated polypyrrole is 72 $mAhg^{-1}$, corresponding to 100% lithiation. The maximum lithiation accomplished in the present work is about 25.8 % only and hence the experimentally obtained capacity is not very close to the theoretical one. The cells based on LiPPy 3, LiPPy 2 and LiPPy 1 deliver initial discharge capacities of 46.7 $mAhg^{-1}$, 41.3 $mAhg^{-1}$ and 35.1 $mAhg^{-1}$ at 0.1 C respectively. The corresponding initial

capacity values at 0.2 C are 39.6 $mAhg^{-1}$,34.5 $mAhg^{-1}$ and 29.5 $mAhg^{-1}$ respectively. The steady capacity values retained in the cells based on LiPPy 3, LiPPy 2 and LiPPy 1 are 37.5 $mAhg^{-1}$, 32.6 $mAhg^{-1}$ and 26.5 $mAhg^{-1}$ at 0.1 C and 31.8 $mAhg^{-1}$, 27.1 $mAhg^{-1}$, 22.5 $mAhg^{-1}$ at 0.2 C respectively. All the cells based on the four lithiated PPy compositions exhibit a capacity retention of about 83.8 % and 75.7% at 0.1 C and 0.2 C respectively. On an average, the coulombic efficiency of all the cells, retains a steady value between 85 % – 88 % for all the charge discharge cycles at 0.1 C and 0.2 C. The realization of lithiated polypyrrole based Li-ion cells with specific capacity near the theoretical limit, high coulombic efficiency and fabulous cycling stability is still in the initial stages of development. In the earlier work described in the previous chapter, the discharge capacity of the cells based on lithiated polypyrrole with maximum lithium substitution is around 30.03 $mAhg^{-1}$ for the first cycle, in which polypyrrole is synthesized using $FeCl_3$ as the oxidant [16]. Compared to the previous work, the charge-discharge behaviour and the cycling stability of the Li ion cells developed in the present work, based on Li substituted PPy, synthesized using APS as the oxidant are much more impressive. The discharge capacity is higher and closer to the theoretical capacity of Li substituted PPy.

6.4 Conclusions

The present work features the superior electrochemical performance offered by the assembled Li ion cells based on lithium substituted PPy, synthesized using APS as the oxidant, compared to the performance of the cells based on lithiated PPy, synthesized using $FeCl_3$

as the oxidant.. The structural studies using FTIR spectroscopy and XRD and the morphological changes observed in the lithiated PPy as per FESEM and TEM investigations strongly support successful lithium substitution in PPy and the enhanced crystallinity acquired. The CV curves and the charge-discharge profiles of the Li ion cells based on lithium substituted PPy, synthesized using APS as the oxidant, reveal excellent electrochemical behaviour, enhanced discharge capacity closer to the theoretical value and superior cycling stability, compared to the earlier work described in the previous chapter. The highlight of the present work is the awareness that the discharge capacity and the energy density of the cells can be enhanced further by optimising the polymer synthesis conditions with proper choice of the oxidants and dopants.

References

[1] X. Gao1, Z. S., Wenbin Luo, Chao Zhong, David Wexler et.al, Novel Germanium/Polypyrrole Composite for High Power Lithium-ion Batteries, Sci. Rep.,4 (2014) 6095

[2] X. Du, T. Yang, J. Lin, T. Feng, J. Zhu, L. Lu, Y. Xu, and J. Wang, Microwave-Assisted Synthesis of SnO 2 @ polypyrrole Nanotubes and Their Pyrolyzed Composite as Anode for Lithium-Ion Batteries, ACS Appl. Mater. Interfaces 8 (2016) 15598–15606

[3] Bruno Scrosati, Jusef Hassoun and Yang-Kook Sun, Lithium-ion batteries. A look into the future. Energy Environ. Sci., 4 (2011) 3287–3295

[4] A. B. Puthirath, B. John, C. Gouri, and S. Jayalekshmi, Lithium doped polyaniline and its composites with, RSC Adv., 5 (2015) 69220–69228

[5] M. Gerard, A. Chaubey, and B. D. Malhotra, Application of conducting polymers to biosensors, Biosens. Bioelectron., 17(5) (2002) 345–359

[6] N. Suhada, M. Tahiruddin, R. Daik, and B. Selangor, Synthesis and characterization of anionic surfactants doped polypyrrole, Der Pharma Chemica, 7(6) (2015) 159–162

[7] A. Kassim, Z. B. Basar, and H. N. M. E. Mahmud , Effects of preparation temperature on the conductivity of polypyrrole conducting polymer, J. Chem. Sci., 114(2) (2002) 155–162

[8] L. Yuan, J. Wang, S. Y. Chew, J. Chen, Z. P. Guo, L. Zhao, K. Konstantinov, and H. K. Liu, Synthesis and characterization of SnO 2 – polypyrrole composite for lithium-ion battery, Journal of Power Sources, 174(2) (2007) 1183–1187

[9] X. Gao, Y. Deng, D. Wexler, G. Chen, S. Chou, H. Liu, Z. Shi, and J. Wang, Improving the electrochemical performance of the LiNi0.5Mn1.5O4 spinel by polypyrrole coating as a cathode material for the lithium-ion battery, J. Mater. Chem. A, 3 (2015) 404–411

[10] C. Basavaraja, W. J. Kim, D. G. Kim, and D. S. Huh, Synthesis and characterization of soluble polypyrrole–poly(ε-caprolactone) polymer blends with improved electrical conductivities, Mater. Chem. Phys., 129 (2011) 787–793

[11] P. Xin, B. Jin, H. Li, X. Lang, C. Yang, W. Gao, Y. Zhu, W. Zhang, S. Dou, and Q. Jiang, Facile Synthesis of Sulfur–Polypyrrole as Cathodes for Lithium–Sulfur Batteries, Chemelectrochem, 4 (2017) 115-121

[12] R. P. Ramasamy, B. Veeraraghavan, B. Haran, and B. N. Popov, Electrochemical characterization of a polypyrrole / Co 0 . 2 CrO x composite as a cathode material for lithium ion batteries, Journal of Power Sources 124 (2003)197–203

[13] X. Liu, Y. Li, Y. Zhao, H. Li, and F. Yin, "In Situ Polymerization Synthesis of Ternary Sulfur / Polypyrrole / Graphene Nanosheet Cathode for Lithium / Sulfur Batteries, Materials Science Forum, 847 (2016) 8-13

[14] W. Wang, G. Li, Q. Wang, G. Li, S. Ye, and X. Gao, Sulfur-Polypyrrole / Graphene Multi-Composites as Cathode for Lithium-Sulfur Battery, J. Electrochem. Soc., 160(6) (2013) A805–A810

[15] P. Xin, B. Jin, H. Li, X. Lang, C. Yang, W. Gao, Y. Zhu, W. Zhang, S. Dou, and Q. Jiang, Facile Synthesis of Sulfur–Polypyrrole as Cathodes for Lithium–Sulfur Batteries, Chemelectrochem, 4 (2017) 115-121

[16] J. John, M. Manoj, K. M. Anilkumar, V. S. Pradeep, and S. Jayalekshmi, Lithium-enriched polypyrrole as a prospective cathode material for Li-ion cells, Ionics, 24 (2018) 2565-2574

[17] M. T. Ramesan, Synthesis, Characterization, and Conductivity Studies of Polypyrrole / Copper Sulfide Nanocomposites, Journal of Applied Polymer Science, 128(3) (2012) 1–7

[18] S. Fujii, S. P. Armes, R. Jeans, R. Devonshire, Synthesis and Characterization of Polypyrrole-Coated Sulfur-Rich Latex Particles, Chem. Mater., 18(11) (2006) 2758–2765

[19] H. Ghalib, I. Abdullah, R.Daik, Electrical Conductivity of Anionic Surfactant-Doped Polypyrrole Nanoparticles Prepared via Emulsion Polymerization, Pertanika Journal of Science and Technology, 21(2) (2013) 459–472

[20] H. K. Chitte, N. V Bhat, V. E. Walunj, and G. N. Shinde, Synthesis of Polypyrrole Using Ferric Chloride (FeCl 3) as Oxidant Together with Some Dopants for Use in Gas Sensors, Journal of Sensor Technology, 1 (2011) 47–56

[21] N. Su, H.B.Li, S.J. Yuan, Synthesis and characterization of polypyrrole doped with anionic spherical polyelectrolyte brushes, Express Polym. Lett., 6(9) (2012) 697–705

[22] S. Bilal, M. Sohail, and A. A. Shah, Synthesis and Characterization of Soluble and Thermally Stable Polypyrrole-DBSA Salts, J Chem. Soc.Pak., 36(6) (2014) 976–982

[23] S. Arunsawad, K. Srikulkit, and S. Limpanart, Effect of Surfactant on Conductivity of Poly (pyrrole- co -formyl pyrrole) via Emulsion Polymerization, Journal of Metals 24(2) (2014) 29–34

[24] M. Trchova and J. Kova, Synthesis and structural study of polypyrroles prepared in the presence of surfactants, Synth. Met., 138 (2003) 447–455

[25] M. Sohail, S. Bilal, and A. A. Shah, Synthesis and characterization of completely soluble polypyrole salts via inverse emulsion polymerization using a mixture of chloroform and 2- butanol as a dispersing medium, JPMS Conference Issue Materials, (2011) 12–15

[26] L. Qie, L. Yuan, W. Zhang, W. Chen, and Y. Huang, Revisit of Polypyrrole as Cathode Material for Lithium-Ion Battery, Journal of the Electrochemical Society, 159(10) (2012) 1624–1629

Chapter 7

SULFUR/POLYPYRROLE COMPOSITE CATHODES FOR APPLICATIONS IN HIGH ENERGY DENSITY LITHIUM-SULFUR CELLS

Lithium–sulfur cells are quite promising devices for the next generation energy storage applications. However, their specific capacity and cycling stability are adversely affected by poor electrical conductivity of sulphur, the shuttling effect of lithium polysulfides and the volume expansion of sulfur during lithium intake. These limitations can be averted through modifying the sulphur cathode by making composites with electrically conducting polymers and carbon nanostructures. The work presented in this chapter mainly deals with the modification of sulphur cathode by making composites with polypyrrole, graphene and polypyrrole/graphene and the investigations carried out to assess their suitability to design Li-S cells with high energy density and good cycling stability.

7.1 Introduction

Rechargeable lithium batteries are being developed for power applications in portable electronic devices, medical implants, hybrid electric vehicles and grid storage because of their higher energy density and cycling stability compared to other types of batteries [1]. Despite the fact that lithium-ion cells are leading power sources for numerous applications, their extensive applications are confined by the cost,

security and toxicity issues. Lithium ion cells based on cathode materials like $LiFePO_4$ and a wide range of derivatives of $LiMn_2O_4$, with higher energy density, less toxicity and low cost have been effectively developed and marketed [2]. However, the theoretical capacity of all of these materials cannot fully satisfy the requirements of large scale applications, such as in hybrid electric vehicles and in the automobile sector requiring quite high energy density. Presently, Li ion batteries use transition metal oxides and phosphates as cathodes, which have an inherent theoretical capacity limit of 300 $mAhg^{-1}$ and most extreme usable limit of just around 210 $mAhg^{-1}$. Along these lines, the capacity limit of lithium batteries is incredibly traded off [3].

The theoretical capacity of sulphur around 1675 $mAhg^{-1}$ is much higher than that of many of the known cathode materials, which permits it to be used as prospective high capacity cathode material for Li based rechargeable cells. Moreover, its low operating voltage of ~2.1 V can offer security preferences over the high voltage intercalation cathodes with operating voltages higher than 3.3 V [4]. Sulfur is abundant in nature and is a progressively appealing cathode material due to its low cost, non-toxicity, environmental benignity and much higher theoretical energy density around 2567 W h Kg^{-1}. These advantageous aspects make it a promising cathode material for applications in the next generation energy storage devices, called as Li-S cells [5]. Regardless of the previously mentioned advantages, there are a few limitations which hinder the progress of the Li-S cell technology. The low electrical conductivity of sulphur cathode which prompts the low usage of sulfur and the poor rate capability of sulfur

are some of the prime disadvantages. The high solubility of the polysulfide ions that are formed during the multistep electrochemical reduction processes, in organic solvent electrolytes causes irreversible loss of sulphur active material over repeated charge-discharge cycles [6]. The rapid degradation of the electrochemical performance happens because of the volume changes during lithium reaction processes and the insulating nature of sulphur used as the cathode material, prompts low coulombic efficiency [7].

The long chain polysulfides (Li_2Sn, $2<n<8$), can diffuse through the electrolyte and move to the Li anode where they react with the lithium electrode to generate lower order polysulfides such as Li_2S or Li_2S_2, which diffuse back to the sulphur cathode and regenerate the higher forms of polysulfides [8]. This cyclic process, called as the shuttle effect is driven by the concentration gradient of polysulfides and it provides a potential benefit for overcharge protection of Li-S cells. In any case, left unchecked, it diminishes the active mass utilization during discharge, triggers current leakage and poor cyclability and markedly reduces the coulombic efficiency of the cell. [9].

To overcome these inadequacies regarding discharge capacity, cyclability and coulombic efficiency of sulphur cathode in Li-S cells, various methods have been developed. They include, proper choice of the organic electrolyte and the modification of the sulphur cathode by making sulfur/carbon and sulfur/conductive polymer composites [10]. Various carbon-sulfur composites using porous hollow carbon, microporous carbon spheres, porous carbon nanospheres and

mesoporous carbon have been developed to encapsulate sulfur in order to enhance the conductivity of sulfur and effectively prevent the dissolution of lithium polysulfides in the electrolyte during cycling [11]. Research work on graphene has been intensified in recent years, owing to its unique electronic, photonic and mechanical properties and the ability to act as a perfect substrate for depositing functional materials for high performance electrochemical devices [12]. Graphene as a conductive matrix for Li-S cells has emerged as one of the most promising materials to modify sulphur cathode by making composites owing to its exceptional two dimensional morphology, high specific surface area of over 2600 m^2/g, superior electrical conductivity, and excellent structural stability [13].

To upgrade the cell capacity and cyclability of Li-S cells, polymer additives are utilized to improve the efficiency of sulfur and furthermore to upgrade the electrochemical connectivity between active material particles. Electrically conducting polymers can be incorporated into the sulfur composites to prevent the diffusion of polysulfides and to improve the electrochemical performance [14]. Among the possible conducting polymers, PPy is one of the most promising candidates to synthesize electrochemically active sulfur composites because of its high electrical conductivity, environmental stability, high specific energy, high theoretical capacity and reversible redox-active property [15]. It can assume various roles as an active material, conducting additive and adsorbing agent in sulphur/PPy composites [16]. The PPy-covered cathode is found to have attractive properties as a modified sulfur cathode [17] and PPy shows good compatibility with sulfur and organic electrolytes. The morphology

of polypyrrole is perfect to enhance the electrochemical conductivity of the sulfur cathode [18].

7.2 Materials and methods

The chemicals used for the synthesis of PPy and PPy composites were of analytical grade and pyrrole monomer obtained from Aldrich Chemicals was purified by distillation. Ammonium persulfate, graphene and sulfur were purchased from Sigma-Aldrich and were used without further purification.

7.2.1 Synthesis of soluble polypyrrole (PPy)

In the present work, polypyrrole (PPy) was synthesized by chemical oxidative polymerization with dodecylbenzene sulfonic acid (DBSA) as the dopant and ammonium persulfate (APS) as the oxidant, the details of which are already given in earlier chapters.

7.2.2 Synthesis of PPy/sulfur composite (PPyS)

In a typical synthesis, 0.4 g of the DBSA doped PPy and 0.6 g of sulphur were dispersed in 20 ml and 40 ml de-ionized water individually at room temperature and both the dispersions were sonicated for 1 hour. The solutions were then mixed together and stirred for 6 hours. The resulting precipitate was filtered, washed and dried in hot air oven at 60 ^{o}C over night to obtain the polypyrrole/sulfur composite labelled as PPyS.

7.2.3 Synthesis of sulfur/graphene (SG) nanocomposite

Sulfur/graphene nanocomposite was synthesized by mixing 0.2 g of graphene and 0.6 g of sulfur in 50 ml deionized water. The mixture

was ultrasonicated for 6 hours to get a uniform suspension. The mixture was then hydrothermally treated for 12 hours at 180 ^{o}C to enable the liquefied sulfur to enter into the layers of graphene. The resulting precipitate was filtered, washed and dried in hot air oven at 60 ^{o}C overnight. The gathered dried powder was marked as sulfur/graphene composite SG.

7.2.4 Synthesis of polypyrrole/ graphene (PPyG) composite

The PPy/graphene composite was synthesized by taking 0.4 g of the synthesized soluble PPy and 0.2 g of graphene in 40 ml deionized water. The mixture was ultrasonicated for 6 hours. The synthesized composite was filtered and rinsed several times with distilled water and methanol. The powder consequently acquired was vacuum dried at 60 ^{o}C for 24 hours and was labelled as PPyG

7.2.5 Synthesis of polypyrrole/ graphene/sulfur composites (PPyGS)

In a typical synthesis, 0.2 g of graphene was dispersed in 100 ml deionized water at room temperature and ultrasonicated for 8 hours. To this solution, 4 g aqueous suspension of sulfur was gradually added and stirred for 6 hours. Then, 0.5 g of the synthesized, DBSA doped, pyrrole was added to this solution and kept under magnetic stirring vigorously for 24 hours. The solution was then hydrothermally treated for 12 hours at 180 ^{o}C. The resulting precipitate was filtered and washed repeatedly in distilled water until the solution became clear. Finally, the synthesized composite was vacuum dried overnight at 70 ^{o}C. The dried powder was labelled as PPyGS

7.2.6 Structural, morphological, elemental and thermal characterization

The synthesized composite samples were subjected to FTIR spectroscopy, XRD and Raman spectroscopy studies and CHNS and thermo-gravimetric analysis as explained in the previous chapters. The surface morphology of the composite samples was analyzed using the Carl Zeiss Sigma field emission scanning electron microscope and the transmission electron microscopy studies were carried out using Jeol/JEM 2100 model machine.

7.2.7 Electrochemical characterization

The cathode electrodes for Li-S cells were prepared by mixing 80 weight % of the active material (PPyS, SG, PPyGS) with 10 weight % of acetylene black as conducting medium and 10 weight % of polyvinylidene difluoride (PVDF) in N-methyl pyrrolidone (NMP) solvent as binder. The homogeneous slurry obtained was coated on a thin aluminum foil by spray coating and was allowed to dry at 60 °C overnight under vacuum. Finally, circular discs were cut from the coating and used as cathode discs. The mass of cathode material on each piece of circular discs was approximately 1.8 mg.

The electrochemical characterizations were carried out by assembling stainless steel Swagelok cells in an argon filled glove box. The electrolyte used was 1 M lithium perchlorate in a mixed solvent of 1, 3-dioxolane (DOL) and 1, 2-dimethoxymethane (DME) at a volume ratio of 1:1 including 0.5 M $LiNO_3$ as an electrolyte additive. Lithium metal was used as the counter/reference electrode and celgard, as the separator.

The cyclic voltammetry (CV) studies were carried out using Bio-Logic SP300 workstation, at a scan rate of 0.1 mV/s between the voltage window of 1.5 - 3 V. The galvanostatic charge-discharge tests of the assembled cells were conducted at various C-rates (1C=1650 $mAhg^{-1}$) using the 8 Channel Battery Analyzer (MTI Corporation-USA) in the potential window of 1.5-3 V.

7.3 Results and discussion

7.3.1 FTIR spectroscopic studies

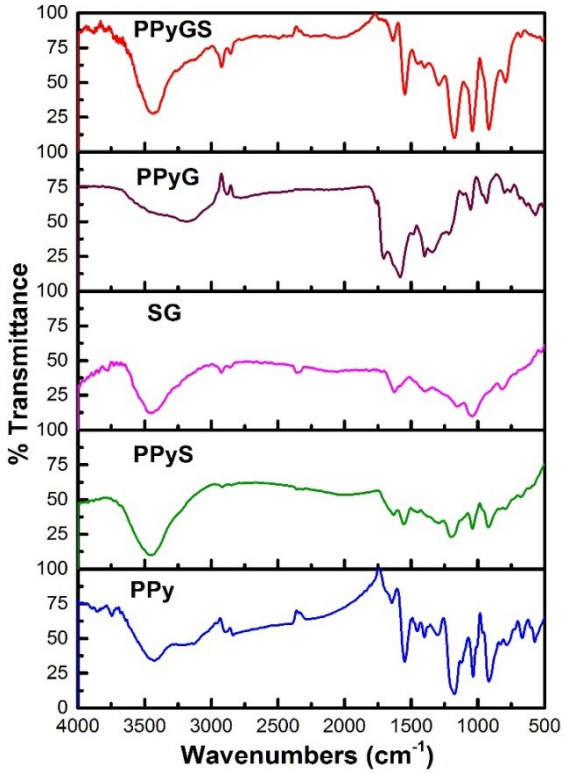

Figure 7.1 FTIR spectra of PPy, PPyS, SG, PPyG sand PPyGS

The FTIR spectra of pure PPy, PPyS, SG, PPyG and PPyGS are shown in figure 7.1. The NH stretch mode is present at 3443 cm^{-1} in PPy and strong peaks due to NH vibrations are observed respectively at 3454 cm^{-1} , 3452 cm^{-1} , 3171 cm^{-1} and 3436 cm^{-1} in the spectra of PPyS, SG, PPyG and PPyGS [19]. The bands in the range 1540 cm^{-1} to 1580 cm^{-1} in PPy and its composites with sulfur and graphene correspond to the C=C stretching vibrations of the pyrrole ring [20]. The spectrum of PPyS is almost identical to that of PPy with slight decrease in the intensity of peaks, showing the effective blending of PPy with sulfur particles. It can also be inferred that there are no chemical reactions between PPy and sulphur in the composite. The peaks at 1585 cm^{-1} and 1548 cm^{-1} in PPyG and PPyGS can be attributed to the skeletal vibrations of graphene sheets and the weak peak at 1625 cm^{-1} in SG is related to the presence of the O-H bending vibrations and additionally, the contribution from epoxide groups and skeletal vibrations [21]. All the characteristic peaks of PPy are seen in the spectrum of PPyG composite, but shifted more or less because of the interaction of the two components [22]. The spectrum of PPyGS composite shows the presence of C-N stretching vibrations from 1301 cm^{-1} to 1398 cm^{-1}, C-H in-plane deformation vibrations from 1159 cm^{-1} to 1198 cm^{-1} and C-H out-of –plane deformation vibrations from 909 cm^{-1} to 937 cm^{-1} [23]. The blended polypyrrole/graphene/sulfur composite has identical peak positions related to the structure of PPy and the PPy structure is retained in all the composite samples.

7.3.2 XRD studies

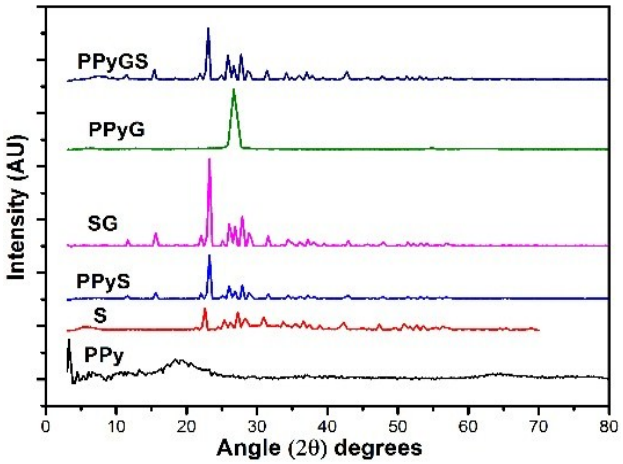

Figure 7.2 XRD patterns of PPy, PPyS, SG, PPyG and PPyGS

The XRD patterns of PPy, PPyS, SG, PPyG and PPyGS composites are shown in figure 7.2. For PPy, the broad peak observed at 18.5^{o} indicates its typical amorphous nature and is in agreement with the previous data in the literature. In the XRD pattern of sulfur, several sharp diffraction peaks are observed in the range of 15° to 60°, indicating its good crystalline structure [24]. The XRD pattern of PPyS shows sharp peaks at 15^{0}, 23.2^{0}, 26.1^{0} and 28.8^{0}, which correspond to those of orthorhombic sulfur [25]. The SG composite also shows well defined peaks at 23.2^{0}, 26.8^{0}, 27.1^{0} and 28^{0}. The sharp peak of PPyG at 26.7 ^{o} and the small peak at 54.8^{o} represent the presence of graphene in the composite [26]. The XRD plot of PPyGS shows a pattern similar to that of PPyS with an intense peak at 23.2° along with the peaks at 25.8^{o} and 27.8^{o} with significantly reduced intensity indicating the higher crystallinity and larger crystalline domains of sulfur. It is obvious from

the XRD pattern of PPyGS that the intensity of the diffraction peaks of graphene diminishes when PPy and sulfur are incorporated onto the surface of graphene.

7.3.3 Raman analysis

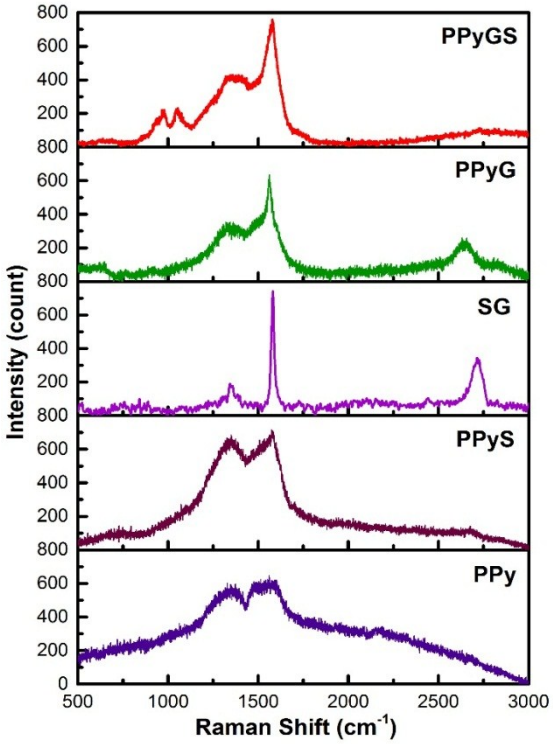

Figure 7.3 Raman spectra of PPy, PPyS, SG, PPyG and PPyGS

The structural information of polypyrrole and its composites with graphene and sulfur is further evaluated by Raman spectroscopy and the spectral details are given in figure 7.3. The Raman spectra confirm the presence of sulfur and graphene in the polypyrrole based composites. The positions of the characteristic G and D bands and the I_D/I_G of the samples are shown in Table 7.1.

Table 7.1 Raman spectral data of PPy and its composites with sulfur and grapheme

Sample	D band cm^{-1}	G band cm^{-1}	I_D/I_G
PPy	1354	1560	0.98
PPyS	1344	1574	0.95
SG	1343	1586	0.26
PPyG	1345	1571	0.52
PPyGS	1345	1382	0.57

The peak intensity proportion of D band and G band (I_D/I_G) is quite low in the polypyrrole/graphene/sulfur and polypyrrole/graphene composites which shows that the conjugated structure of PPy is improved with the expansion of the molecular chains and the level of imperfections of PPy has been reduced after forming composites with sulfur and graphene [27]. The tremendous decrease of I_D/I_G for the SG composite shows the significant improvement of the level of disorder in the composite which implies that the incorporation of sulfur can effectively diminish a portion of the functional groups on the graphene surface and repair lattice defects [24]. The presence of PPy in the composite PPyGS is revealed by the small peak at 1054 cm^{-1} which is assigned to the C-H in plane deformation vibration [28] and also by the peak at 979 cm^{-1}, which is related to the bipolaron and polaron structure of PPy [27].

7.3.4 CHNS Analysis

Table 7.2 CHNS analysis data of PPy, PPyS, SG, PPyG and PPyGS

Sample number	Sample name	N%	C%	S%	H%
1	**PPy**	13.74	46.22	**1.26**	3.00
2	**PPyS**	2.06	5.91	**67.65**	0.56
3	**SG**	1.25	5.29	**87.15**	ND
4	**PPyG**	2.15	6.56	**12.14**	0.76
5	**PPyGS**	1.70	9.43	**88.67**	0.68

Using CHNS elemental analysis, the sulfur content in the composites was determined and the percentage concentrations of all the relevant elements in the composites are shown in Table 7.2. The analysis shows that the sulfur content in the SG and PPyGS composites is about 87 % and 88 % respectively. The presence of graphene as a template facilitates the better dispersion of sulfur in the composites which is desirable in the designing of practical Li-S cells [29].

7.3.5 TGA Analysis

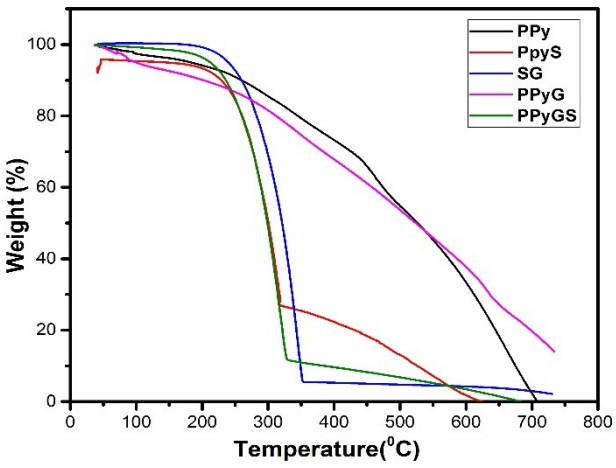

Figure 7.4 TG curves of PPy, PPyS, SG, PPyG and PPyGS

The thermo-gravimetric (TG) curves of PPy, PPyS, SG, PPyG and PPyGS are shown in figure 7.4. Polypyrrole shows weight loss at around 66 °C to 137 °C which is due to the loss of moisture bound in the polypyrrole matrix and the decomposition of PPy starts at 325 °C. The composite, PPyS loses about 3 % of its weight in the temperature range of 107 °C to 121 °C which is a direct result of the vanishing of water content. A second weight reduction of around 67 % happens in PPyS composite which begins at 212 °C because of the loss of sulfur and is complete before 307 °C. The SG composite exhibits a weight loss of 87 % starting from 217^0 C to 310 °C due to the loss of sulphur. This tendency comparison enables one to estimate the weight loss in the PPyGS composite as 89 % from the exceptionally permeable structure of the composite [30]. The TG curves demonstrate that, for the sulfur composites, the shift of the decomposition temperature to the lower temperatures, compared to that of PPy is due to the lower melting point of sulfur. The quantity of sulfur estimated in the sulphur composites perfectly matches with the results obtained by the CHNS chemical analysis The TG plots of pure PPy and PPyG composite show similar shapes, but the thermal stability of the PPyG composite is better than of PPy.

7.3.6 FESEM studies

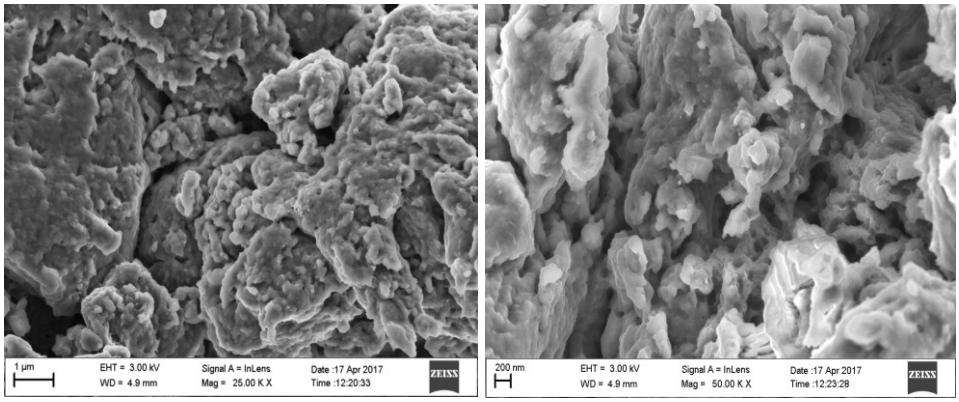

(a)

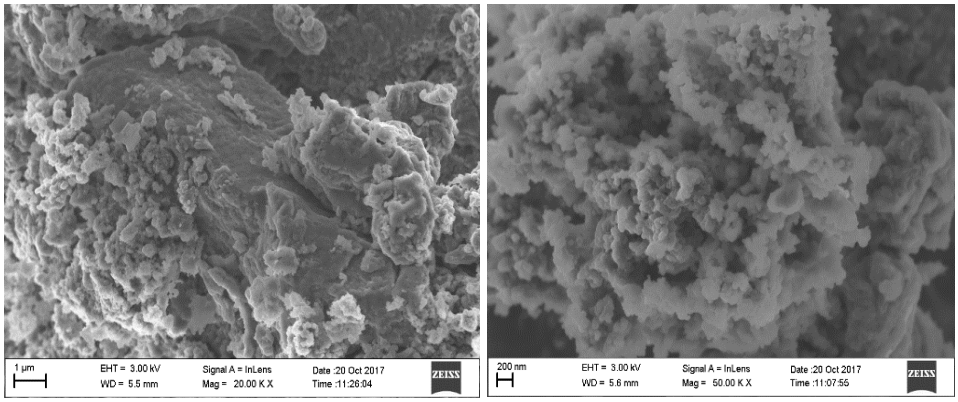

(b)

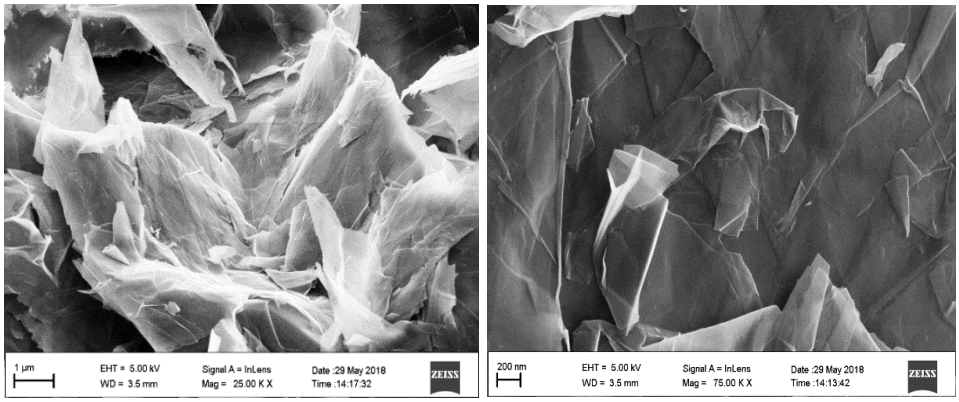

(c)

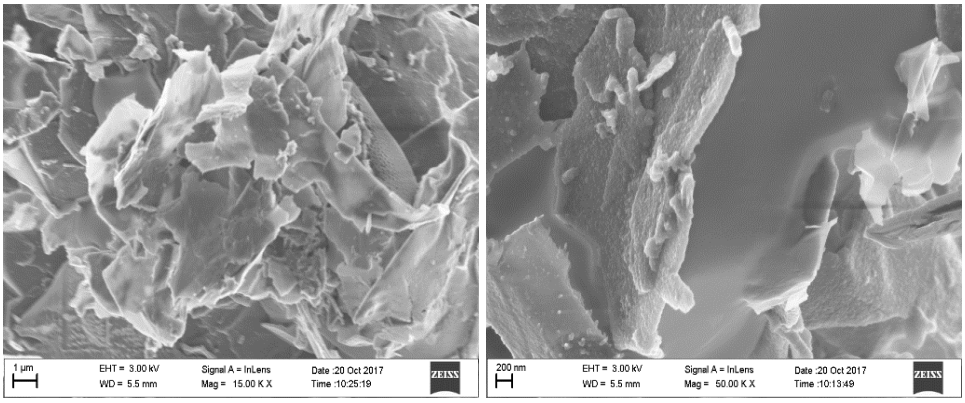

(d)

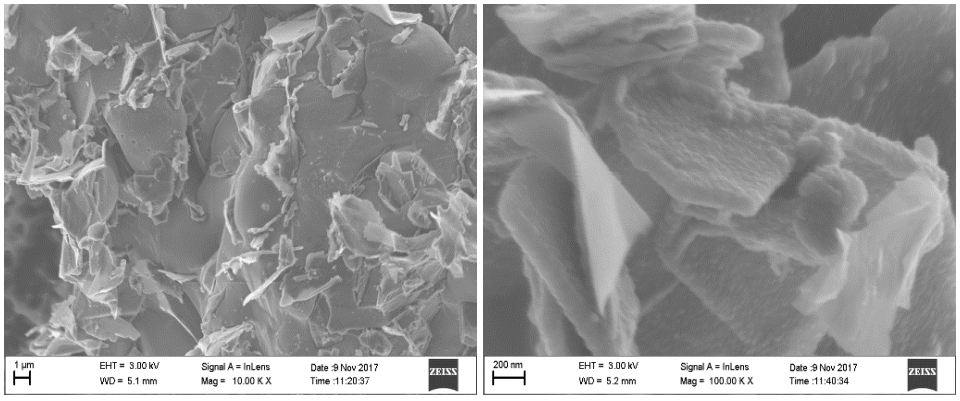

(e)

Figure 7.5 FESEM images of (a) PPy (b) PPyS (c) SG (d) PPyG and (e) PPyGS

Field emission scanning electron microscopy (FESEM) images of PPy and the composites are shown in figure 7.5. The images of PPy shown in figure 7.5 (a) exhibit the typical globular structure of PPy in which no phase division is seen which indicates good compatibility of the dopant DBSA and polypyrrole [31]. The images of PPy/sulfur composite illustrated in figure 7.5 (b) give a clear vision of sulphur particles being covered by PPy. Spherically moulded sulfur particles efficiently covered by graphene sheets are seen in the images shown in figure 7.5 (c). The image at 200 nm in figure 7.5 (d) obviously shows the presence of PPy over the graphene layers and the composite is having a layered structure. Because of the electrostatic attraction between polypyrrole and graphene, polypyrrole can easily get absorbed onto the surface of graphene [32]. The images of PPyGS composite presented in figure 7.5 (e) illustrate that the composite is having a layered structure. However the layer surface seems to be granular or it is more harsh than the layered structure of PPyG composite which is due to the presence of sulphur particles.

7.3.7 TEM studies

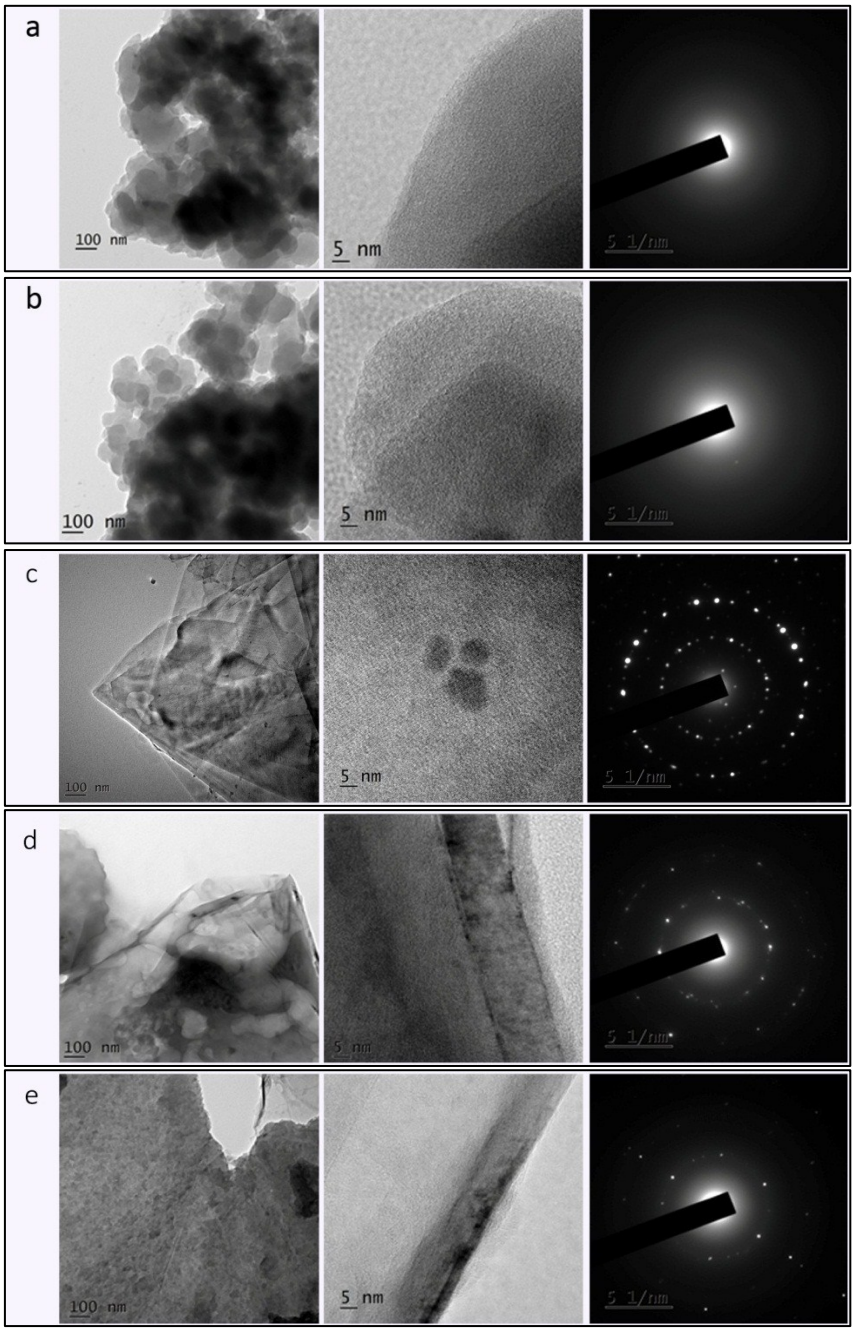

Figure 7.6 TEM images of (a) PPy (b) PPyS (c) SG (d) PPyG and (e) PPyGS

The TEM images of PPy, PPyS, SG, PPyG and PPyGS are shown in figure 7.6. The images of PPy in figure 7.6 (a) demonstrate the typical densely packed globular structure of PPy in which the PPy particles are strongly interconnected with the dopant DBSA and the SAED pattern affirms the amorphous nature of the doped polymer. In the TEM images of PPyS composite at 100 nm and 5 nm scales shown in figure 7.6 (b), sulfur particles are seen with a covering of PPy over it. Here it is confirmed from the SAED pattern that the presence of sulfur makes the composite, more crystalline in nature. Graphene layers covered with PPy are obviously noticeable in the TEM images of PPyG composite shown in figure 7.6 (c) and the layer surface seems, by all accounts, to be smooth [33]. The SAED pattern comprises of spots and diffused rings, which affirms the presence of crystalline graphene and amorphous PPy. The TEM images of PPyGS composite given in figure 7.6 (d) expose the layered structure of the composite and it is obviously noticeable in the images that the graphene layers are covered with PPy and with sulfur particles over it which resemble the images of a mosaic floor. The SAED pattern of SG composite shows the normal pattern of six membered ring. However, that of PPyGS demonstrates the decrease in the rings because of the amorphous nature of PPy and the pattern additionally affirms the crystalline nature of the composite [34].

7.3.8 Cyclic voltammetry studies

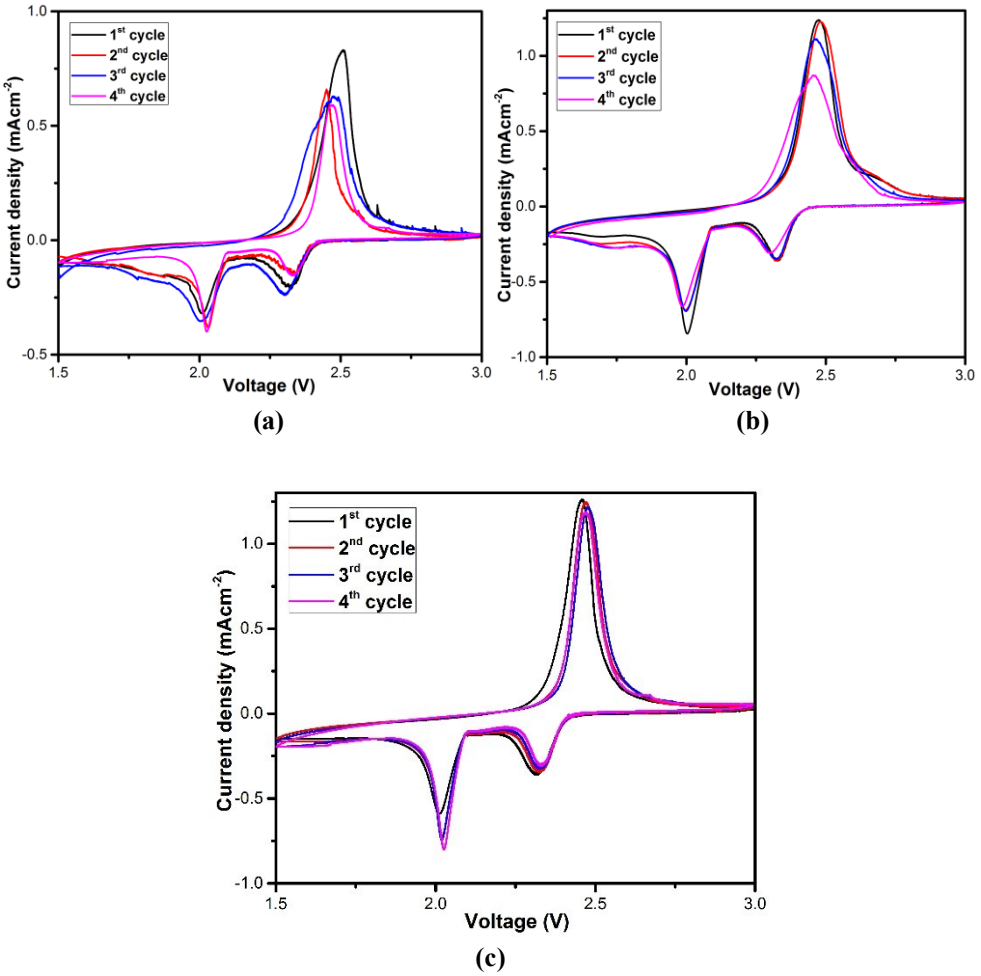

Figure 7.7 Cyclic voltammetry curves of (a) PPyS, (b) SG and (c) PPyGS based Li-S cells at a sweep rate of 0.1 mV/s

Cyclic voltammetry (CV) curves of the Li-S cells assembled using PPyS, SG and PPyGS composites as cathodes are shown in figures 7.7 (a), (b) and (c) respectively. All the CV curves indicate two reduction peaks and one oxidation peak, consistent with the typical behavior of sulfur cathodes. The origin of the reduction peak close to 2.32 V, during the

cathodic scan can be related to the conversion of higher-order polysulfides to lower-order polysulfides (Li_2Sx, $8 > x \geq 4$) and the second reduction peak at 2.0 V corresponds to the further diminishing of lithium polysulfides to insoluble Li_2S_2 and at last to Li_2S [35]. In the anodic sweep, there is only a single broad oxidation peak at around 2.45 V, representing the change of Li_2S_2/Li_2S to polysulfides and sulfur [36]. An increase in the redox currents is seen in the CV curves of the cells based on the composites SG and PPyGS, which indicates better usage of active cathode material. The cell based on PPyGS composite exhibits narrower peaks with slight shift with cycling, signifying its excellent electrochemical stability. The slight shift and broadening of redox peaks observed in all the CV curves are due to quick conversion between polysulfides and sulfur. The slight changes in the cathodic and anodic peaks of the CV curves of the cells based on the SG and the PPyGS composites vanish after the first cycle because of the rearrangement of the active material to electrochemically active positions and the peaks are well positioned indicating reversibility in the accompanying cycles.

7.3.9 Charge/discharge profiles of the Li-S cells

Table 7.3 Discharge capacities of the PPyGS composite cathode based cells at 0.1C rate.

1^{st} cycle	1444 mAhg-1
30^{th} cycle	1210 mAhg-1
100^{th} cycle	1005 mAhg-1

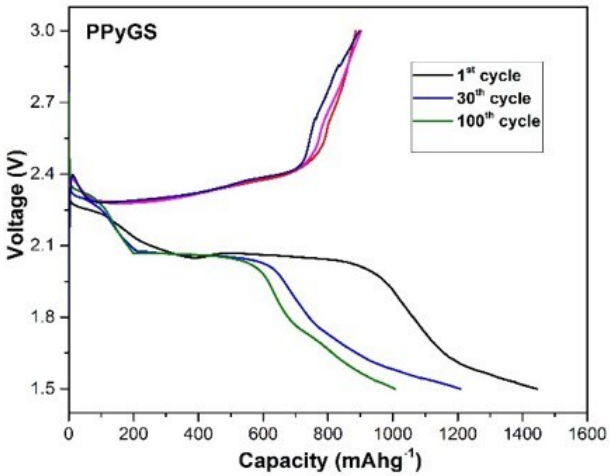

Figure 7.8 Charge-discharge profiles of PPyGS composite based Li-S cells after various number of cycles at 0.1C.

The charge-discharge profiles and the discharge capacities of the PPyGS composite based Li-S cells for the 1st, 30th and 100th cycles at 0.1 C are shown in figure 7.8 and Table 7.3. The capacities are determined by considering the weight of sulfur in the cathode active materials. Figure 7.9 shows the charge-discharge profiles of PPyS, SG and PPyGS based cells at 0.1 C, 0.2 C and 0.5 C current rates and the discharge capacities at various currents rates are given Table 7.4 respectively. The higher discharge capacity of the PPyGS based Li-S cells can be ascribed to the higher sulphur content in the above composite compared to the other composites, as obvious from the CHNS analysis.

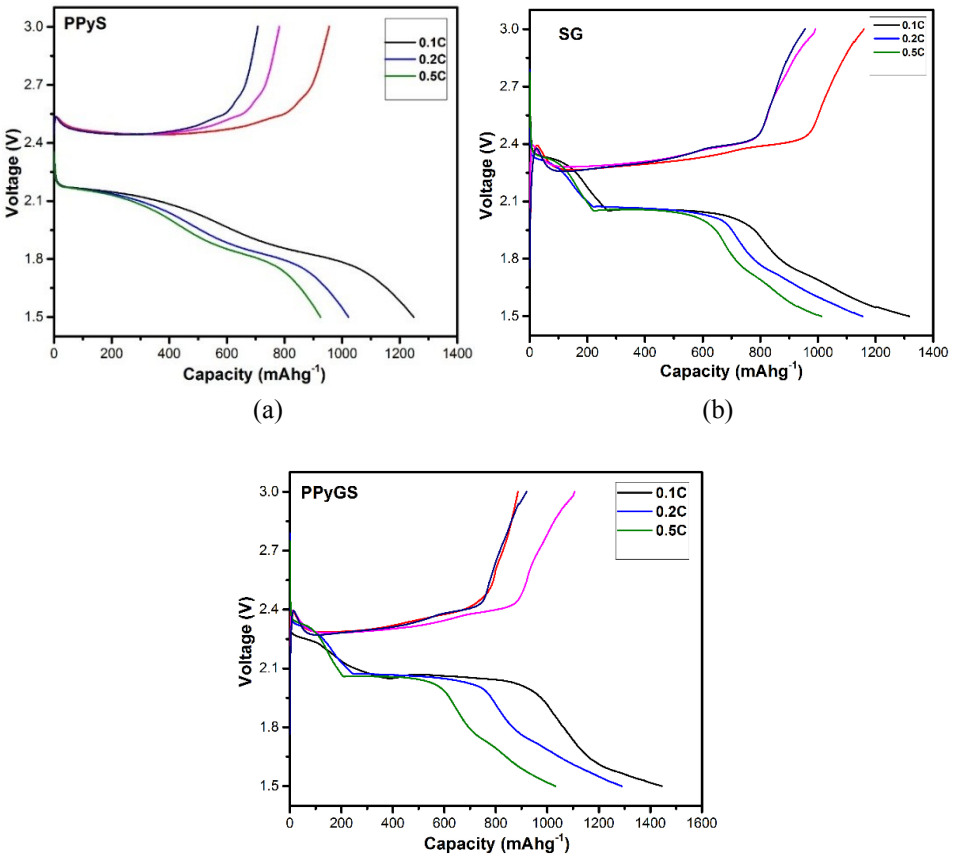

Figure 7.9 Charge-discharge profiles of (a) PPyS (b) SG and (c) PPyGS based Li-S cells at various C-rates.

Table 7.4 Discharge capacities of PPyS, SG and PPyGS based Li-S cells at various C-rates.

C rate	PPyS based cell	SG based cell	PPyGS based cell
0.1 C	1248 $mAhg^{-1}$	1317 $mAhg^{-1}$	1444 $mAhg^{-1}$
0.2 C	1022 $mAhg^{-1}$	1154 $mAhg^{-1}$	1367 $mAhg^{-1}$
0.5 C	925 $mAhg^{-1}$	1012 $mAhg^{-1}$	1243 $mAhg^{-1}$

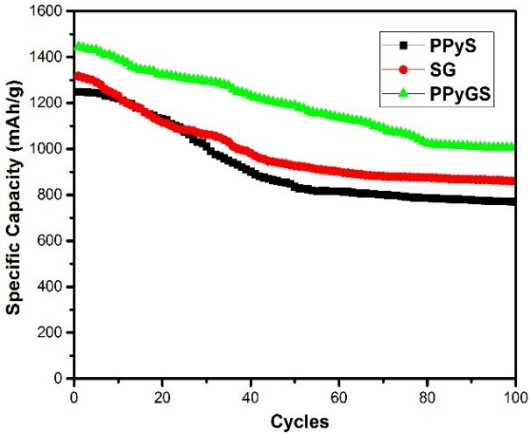

Figure 7.10 Cycling stability of PPyS, SG and PPyGS based Li-S cells at 0.1 C

The cycling stability of PPyS, SG and PPyGS based Li-S cells at 0.1 C is illustrated in figure 7.10. Capacity drop is observed for a few cycles for all the cells which is a direct result of the presence of a large number of sulfur particles, failing to achieve good electrochemical contact inside the new electrodes initially and afterwards steady cycling at 0.1 C is acquired due to the polypyrrole covering which gives a steady interface between the liquid electrolyte and lithium polysulfides, permitting quick ion and charge transfer with least loss of active materials. The PPyGS composite based cell offers more impressive cyclic execution compared with PPyS and SG based cells, under comparative cycling conditions, which can be attributed to the multiplex mix of sulfur with amorphous PPy and graphene [21]. Capacity retention of PPyS, SG and PPyGS composite cathodes based Li-S cells are 61%, 63% & 69% respectively. The improved cycle life of the cells based on the PPyGS composite cathode, compared to the cells based on the other sulphur composite cathodes of the present work can be a consequence of

the capability of doped PPy to incorporate large volume of sulfur on its branched structure and the efficient absorption of polysulfides into the pores of PPy, thereby inhibiting the adverse effects of the volume expansion of sulfur during Li intake and the polysulfide shuttling phenomenon. This fascinating effect is more pronounced in the PPyGS composite based cell, since this composite has the maximum sulfur content as observed from the CHNS investigation.

7.4 Conclusions

Polypyrrole with improved solubility was synthesized by chemical oxidative polymerization using ammonium persulfate as the oxidant and dodecylbenzene sulfonic acid (DBSA) as the dopant. Polypyrrole/sulfur (PPyS), sulfur/graphene (SG) and polypyrrole/graphene/sulfur (PPyGS) composites were synthesized and were investigated to assess their suitability as cathode active materials in Li-S cells. The FTIR studies reveal the presence of polypyrrole, sulphur and graphene in the composites. The XRD patterns indicate that the synthesized composites are semi-crystalline in nature. Using CHNS analysis, the sulphur content in the composites is determined and the results are in good agreement with those from thermo-gravimetric analysis. The surface morphology studies using FESEM and TEM techniques clearly indicate the presence of PPy, graphene sheets and sulphur in the composites. The electrochemical studies carried out on Li-S cells assembled using the modified sulphur cathodes constituted by the synthesized composites of sulphur with PPy, graphene and PPy/graphene offer quite promising cell performance. The CV curves and the charge discharge profiles of the assembled cells

establish the impressive electrochemical performance of the cells with capacity retention close to 70% after 100 cycles for the cells based on PPyGS composite cathode. The specific capacity of these cells between 1444-1240 mAh/g corresponding to 0.1,.0.2 and 0.5 current rates offers high scope for their applications in the design of high energy density Li-S cells. The capability of doped PPy to incorporate large volume of sulfur on its branched structure and facilitate the efficient absorption of polysulfides into its pores, thereby inhibiting the adverse effects of the volume expansion of sulfur during Li intake and the polysulfide shuttling phenomenon is the prime advantage of the strategies adopted in the present work for modifying the sulfur cathode to improve the capacity and cycling stability of the cells. This fascinating effect is more pronounced in the PPyGS composite cathode based cell, since this composite has the maximum sulfur content as observed from the CHNS investigation.

References

[1] Y. Su, Y. Fu, A. Manthiram, Challenges and Prospects of Lithium-Sulfur Batteries, Acc. Chem. Res., 46(5) (2013) 1125–1134

[2] Zhang, Sulfur based Composite Cathode Materials for Rechargeable Lithium Batteries, Ph.D Thesis http://hdl.handle.net/10012/7769 (2013)

[3] G. Zheng, Y. Yang, J. J. Cha, S. S. Hong, and Y. Cui, Hollow Carbon Nanofiber-Encapsulated Sulfur Cathodes for High Specific Capacity Rechargeable Lithium Batteries, Nano Lett., 11(10) (2011) 4462–4467

[4] Y. Fu and A. Manthiram, Core-shell structured sulfur-polypyrrole composite cathodes for lithium- sulfur batteries, RSC Adv., 2(14) (2012)5927–5929

[5] J. Guo, Y. Xu, and C. Wang, Sulfur-Impregnated Disordered Carbon Nanotubes Cathode for Lithium-Sulfur Batteries, Nano Lett.,11(10) (2011) 4288–4294

[6] L. Ji, M. Rao, H. Zheng, L. Zhang, O. Y. Li, and W. Duan, Graphene Oxide as a Sulfur Immobilizer in High Performance Lithium/Sulfur Cells, 133(46 (2011) 18522–18525

[7] H. Wang, Y. Yang, Y. Liang, J. T. Robinson, Y. Li, and A. Jackson, Graphene-Wrapped Sulfur Particles as a Rechargeable Lithium - Sulfur Battery Cathode Material with High Capacity and Cycling Stability,Nano Lett., 11(7) (2011) 2644–2647

[8] G. Zhou, S. Pei, L. Li, D. Wang, S. Wang, and K. Huang, A Graphene–Pure-Sulfur Sandwich Structure for Ultrafast, Long-Life Lithium–Sulfur Batteries,Adv. Mater., 26(4) (2014) 625–631

[9] N. Jayaprakash, J. Shen, S. S. Moganty, A. Corona, and L. A. Archer, Porous Hollow Carbon@Sulfur Composites for High-Power Lithium-Sulfur Batteries, Angewandte Chemia 123(26) (2011) 6026–6030

[10] N. Li, M. Zheng, H. Lu, Z. Hu, C. Shen, and X. Chang, High-rate lithium – sulfur batteries promoted by reduced graphene oxide coating , Chem. Commun., 48 (2012) 4106–4108

[11] A. Fedorková, R. Oriňáková, O. Čech, and M. Sedlaříková, New Composite Cathode Materials for Li / S Batteries : A Review, 8(8) (2013) 10308–10319

[12] X. Liu, Y. Li, Y. Zhao, H. Li, and F. Yin, In Situ Polymerization Synthesis of Ternary Sulfur / Polypyrrole / Graphene Nanosheet Cathode for Lithium / Sulfur Batteries, Materials Science Forum, 847 (2016) 8-13

[13] Y. Qiu, W. Li, W. Zhao, G. Li, Y. Hou, M. Liu, L. Zhou, F. Ye, H. Li, Z. Wei, S. Yang, W. Duan, Y. Ye, J. Guo, and Y. Zhang, High-Rate, Ultralong Cycle-Life Lithium/Sulfur Batteries Enabled by Nitrogen-Doped Graphene, Nano Lett., 14(8) (2014) 4821-4827

[14] Y. Fu and A. Manthiram, Enhanced Cyclability of Lithium − Sulfur Batteries by a Polymer Acid- Doped Polypyrrole Mixed Ionic − Electronic Conductor, Chem. Mater., 24(15) (2012) 3081-3087

[15] C. Su, L. Wang, L. Xu, and C. Zhang, Synthesis of a novel ferrocene-contained polypyrrole derivative and its performance as a cathode material for Li-ion batteries, Electrochim. Acta, 104 (2013) 302–307

[16] B. Jin, H. Li, X. Lang, C. Yang, W. Gao, Y. Zhu, W. Zhang, S. Dou, and Q. Jiang, Facile Synthesis of Sulfur-Polypyrrole as Cathodes for Lithium-Sulfur Batteries, Chemelectrochem, 4(1) (2017) 115-121

[17] N. Nakamura, T. Yokoshima, H. Nara, T. Momma, and T. Osaka, Suppression of polysul fi de dissolution by polypyrrole modification of sulfur-based cathodes in lithium secondary batteries, J. Power Sources, 274 (2015) 1263–1266

[18] X. Liang, Y. Liu, Z. Wen, L. Huang, X. Wang, and H. Zhang, A nano-structured and highly ordered polypyrrole-sulfur cathode for lithium – sulfur batteries, J. Power Sources, 196(16) (2011) 6951–6955

[19] S. Deivanayaki, V. Ponnuswamy, R. Mariappan, and P. Jayamurugan, Synthesis and characterization of polypyrrole/TiO2 composites by chemical oxidative method, Optik (Stuttg)., 124 (12) (2013) 1089–1091

[20] C. Basavaraja, W. J. Kim, D. G. Kim, and D. S. Huh, Synthesis and characterization of soluble polypyrrole–poly(ε-caprolactone) polymer blends with improved electrical conductivities, Mater. Chem. Phys., 129 (3) (2011) 787–793

[21] W. Wang, G. Li, Q. Wang, G. Li, S. Ye, and X. Gao, Sulfur-Polypyrrole / Graphene Multi-Composites as Cathode for Lithium-Sulfur Battery, J. Electrochem. Soc., 160 (6) (2013) 805–810

[22] X. Feng, R. Li, Z. Yan, X. Liu, R. Chen, Y. Ma, and X. Li, Preparation of Graphene / Polypyrrole Composite Film via Electrodeposition for Supercapacitors, IEEE Transactions on Nanotechnology, 11 (6) (2012),1080–1086

[23] H. Eisazadeh, Studying the Characteristics of Polypyrrole and its Composites, World J. Chem., 2(2) 2007 67–74

[24] H. Li, M. Sun, T. Zhang, Y. Fang, and G. Wang, Improving the performance of PEDOT-PSS coated sulfur@activated porous graphene composite cathodes for lithium–sulfur batteries, J. Mater. Chem. A, 2(43) (2014) 18345–18352

[25] R. Ghosh Chaudhuri and S. Paria, Visible light induced photocatalytic activity of sulfur doped hollow TiO2 nanoparticles, synthesized via a novel route, Dalt. Trans., 43(14) (2014) 5526–5534

[26] S. Konwer and S. K. Dolui, Synthesis and characterization of polypyrrole / graphite composites and study of their electrical and electrochemical properties, Mater. Chem. Phys., 124(1) (2010) 738–743

[27] X. Tang, T. Liu, H. Li, D. Yang, and L. Chen, Notably enhanced thermoelectric (2017) properties of lamellar polypyrrole by doping with β -naphthalene sulfonic acid, RSC Adv., 7 20192–20200

[28] Pullarkat P. Jeeju, Sreekanath J. Varma, S. Jayalekshmi, Novel polypyrrole films with excellent crystallinity and good thermal stability, Materials Chemistry and Physics, 134(2-3) (2012) 803-808

[29] J.L. Gómez-Urbanoa, J.L. Gómez-Cámera, C. Botasa, N. Díeza, J.M. López del Amoa, L.M. Rodríguez- Martineza, D. Carriazo T. Rojoa, Hydrothermally reduced graphene oxide for the effective wrapping of sulfur particles showing long term stability as electrodes for Li-S Batteries, Carbon, 139 (2018) 226-233

[30] Fuxing Yin, Xinyi Liu , Yongguang Zhang , Yan Zhao , Almagul Menbayeva , Zhumabay Bakenov , Xin Wang ,Well-dispersed sulfur anchored on interconnected polypyrrole nanofiber network as high performance cathode for lithium-sulfur batteries, Solid State Sciences 66 (2017) 44-49

[31] P. Jayamurugan, V. Ponnuswamy, S. Ashokan, R. N. Jayaprakash, and N. Ashok, DBSA doped polypyrrole blended with Poly (4-styrenesulfonic acid) by mechanical mixing , Materials Science-Poland, 32(4) (2014) 648–651

[32] J. Zhu, Y. Xu, J. Wang, J. Wang, Y. Bai, and X. Du, Morphology controllable nano-sheet polypyrrole – graphene composites for high-rate supercapacitor, Phys. Chem. Chem. Phys., 17(30) (2015) 19885–19894

[33] Amir Reza Sadrolhosseini, Suraya Abdul Rashid, A. S. M. Noor, Optical Band Gap and Thermal Diffusivity of Polypyrrole-Nanoparticles Decorated Reduced Graphene Oxide Nanocomposite Layer, Journal of Nanomaterials, 2016 (2015)

[34] Sumanta Sahoo, G. C. Nayak, Chapal Kumar Das, Synthesis and Electrochemical Characterization of Modified Graphene/Polypyrrole Nanocomposites, Macromolecular Symposia, 315 (1) (2012) 177-187

[35] Zhao MQ , Zhang Q, Huang JQ, Tian GL, Nie JQ, Peng HJ, Wei F, Unstacked double-layer templated graphene for high-rate lithium-sulphur batteries, Nat. Commun. 5 (2014) 1-8

[36] Zhou G, Yin LC, Wang DW, Li L, Pei S, Gentle IR, Li F, Cheng HM, Fibrous hybrid of graphene and sulfur nanocrystals for high-performance lithium-sulfur batteries, ACS Nano, 7 (6) (2013) 5367-5375.

Chapter 8
SUMMARY AND CONCLUSIONS

The work presented in the thesis is focussed on investigating the structural, morphological, optical, electrical and electrochemical properties of polypyrrole in bulk and thin film forms, synthesized using two different routes, and assessing its application prospects in various technological fields. The effect of long alkyl chain containing dopants like NaDEHS, DBSA and NaDBSA on improving the solubility and processability of polypyrrole has been investigated in depth. Much importance is given for assessing the prospective applications of lithium substituted polypyrrole, doped polypyrrole and its nanocomposites as cathode active materials in Li ion cells and as materials to modify the sulphur cathode to improve the capacity and cycling stability of Li-S cells.

Plasma polymerization and chemical oxidative polymerization are the synthesis routes adopted in the present work to polymerize pyrrole. The first part of the thesis is devoted to the investigations on the structural, electrical and optical properties of plasma polymerized pyrrole thin films in pristine and iodine doped forms. Space charge limited type conduction has been identified as the dominant carrier transport mechanism in plasma polymerized pyrrole films. Iodine doping brings about quite significant changes in the structural, optical, and

electrical properties of polypyrrole films, compared to the pristine ones. The method of Urbach tail analysis is used to understand the enhancement of defect levels by iodine doping and it is observed that iodine doping results in the creation of charged defects in the polymer chain. The analysis further suggests that the disorders created by doping are more prominent in the visible region than in the NIR region.

Chemical oxidative polymerization technique, using ammonium persulfate as the oxidant and NaDEHS, DBSA and NaDBSA as the dopants is used to synthesize doped polypyrrole compositions with appreciable solubility in organic solvents which include m-cresol, NMP, DMF and DMSO. The effective incorporation of the dopants into the PPy structure has been demonstrated through FTIR spectroscopy studies and elemental analysis. The significant impact of the dopants in modifying the morphology of PPy structure is evident from the FESEM and TEM studies and the XRD patterns and the SAED patterns support the enhanced crystalline order of the doped PPy compositions. The increased structural order in PPy, brought about by doping has also been established by the increase in the glass transition temperature and the melting temperature of the doped PPy compositions as per the DSC studies.

The significant extent of solubility and processability attained through doping and the enhanced crystalline order and electrical conductivity achieved consequently make the chemically synthesized, doped polypyrrole, a potential candidate for various device applications. The present studies highlight the superb power of appropriate dopants to control the structural and morphological features of chemically

synthesized polypyrrole and to offer means of designing doped polypyrrole compositions with desired structural, electrical and optical characteristics suitable for different types of device applications.

The synthesis of DBSA doped, polypyrrole/graphene composites using various solvents like DMF, DMSO, NMP and m-cresol and the investigations on the structural, morphological, electrical and optical characteristics of the spin coated and electro-sprayed films of these composites comprise another important work on doped polypyrrole. From the XRD, FTIR and Raman spectroscopy and the FESEM and TEM studies, it can be established that the dopant DBSA and graphene bring more structural order to the DBSA doped, PPy/graphene nanocomposite and enhance the crystalline nature of the nanocomposite to a significant extent. Raman spectroscopy studies of the electro-sprayed films of the DBSA doped PPy/graphene nanocomposite illustrate the presence of the G bands of graphene with quite high intensity and that of the D bands with much less intensity, indicating the overall defect free nature of the nanocomposite. The electro-sprayed films of the nanocomposite dissolved in m-cresol, show maximum electrical conductivity around 4.2 S/cm, .which is much higher than that of the spin coated films. The morphological features of the spin coated and electro-sprayed films of the nanocomposite, revealed by the FESEM and TEM studies show that, in the nanocomposite, the graphene layers are covered by the DBSA doped PPy matrix. The doped PPy can steadily hold onto the surface of graphene due to the electrostatic attraction between the doped PPy and graphene.

The second part of the research work is devoted for investigating the suitability of polypyrrole, synthesized using $FeCl_3$ as the oxidant, to serve as the electrode material for applications in the development of flexible Li ion cells with high energy density and excellent cycling stability. The interesting aspect of the work is the introduction of a relatively less expensive lithium salt, n-butyllithium in hexanes (n-BuLi), compared to the expensive counterparts like $LiPF_6$ and $LiBF_4$, as a dopant for synthesizing lithium substituted polypyrrole to be used as the cathode active material in rechargeable Li ion cells The amount of lithium content in the lithiated PPy compositions is evaluated using ICP-AES technique which reveals that the lithium content increases by increasing the n-BuLi concentration. Studies using FTIR spectroscopy, XRD, FESEM and TEM techniques strongly support fruitful lithium substitution in PPy and the increase in the crystalline order of the polymer structure, with increase in the extent of lithiation. The Li ion cells assembled, using the lithiated PPy as the cathode, lithium metal as the anode and lithium hexaflurophosphate ($LiPF_6$) as the electrolyte demonstrate an open circuit voltage of 3.3 V. The features of the CV curves of the coin cells indicate that the lithiated PPy based Li ion cells are electrochemically active. All the assembled four cells show stable charge - discharge cycling behaviour up to 60 cycles, specific capacity about 30.03 mAh/g for the cell with maximum lithium substitution of 21.56 % and coulombic efficiency around 85 %. The present studies highlight the meritorious features of the n-BuLi doped polypyrrole as a promising cathode active material to develop conducting polymer based Li ion cells with the inherent

advantages of flexibility in cell design, reduced material cost and environmental friendliness. There is ample scope for bringing the specific capacity of the cells closer to the theoretical capacity of polypyrrole around 72 mAh/g by the proper choice of the dopants to achieve much enhanced Li substitution in PPy.

The investigations on the superior electrochemical performance offered by the assembled Li ion cells based on lithium substituted PPy, synthesized using APS as the oxidant, compared to the performance of the cells based on lithiated PPy, synthesized using $FeCl_3$ as the oxidant form another significant part of the research work. The structural studies using FTIR spectroscopy and XRD and the morphological changes observed in the lithiated PPy as per FESEM and TEM investigations strongly support successful lithium substitution in PPy and the enhanced crystallinity acquired. The CV curves and the charge-discharge profiles of the Li ion cells based on lithium substituted PPy, synthesized using APS as the oxidant, reveal excellent electrochemical behaviour, enhanced discharge capacity around 52.02 mAh/g, closer to the theoretical value and superior cycling stability up to 85 cycles, compared to the earlier work on Li ion cells based on lithiated PPy, synthesized using $FeCl_3$ as the oxidant. The highlight of the work is the awareness that the discharge capacity and the energy density of the cells can be enhanced further by optimising the polymer synthesis conditions with proper choice of the oxidants and dopants.

The last part of the research work features the attempts carried out to assess the suitability of polypyrrole and its composite with graphene

in the modification of the sulphur cathode to develop Li-S cells with high energy density and excellent cycling stability for the next generation energy storage applications. Lithium–sulfur cells are quite promising devices for energy storage applications with high theoretical capacity of 1675 $mAhg^{-1}$. However, their specific capacity and cycling stability are adversely affected by poor electrical conductivity of sulfur, the shuttling effect of lithium polysulfides and the volume expansion of sulfur during lithium intake. These limitations can be averted through modifying the sulphur cathode by making composites with electrically conducting polymers and carbon nanostructures. The research work is hence focused on the modification of sulphur cathode by making composites with polypyrrole, graphene and polypyrrole/graphene.

Polypyrrole with improved solubility is synthesized by chemical oxidative polymerization using ammonium persulfate as the oxidant and dodecylbenzene sulfonic acid (DBSA) as the dopant. Polypyrrole/sulfur (PPyS), sulfur/graphene(SG) and polypyrrole/graphene/sulfur (PPyGS) composites are synthesized and subjected to detailed investigations to assess their suitability as cathode active materials in Li-S cells. The sulphur content in the composites is determined using CHNS analysis and the results are in good agreement with those from thermo-gravimetric analysis. The surface morphology studies using FESEM and TEM techniques clearly establish the presence of PPy, graphene sheets and sulphur in the composites. The electrochemical studies carried out on Li-S cells assembled using the modified sulphur cathodes constituted by the synthesized composites of sulphur with PPy, graphene and PPy/graphene termed respectively as PPyS, SG and PPyGS offer quite

promising cell performance. The CV curves and the charge discharge profiles of the assembled cells establish the impressive electrochemical performance of the cells with capacity retention close to 70% after 100 cycles for the cells based on PPyGS composite cathode. The specific capacity of these cells between 1444-1240 mAh/g corresponding to 0.1, 0.2 and 0.5 current rates offers high scope for their applications in the design of high energy density Li-S cells. The competence of doped PPy to incorporate large volume of sulfur on its branched structure and facilitate the efficient absorption of polysulfides into its pores, thereby inhibiting the adverse effects of the volume expansion of sulfur during Li intake and the polysulfide shuttling phenomenon is the prime advantage of the strategies adopted in the present work for modifying the sulfur cathode to improve the capacity and cycling stability of the cells. This intriguing effect is more pronounced in the PPyGS composite cathode based cell, since this composite has the maximum sulfur content as observed from the CHNS analysis.

Future Prospects

- The present work proposes sufficient and ample scope for further investigations, in view of the consequences of the present studies and the appropriate changes proposed to be made for making the research outcomes viable for practical situations.
- The synthesis conditions of polypyrrole using chemical oxidation method with various oxidants and dopants can be optimized furthermore to improve the electrical conductivity and solubility.

- Attempts should be made to optimize the film deposition conditions by spin coating and electro-spraying techniques, to develop high quality films of PPy and its composites, for conceivable applications in energy storage devices.
- Development of lithiated polypyrrole based Li ion cells with improved specific capacity close to the theoretical value of 72 mAh/g for possible applications as biocompatible, flexible cells.
- Development of Li-S cells with high capacity, energy density and excellent cycling stability, using polypyrrole composite cathodes, capable of operation at higher current rates.

.....ꕥ.....